INTERNATIONAL UNIVERSITY LIAISON INDONESIA

BACHELOR'S THESIS

PERFORMANCE CALCULATION OF BOMBARDIER CRJ 1000 NEXTGEN AIRCRAFT CONVERSION TO BUSINESS JETS

By

Florensia Yovita

11201501014

Presented to the Faculty of Engineering

In Partial Fulfilment Of the Requirements for the Degree of

SARJANA TEKNIK

In

AVIATION ENGINEERING

FACULTY OF ENGINEERING

BSD City 15345

Indonesia

August 2021

APPROVAL PAGE

PERFORMANCE CALCULATION OF BOMBARDIER CRJ 1000 NEXTGEN AIRCRAFT CONVERSION TO BUSINESS JETS

FLORENSIA YOVITA
11201501014

Presented to the Faculty of Engineering
In Partial Fulfillment of the Requirements for the Degree of

SARJANA TEKNIK
In
AVIATION ENGINEERING

FACULTY OF ENGINEERING

Triwanto Simanjuntak, Ph.D.	_____
Thesis Advisor	Date:
Ananta Wijaya, S.T., M. Sc. Tech.	_____
Thesis Co-Advisor	Date:
Tutun Nugraha, BASc, MASc, Ph.D.	_____
Vice Rector of Academic Affairs	Date:

EXAMINERS APPROVAL PAGE

Dr. Ir. Erie Sandhita, MsAe, DEA _____
Examiner 1 Date:

Dr. Eng. Ressa Octavianty, S.T., M. Eng _____
Examiner 2 Date:

Triwanto Simanjuntak, Ph.D. _____
Examiner 3 Date:

Ananta Wijaya, S.T., M. Sc. Tech. _____
Examiner 4 Date:

STATEMENT BY THE AUTHOR

I hereby declare that this submission is my own work and to the best of my knowledge, it contains no material previously published or written by another person, nor material which to a substantial extent has been accepted for the award of any other degree or diploma at any educational institution, except where due acknowledgement is made in the thesis.

Florensia Yovita _____ _____

Student Date

ABSTRACT

Performance Calculation Of Bombardier CRJ 1000 Nextgen Aircraft Conversion To Business Jets

by

Florensia Yovita

Triwanto Simanjuntak, Ph.D., Advisor

Ananta Wijaya, S.T., M. Sc. Tech., Co-Advisor

The CRJ1000 operational has caused a great burden on Airline X. The operational of this aircraft has never made any profit since its first operated. The COVID-19 pandemic makes the situation worse. There is a most probable solution for the airline to override this problem by joining the ongoing aviation trend rises across the world during this pandemic, converting these aircraft into business jets. Therefore, the objectives of this study are to check the feasibility of conversion to Biz Jet with the main considerations are airfield and cruising performance and to assess how the performance of the aircraft are changed by the conversion. There are two proposed configurations used for this study. The analysis includes the MTOW, range, endurance, take-off and landing ground roll distance, actual and required landing distance, and landing speed. In conclusion, both proposed configurations have lighter MTOW as far as 20.18% lower, therefore both range and endurance for option 1 are increased up to 29.5 % and 26.8 % for option 2. The required landing distance for option 1 is 27.1% lower and 26% lower for option 2. The landing distance can be obtained by using linear regressions from the landing distance chart and approximations. The take-off and landing ground roll distance, actual landing distance, and landing speed for both configurations are also lower.

Keyword: *aircraft performance, CRJ 1000, business jets, conversion, airfield performance, range, endurance*

ACKNOWLEDGEMENTS

My deep gratitude goes first to both Mr. Ananta Widjaja and Mr. Triwanto Simanjuntak who expertly guided me through my undergraduate study. Thank you so much for willing to be my thesis advisors when I've almost lost hope, for bearing with me, for spending your time and energy, especially in this hard time during the pandemic. Thank you for always being the most supportive and understanding lecturers during my study in IULI, making my study enjoyable and bearable.

My deep gratitude also extends to Mr. Erie Sandhita and Ms. Ressa Octavianty for the knowledge during my study and for the input as my thesis examiners. Thank you as well to Mr. Neno Ruseno as the former head of AVE, Mr. Prianggada Indra Tanaya as the former dean of engineering faculty, Mr. Setyo and Mr. Derajat as my former thesis advisors, all of the aviation engineering lecturers, IULI staffs, Tama, Teddy, Nadia, Luci, Sheren, Jordy, Bagas, Davion, Nini, Mazay, and AVE15 for the kindness, support, and knowledge during my study.

I would also like to thank Agha, Rao, Tazkya, Billy, and Nael for their help with my thesis.

To Inca Maya Sari, thank you for your support, guidance, and encouragement.

To Jasmine, Catherine, Andrean, Verdy, my psychologists, I am grateful that you are part of my life.

To members of Kiki, Youth Coalition for Girls, A*I, Asymmetric, floorball and fencing mates, Sinar Medan, Kos 446, I am thankful for nights that turned into mornings, friends that turned into family, and dreams that turned into reality.

And finally, to my family, thank you for everything.

Contents

List of Figures

List of Tables

List of Abbreviations

COG	**C**enter **O**f **G**ravity
CRJ	**C**anadair **R**egional **J**et
FAA	**F**ederal **A**viation **A**dministration
ISA	**I**nternational **S**tandard **A**tmosphere
MLW	**M**aximum **L**anding **W**eight
MTOW	**M**aximum **T**ake-Off **W**eight
MZFW	**M**aximum **Z**ero **F**uel **W**eight
OEW	**O**perational **E**mpty **W**eight

Dedicated to my parents

CHAPTER 1
INTRODUCTION

1.1 Background

A regional jet is a narrow-body aircraft that is used by airlines operating regional flights which typically has less than 150 seats and is used for short-haul flights, usually within a country or a certain area of a continent (www.alternativeairlines.com, 2021).

Bombardier CRJ1000 is the last regional aircraft series that is made by Bombardier Inc., first delivered in 2011. This twin turbofan passenger aircraft is capable to transport up to 104 passengers, certified to fly at maximum altitude of 41,000 feet, airspeed up to Mach 0.84, and maximum range of 2760 km. Bombardier CRJ1000 is also claimed to be more eco-friendly with lower operating cost, fuel efficient, and more comfortable for the passengers compared to previous aircraft series.

Airline X, bought 6 Bombardier CRJ1000 aircrafts in 2011 from Bombardier Inc. and leased 12 Bombardier CRJ1000 aircrafts from Nordic Aviation Capital (NAC) in 2012. However, operating Bombardier CRJ1000 aircrafts created a big lost to Airline X. Twelve Bombardier CRJ1000 aircrafts will be returned to NAC despite the fact that the contrac will be ended by 2027 (Herman, 2021).

The Bombardier CRJ1000 aircrafts cost US$ 30 million annually to operate and cause airline money losses while the leasing cost itself is US$ 27 million (Curran, 2021). With only 96 seats and a restricted baggage capacity, the aircraft was never a good fit for Indonesia's generally crowded domestic aviation industry. Bombardier's jets were an odd fit to Airline X's existing set of aircraft, dominated by Boeing, Airbus, and ATR aircrafts, which results in making the jets' maintenance cost more expensive for the airline.

CRJ 1000 requires a take-off distance of 2120 m, which is incompatible with the typical runway in East Indonesia, which is less than 2000 m. Therefore, it limits Airline X to expand its route.

If Airline X terminates it now, until the end of the contract period, the airline will be capable of saving about US$ 220 million (Handayani & Kuniawan, 2021). This is part of the effort to curtail losses from the use of these aircrafts at Airline X. Those twelve aircrafts are currently grounded at its maintenance facility hangar since February 1st, 2021 while waiting for the negotiation outcome with NAC regarding the early contract termination (Puspa, 2021).

Along the year 2020, COVID-19 has became a fully blown pandemic, which throw a global risk to our health and also economics. Across all industries, probably at the aviation sector is among the industries who is hit the hardest. The unprecedented decrease in passenger demand (along with the flight restriction), led to a halt of most airlines; many companies had to cease almost all their operations and grounded entire fleets, many airports have closed their runways in order to free up space for aircraft parking or just shutting down indefinitely, most companies in the aviation sector are working with minimum staffing on strict rotations, and aircraft manufacturers and downstream industry have largely shut-down their production lines (Sun, Wandelt, Zheng, & Zhang, 2021).

The Covid-19 pandemic makes the situation worse as the aircraft utilization is very low. While the Covid-19 pandemic has had a significant impact on the commercial flight industry, the business or private jet industry has had relatively healthy trends. Private jets enable consumers to travel without encountering other passengers on the flight or in the airport. According to private jet membership business Airshare, a passenger on a commercial flight will meet 700 points of contact during the flight, including check-in, security, and boarding, whereas a client on a private jet will only see 20 touchpoints. Numerous private jet firms are witnessing an increase in memberships as a result of this (Swindells, 2021).

Business flights, by September 2020, has back to almost to 2019 volume following a smaller drop between March and June. These global trends were also seen in data for the United States, the world's largest market for private jet flights, with business flight volume recovering at a considerably faster and greater rate than the aviation industry as a whole. Global flights plummeted to a fifth of their 2019

volume in April, while business flights fell to 36Monarch Air Group, a US-based charter company, announced that they have seen an increase (Year-on-Year) of 125% in total bookings till June 2020 compared to June 2019, and approximately half of its new charter contracts were received in June 2020 (Linker, 2021). Globally, flight volume has recovered slowly and has been hovering around half of what it was in 2019.

The same trend is also followed by Asia, especially in Japan (T. J. Times, 2021), China, Hongkong, and Indonesia (Neubauer, 2021). In China, domestic flights are either hired privately or flown exclusively for their owners are up 87 percent this year compared to the same period two years earlier, according to data from WingX Advance GmbH (F. Times, 2021). While the frequency of commercial flights globally is still down by 29 percent this year compared to last year, private jets are 18 percent busier but remain down on 2019.

The aircraft conversion process is not a new thing in the aviation industry. Generally, the aircraft is designed and used for passenger aircraft, but then it is converted into other kinds of aircraft for other needs such as freighter, medical evacuation, business jets, and others, depends on the users' needs. For example, it has been done on A320, A300B4, A310-200/-300, A300-600, A330-200/-300 from passenger into freighter by EWF, who has already done the aircraft conversion for more than 25 years. Precision Aircraft Solusion has also converted A321-200 and B757-200 into freighter and B757-200 into a combination of passenger and freighter aircraft. An Embraer Legacy 650 is converted to medical evacuation aircraft by Jet Aviation. A Boeing B737-524 corporate jet is converted into a VIP business jet by FL Technics and a B787 into private jet by Kestrel Aviation Management.

Looking from the uprising trend of business jets industry and the uncertainty during Covid-19, converting Bombardier CRJ1000 aircrafts to business jets could be one of the most beneficial and profitable options for Garuda Indonesia, considering the current situation with NAC as well as the Covid-19 pandemic. However, converting these aircrafts also means changing the seat configuration, overall interior, and perhaps adding auxiliary fuel tanks generally in the baggage hold. This conversion means there will be differences in terms of weight, payload, range, take-off, and landing distance, and other aircraft performance factors, which needs to

be recalculated to ensure the flight performance and also to comply with the regulations.

1.2 Problem Statement

These Bombardier CRJ1000 aircrafts are currently grounded which means these aircrafts are frozen assets as the airline waits for an indefinite period of time waiting for the negotiation with NAC to complete. This also means that space currently used for these aircrafts to park is unavailable for its maintenance facility to utilize for other clients' needs. Even if the negotiation comes to a mutual agreement, there is a certain amount of penalty that needs to be paid. Converting these aircrafts to business jets also means changes in the overall aircraft flight performance, including but not limited to weight, range, payload, takeoff and landing distance that needs to be recalculated and ensured that it complies with the regulations.

The problem statements are:

- How to utilize CRJ1000 leased by Airline X as business jets?
- Specifically, how the aircraft performance of CRJ1000 will be changed if converted into business jets?
- What kind of configurations are available for the conversion?

1.3 Research Purpose

The purpose of this thesis are to investigate:

- To check the feasibility of conversion to Business Jet; the main consideration are airfield and cruising performance.
- There are two configurations being considered.
- To assess or calculate how the aircraft performance is changed by the conversion.

1.4 Research Scope

- The object of this study is Bombardier CRJ1000 aircraft.
- The Bombardier CRJ1000 data is taken from Airline X.
- The modification of Bombardier CRJ1000 is only within the aircraft's interior.
- None of the aircraft's exterior is modified, therefore there is no changes within aerodynamics aspect.
- The fuel used for take=off and landing is considered negligible.

1.5 Thesis Organization

This thesis consists of five chapters and organized as follows:

1. Chapter 1: Introduction The first chapter introduces a brief overview of the thesis topic in general, as well as problem statement, research purpose, and research scope.
2. Chapter 2: Literature Review The second chapter describes the literature that is related to this study.
3. Chapter 3: Methodology The third chapter explains the methodology applied to gather data to be analyzed and solve the problems on this chapter.
4. Chapter 4: Result and Discussion The fourth chapter presents the result of the analyzed data. Furthermore, promising solution will be discussed to find the solution of the problem.
5. Chapter 5: Conclusion and Recommendation The fifth chapter presents the thesis conclusions and its recommendation, that could be used to solve the problems.

CHAPTER 2
LITERATURE REVIEW

2.1 Pandemic

A pandemic is an epidemic of an infectious illness that has spread everywhere, crossing multiple continents or the entire world, and has affected a huge number of people. The COVID-19 pandemic, alternatively referred to as the coronavirus pandemic, is a global pandemic of coronavirus disease 2019 (COVID-19), which is caused by coronavirus 2 causing severe acute respiratory syndrome (SARS-CoV-2). It was discovered for the first time in December 2019 in Wuhan, China (University, 2021).

On 30 January 2020, the World Health Organization (WHO) declared COVID-19 a Public Health Emergency of International Concern, which was later elevated to a pandemic by 11 March 2020. As of 10 June 2021, over 174 million verified cases had been reported, with over 3.75 million confirmed deaths, making COVID-19 one of the worst pandemics throughout history.

COVID-19 symptoms are widely diverse in intensity, ranging from no symptoms at all to life-threatening. COVID-19 is spread via the air when droplets and small airborne particles are breathed in. While the risk is greatest when people are near together, they can be breathed over greater distances, particularly indoors. Transmission can also occur if contaminated fluids are sprayed into the eyes, nose, or mouth, or, quite rarely, via infected surfaces. According to existing research, the incubation period (the time period between exposure and development of symptoms) for SARS-CoV-2 is between 2 and 14 days, and infected individuals can spread the virus even if they do not develop symptoms (for Diseases Control & Prevention, 2021).

Social distancing, ventilation, wearing face masks in public, hand washing or cleaning, covering one's mouth when sneezing or coughing, sanitizing surfaces, and

monitoring and self-isolation for those exposed or sick are all the preventive methods. Since December 2020, vaccines have been created and widely delivered. Globally, authorities have responded with travel restrictions, lockdowns and quarantines, occupational hazard controls, and business closures.

The pandemic has caused tremendous economic and social disruptions on a global scale, including the greatest global recession since the 1930s Great Depression (Gopinath, 2021). It has resulted in significant supply shortages, which have been worsened further by panic buying, food scarcity, and agricultural disruption. Numerous educational institutions and public spaces have been shuttered and numerous activities have been either canceled or rescheduled. Through social media and traditional media, misinformation has spread, escalating political tensions.

2.2 Aviation Industry during the Pandemic

As the pandemic continues, the world faces uncertainty about when the pandemic will end. Many countries are back to lockdown again and traveling is very restricted, although the travel restriction varies between countries.

The pandemic has an enormous impact on the aviation industry, affecting passenger traffic, air cargo demand, airport workforce, and incoming revenues. There are significant reductions in passenger traffic in flights being canceled or aircrafts flying empty between airports, which then affect the revenues reduction for airlines and forced some to lay off employees or worst, bankrupt. Oliver Wyman, an American management consulting firm reported that airlines in Asia has reduced their available seat miles by 23% in March 2020 (Team, 2021).

By June 2020, 10,500 aircrafts were grounded while 11,500 were active, with the average daily utilization down by 35% from 2019; led by Asia-Pacific airlines with almost 75% of the fleet flying, then Europe with two-thirds of the fleet flying, then North America with 50% (Kingsley-Jones, 2021a). Major airliner deliveries dopped from a typical 90-100 aircrafts a month to an average of less than 40 aircrafts in the first six months of 2020 (Kingsley-Jones, 2021b).

By March 2021, Airports Council International (ACI) World has released an assessment, which will examine the economic consequences of the COVID-19 pandemic, its influence on the worldwide airport sector, and the path to recovery. In

light of the unprecedented impact of the COVID-19 situation on airport traffic, ACI World has released the latest passenger traffic impact estimates. On 2021:

- The COVID-19 crisis impacted almost 1 billion travelers in 2020, compared to the expected baseline (pre-COVID-19 projection for 2020), resulting in a 64.6 percent drop in worldwide passenger traffic (see Table 1). In comparison to the 2019 level, the drop is 63.3 percent.

- Europe and the Middle East were the two regions hardest hit, both experiencing 5% decreases in comparison to the predicted baseline.

- After being hit initially, Asia-Pacific recovered earlier and more rapidly than other areas — mostly due to China's enormous domestic market — and ended 2020 with a 61.3 percent decrease in GDP relative to the predicted baseline (59.8 percent decline compared to 2019). Asia-Pacific, on the other hand, saw the greatest traffic loss of any area, losing 2.15 billion passengers in 2020 relative to the predicted baseline.

- Latin America-Caribbean experienced the least impact of any area, down by 61.1 percent from the expected baseline (-59.8 percent compared to 2019 level).

- International passenger movement was almost non-existent in the second half of 2020 following the "Great Lockdown" in April 2020. International passenger volume ended the year below 1 billion, a decline of more than 75% from 2019.

- The early recovery of large domestic markets such as China, Russia, and the United States aided domestic passenger traffic volume. Globally, domestic traffic volume was slightly more than 2.4 billion passengers in 2020, a fall of 54.7 percent from the number in 2019.

While projections for 2021:

- By end of 2021, the COVID-19 crisis is expected to have displaced an extra 4.7 billion passengers relative to the predicted baseline (pre-COVID-19 prediction for 2021), indicating a 47.5 percent reduction in global passenger

traffic. By year end, the reduction is expected to be -43.6 percent when compared to the 2019 level. The first quarter of 2021 is predicted to exhibit modest improvement over the fourth quarter of 2020. As vaccination coverage and uptake grow, more passengers are predicted to return to travel, with the greatest rise occurring in 2021's Q3 and Q4 quarters.

- Similar to 2020, Europe and the Middle East are expected to remain the two most impacted regions, with declines of 1% and 58.9 percent, respectively, relative to the projected baseline, due to their high reliance on international travel and connectivity, which are recovering more slowly than domestic travel.

- North America's prediction for 2021 is likely to dramatically improve, with the area ending the year at -43.5 percent below the anticipated baseline.

- Foreign passenger traffic is projected to remain low in the first half of 2021, but early indications consider the increase of air travel demand in the second half of 2021 as more people get vaccinated and international travel restrictions are gradually removed.

- Domestic passenger travel began its comeback earlier than international passenger traffic. Domestic traffic will continue to grow globally in 2021, reaching near to 5 billion passengers by the end of the year, or 65.6 percent of the level in 2019.

Table 1: The impact of the COVID-19 crisis on quarterly passenger traffic by region (2020–2021, rounded in million passengers)

Region	2020 Q1	Q2	Q3	Q4	TOTAL	2021 Q1	Q2	Q3	Q4	TOTAL
	Projected baseline (pre-COVID-19)*					Projected baseline (pre-COVID-19)*				
Africa	56	58	68	62	244	60	63	74	67	263
Asia-Pacific	860	858	893	894	3,505	899	897	932	932	3,660
Europe	495	663	779	565	2,502	508	680	798	579	2,565
Latin America-Caribbean	178	169	182	180	708	184	176	189	188	737
Middle East	105	105	117	104	431	110	111	123	109	453
North America	477	542	553	518	2,089	491	558	569	534	2,152
World	**2,170**	**2,395**	**2,592**	**2,323**	**9,480**	**2,253**	**2,484**	**2,684**	**2,409**	**9,830**
	Estimated under COVID-19**					Estimated under COVID-19**				
Africa	46	1.5	11	21	79	26	27	32	31	116
Asia-Pacific	545	152	304	355	1,356	437	459	568	722	2,186
Europe	381	25	213	119	739	110	209	453	303	1,075
Latin America-Caribbean	152	10	37	77	275	77	85	102	113	377
Middle East	81	3.7	16	26	127	31	37	58	60	186
North America	386	59	155	182	783	207	255	365	389	1,216
World	**1,592**	**251**	**737**	**779**	**3,359**	**888**	**1,073**	**1,578**	**1,619**	**5,157**
	Estimated traffic loss					Estimated traffic loss				
Africa	-10	-56	-57	-41	-165	-34	-35	-42	-36	-147
Asia-Pacific	-315	-706	-588	-539	-2,148	-462	-438	-363	-211	-1,474
Europe	-114	-638	-566	-445	-1,764	-398	-471	-345	-276	-1,490
Latin America-Caribbean	-25	-159	-145	-104	-433	-107	-91	-87	-75	-360
Middle East	-23	-102	-101	-78	-304	-79	-74	-65	-49	-267
North America	-90	-483	-397	-336	-1,307	-284	-303	-204	-144	-936
World	**-578**	**-2,145**	**-1,855**	**-1,543**	**-6,121**	**-1,364**	**-1,412**	**-1,106**	**-790**	**-4,673**
	Estimated traffic loss (%)					Estimated traffic loss (%)				
Africa	-17.2%	-97.4%	-83.9%	-66.8%	-67.6%	-56.9%	-56.3%	-56.7%	-53.4%	-55.8%
Asia-Pacific	-36.6%	-82.3%	-65.9%	-60.3%	-61.3%	-51.4%	-48.8%	-39.0%	-22.6%	-40.3%
Europe	-23.0%	-96.2%	-72.7%	-78.8%	-70.5%	-78.3%	-69.3%	-43.3%	-47.6%	-58.1%
Latin America-Caribbean	-14.3%	-94.2%	-79.8%	-57.6%	-61.1%	-58.1%	-51.8%	-46.0%	-39.7%	-48.8%
Middle East	-22.4%	-96.5%	-86.1%	-75.0%	-70.5%	-71.8%	-66.4%	-52.9%	-44.9%	-58.9%
North America	-19.0%	-89.1%	-71.9%	-64.9%	-62.5%	-57.9%	-54.3%	-35.9%	-27.1%	-43.5%
World	**-26.6%**	**-89.5%**	**-71.6%**	**-66.5%**	**-64.6%**	**-60.6%**	**-56.8%**	**-41.2%**	**-32.8%**	**-47.5%**

*Projected baseline (pre-COVID-19) scenario based on adjusted World Airport Traffic Forecasts (WATF) 2020–2040 considering latest insights provided by ACI Regional offices and other inputs

**Estimated passenger traffic volumes based on a broad range of inputs provided by ACI Regional offices and industry experts

Source: ACI World

FIGURE 2.1: The impact of the COVID-19 crisis on quarterly passenger traffic by region (2020-2021, rounded in million passengers)

Table 2: The impact of the COVID-19 crisis on quarterly passenger traffic by region (2020–2021, rounded in million passengers, percentage of change compared to 2019)

Region	Q1	Q2	Q3	Q4	TOTAL	Q1	Q2	Q3	Q4	TOTAL
	2019					2019				
Africa	52	55	64	58	229	-	-	-	-	-
Asia-Pacific	836	822	858	854	3,370	-	-	-	-	-
Europe	478	652	755	552	2,437	-	-	-	-	-
Latin America-Caribbean	172	163	175	174	684	-	-	-	-	-
Middle East	97	100	111	99	406	-	-	-	-	-
North America	461	527	534	503	2,025	-	-	-	-	-
World	**2,095**	**2,318**	**2,498**	**2,240**	**9,151**	-	-	-	-	-
	Estimated under COVID-19**					**Compared to 2019 (%)**				
	2020					2020				
Africa	46	1.5	11	21	79	88.6%	2.7%	17.1%	35.5%	34.6%
Asia-Pacific	545	152	304	355	1,356	65.3%	18.4%	35.5%	41.5%	40.2%
Europe	381	25	213	119	739	79.7%	3.8%	28.2%	21.7%	30.3%
Latin America-Caribbean	152	10	37	77	275	88.7%	6.0%	21.0%	43.9%	40.2%
Middle East	81	3.7	16	26	127	83.5%	3.7%	14.6%	26.3%	31.2%
North America	386	59	155	182	783	83.8%	11.3%	29.1%	36.1%	38.7%
World	**1,592**	**251**	**737**	**779**	**3,359**	**76.0%**	**10.8%**	**29.5%**	**34.8%**	**36.7%**
	2021					2021				
Africa	26	27	32	31	116	49.8%	50.2%	49.8%	53.9%	50.9%
Asia-Pacific	437	459	568	722	2,186	52.3%	55.8%	66.3%	84.5%	64.9%
Europe	110	209	453	303	1,075	23.0%	32.0%	60.0%	55.0%	44.1%
Latin America-Caribbean	77	85	102	113	377	45.0%	51.9%	58.2%	64.9%	55.1%
Middle East	31	37	58	60	186	31.9%	37.4%	51.9%	61.1%	45.8%
North America	207	255	365	389	1,216	44.9%	48.5%	68.3%	77.3%	60.1%
World	**888**	**1,073**	**1,578**	**1,619**	**5,157**	**42.4%**	**46.3%**	**63.2%**	**72.3%**	**56.4%**

*Projected baseline (pre-COVID-19) scenario based on adjusted World Airport Traffic Forecasts (WATF) 2020–2040 considering latest insights provided by ACI Regional offices and other inputs
**Estimated passenger traffic volumes based on a broad range of inputs provided by ACI Regional offices and industry experts
Source: ACI World

FIGURE 2.2: The impact of the COVID-19 crisis on quarterly passenger traffic by region (2020-2021, rounded in million passengers, percentage of change compared to 2019)

Chart 1: Projected global quarterly passenger losses due to the COVID-19 crisis (2019/2020/2021, in billion passengers)

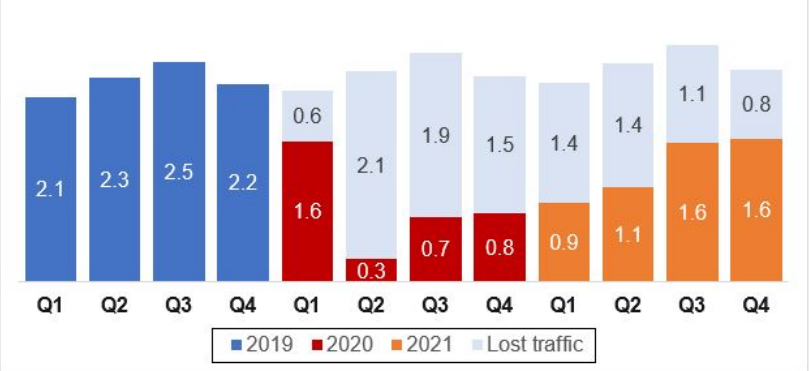

Source: ACI World

FIGURE 2.3: Projected global quarterly passenger losses due to the COVID-19 crisis (2019/2020/2021, in billion passengers)

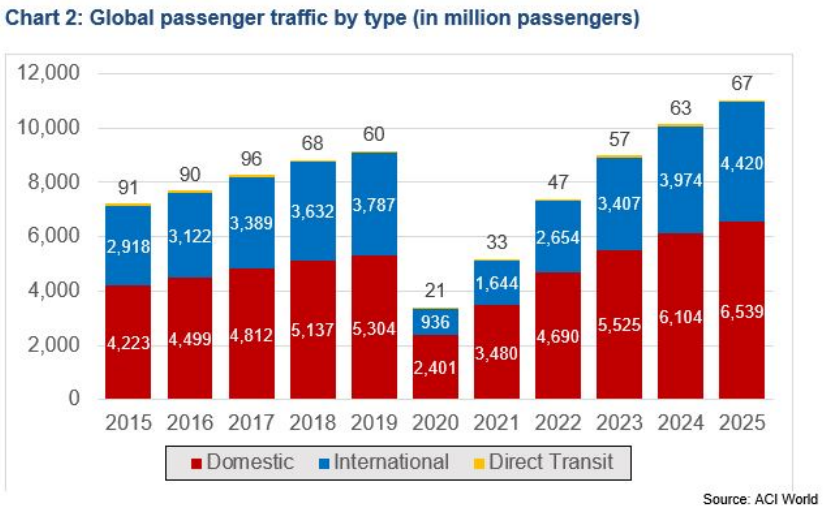

FIGURE 2.4: Global passenger traffic by type (in million passengers)

ACI World forecasts the following related to COVID-19 catastrophic impact on airport revenues. On 2021:

- Prior to the COVID-19 outbreak, the airport industry was predicted to generate approximately $188 billion in 2020. The COVID-19 issue had an unprecedented impact on airport revenues, lowering them by close to 125 billion USD in 2020 compared to the predicted baseline (pre-COVID-19 income prediction), a loss of 66.3 percent.

- The second quarter of 2020 alone contributed to a revenue decline of over $43.5 billion, or more than 1%, compared to the predicted baseline.

- As with passenger transportation, Europe and the Middle East were hardest hit. In absolute terms, Europe's revenue gap for 2020 is anticipated to be $4 billion. Europe and the Middle East reported a 70.5 percent decline in income for 2020 when compared to the predicted baseline.

Projections for 2021:

- The COVID-19 situation will continue to have a significant influence on airport revenues in 2021. Globally, airports are expected to lose more than 94 billion USD in income by 2021, effectively halving airport income forecasts

(-50.0 percent) compared to the forecast baseline (-48.1 percent compared to 2019 level).

- Each quarter of 2021 is forecast to improve on the previous one, progressing from a reduction of 7% in the first quarter to a decline of 35.2 percent in the fourth quarter relative to the predicted baseline.

- Europe will continue to be the most impacted region in absolute terms, with a revenue loss of more than 4 billion USD predicted by year end 2021. In proportional terms, the Middle East and Europe will take the heaviest impact, losing 58.9 percent and 58.1 percent of their population, respectively. Asia-Pacific will experience the fastest recovery, recovering to 59.7% of the anticipated baseline.

Table 3: Impact of the COVID-19 crisis on quarterly revenues* by region (2020–2021) (rounded in million USD)

Region	2020 Q1	2020 Q2	2020 Q3	2020 Q4	2020 TOTAL	2021 Q1	2021 Q2	2021 Q3	2021 Q4	2021 TOTAL
	Projected baseline (pre-COVID-19)*					Projected baseline (pre-COVID-19)*				
Africa	900	938	1,108	1,003	3,950	971	1,012	1,196	1,083	4,263
Asia-Pacific	14,501	14,457	15,043	15,058	59,060	15,157	15,113	15,699	15,714	61,684
Europe	12,456	16,684	19,604	14,209	62,953	12,774	17,101	20,087	14,569	64,530
Latin America-Caribbean	2,906	2,785	2,972	2,953	11,596	3,020	2,883	3,086	3,071	12,060
Middle East	3,707	3,731	4,145	3,677	15,260	3,902	3,926	4,341	3,872	16,041
North America	8,073	9,185	9,383	8,777	35,398	8,314	7,226	7,367	6,906	29,813
World	**42,542**	**47,760**	**52,235**	**45,679**	**188,217**	**44,138**	**47,262**	**51,775**	**45,216**	**188,390**
	Estimated under COVID-19**					Estimated under COVID-19**				
Africa	745	24	178	333	1,280	419	443	518	505	1,885
Asia-Pacific	9,190	2,555	5,129	5,980	22,855	7,369	7,738	9,580	12,159	36,847
Europe	9,590	627	5,361	3,006	18,584	2,767	5,248	11,397	7,632	27,044
Latin America-Caribbean	2,492	161	601	1,253	4,506	1,265	1,388	1,666	1,851	6,170
Middle East	2,875	130	574	919	4,498	1,099	1,319	2,045	2,133	6,597
North America	6,542	767	2,010	2,354	11,674	2,676	3,306	4,722	5,037	15,741
World	**31,434**	**4,264**	**13,854**	**13,844**	**63,397**	**15,595**	**19,442**	**29,929**	**29,318**	**94,284**
	Estimated revenue loss					Estimated revenue loss				
Africa	-155	-914	-930	-671	-2,670	-553	-569	-678	-578	-2,378
Asia-Pacific	-5,311	-11,903	-9,914	-9,078	-36,206	-7,787	-7,376	-6,119	-3,555	-24,837
Europe	-2,866	-16,057	-14,242	-11,203	-44,368	-10,008	-11,853	-8,689	-6,936	-37,486
Latin America-Caribbean	-414	-2,605	-2,371	-1,701	-7,090	-1,755	-1,495	-1,420	-1,220	-5,889
Middle East	-832	-3,601	-3,571	-2,758	-10,762	-2,803	-2,607	-2,295	-1,739	-9,444
North America	-1,531	-8,417	-7,352	-6,424	-23,723	-5,638	-3,921	-2,644	-1,869	-14,071
World	**-11,108**	**-43,496**	**-38,381**	**-31,834**	**-124,820**	**-28,543**	**-27,820**	**-21,846**	**-15,898**	**-94,106**
	Estimated revenue loss (%)					Estimated revenue loss (%)				
Africa	-17.2%	-97.4%	-83.9%	-66.8%	-67.6%	-56.9%	-56.3%	-56.7%	-53.4%	-55.8%
Asia-Pacific	-36.6%	-82.3%	-65.9%	-60.3%	-61.3%	-51.4%	-48.8%	-39.0%	-22.6%	-40.3%
Europe	-23.0%	-96.2%	-72.7%	-78.8%	-70.5%	-78.3%	-69.3%	-43.3%	-47.6%	-58.1%
Latin America-Caribbean	-14.3%	-94.2%	-79.8%	-57.6%	-61.1%	-58.1%	-51.8%	-46.0%	-39.7%	-48.8%
Middle East	-22.4%	-96.5%	-86.1%	-75.0%	-70.5%	-71.8%	-66.4%	-52.9%	-44.9%	-58.9%
North America	-19.0%	-91.6%	-78.5%	-73.2%	-67.0%	-67.8%	-54.3%	-35.9%	-27.1%	-47.2%
World	**-26.1%**	**-91.1%**	**-73.5%**	**-69.7%**	**-66.3%**	**-64.7%**	**-58.9%**	**-42.2%**	**-35.2%**	**-50.0%**

* Revenues estimated assuming constant airport revenues on a per-passenger basis and based on KPIs from the ACI 2021 Economic Report as well as input from ACI Regional offices. Financial figures are rounded for ease of reading. Percentage of change use exact figures.
** Projected baseline (pre-COVID-19) scenario based on adjusted World Airport Traffic Forecasts (WATF) 2020–2040 considering latest insights provided by ACI Regional offices and other inputs.
*** Estimated passenger traffic volumes based on a broad range of inputs provided by ACI Regional offices and industry experts
Source: ACI World

FIGURE 2.5: Impact of the COVID-19 crisis on quarterly revenues by region in (2020-2021, rounded in million USD)

Table 4: Impact of the COVID-19 crisis on quarterly revenues* by region (2020–2021) (rounded in million USD, percentage of change compared to 2019)

Region	Q1	Q2	Q3	Q4	TOTAL	Q1	Q2	Q3	Q4	TOTAL
	2019					2019				
Africa	843	879	1,038	940	3,700	-	-	-	-	-
Asia-Pacific	13,946	13,904	14,468	14,482	56,800	-	-	-	-	-
Europe	12,129	16,246	19,089	13,836	61,300	-	-	-	-	-
Latin America-Caribbean	2,807	2,671	2,870	2,852	11,200	-	-	-	-	-
Middle East	3,498	3,521	3,912	3,470	14,400	-	-	-	-	-
North America	7,823	8,900	9,072	8,505	34,300	-	-	-	-	-
World	**41,045**	**46,120**	**50,449**	**44,086**	**181,700**	-	-	-	-	-
	Estimated under COVID-19**					**Compared to 2019 (%)**				
	2020					2020				
Africa	745	24	178	333	1,280	88.4%	2.8%	17.1%	35.4%	34.6%
Asia-Pacific	9,190	2,555	5,129	5,980	22,855	65.9%	18.4%	35.5%	41.3%	40.2%
Europe	9,590	627	5,361	3,006	18,584	79.1%	3.9%	28.1%	21.7%	30.3%
Latin America-Caribbean	2,492	161	601	1,253	4,506	88.8%	6.0%	20.9%	43.9%	40.2%
Middle East	2,875	130	574	919	4,498	82.2%	3.7%	14.7%	26.5%	31.2%
North America	6,542	767	2,010	2,354	11,674	83.6%	8.6%	22.2%	27.7%	34.0%
World	**31,434**	**4,264**	**13,854**	**13,844**	**63,397**	**76.6%**	**9.2%**	**27.5%**	**31.4%**	**34.9%**
	2021					2021				
Africa	419	443	518	505	1,885	49.7%	50.4%	49.9%	53.7%	50.9%
Asia-Pacific	7,369	7,738	9,580	12,159	36,847	52.8%	55.7%	66.2%	84.0%	64.9%
Europe	2,767	5,248	11,397	7,632	27,044	22.8%	32.3%	59.7%	55.2%	44.1%
Latin America-Caribbean	1,265	1,388	1,866	1,851	6,170	45.1%	52.0%	68.0%	64.9%	55.1%
Middle East	1,099	1,319	2,045	2,133	6,597	31.4%	37.5%	52.3%	61.5%	45.8%
North America	2,676	3,306	4,722	5,037	15,741	34.2%	37.1%	52.1%	59.2%	45.9%
World	15,595	19,442	29,929	29,318	94,284	38.0%	42.2%	59.3%	66.5%	51.9%

* Revenues estimated assuming constant airport revenues on a per-passenger basis and based on KPIs from the ACI 2021 Economic Report as well as input from ACI Regional offices. Financial figures are rounded for ease of reading. Percentage of change use exact figures.
** Projected baseline (pre-COVID-19) scenario based on adjusted World Airport Traffic Forecasts (WATF) 2020–2040 considering latest insights provided by ACI Regional offices and other inputs.
*** Estimated passenger traffic volumes based on a broad range of inputs provided by ACI Regional offices and industry experts.
Source: ACI World

FIGURE 2.6: Impact of the COVID-19 crisis on quarterly revenues by region (2020-2021, rounded in million USD, percentage of change compared to 2019)

Numerous industry analysts predict an increase in travel in the second half of 2021. However, much uncertainty surrounds the aviation industry's recovery, and estimating the route to recovery at this stage requires caution. Three scenarios with the following assumptions are utilized to examine the potential recovery trajectory. The following three scenarios are predicated on the following assumptions.

1. WATF 2020–2040: Developed in December 2020 and published in January 2021, the WATF 2020–2040 was predicated on effective vaccines being widely distributed in the second half of 2021, as well as passenger eagerness to resume flying and a respectable airline fleet recovery. This scenario is still possible, but it is dependant on governments' capacity to restrict the spread of new viral varieties.

2. Revised Projection (Baseline): Effective vaccines are widely delivered in the second half of 2021, complemented by passenger eagerness to resume flying in the second half of 2021 and a decent airline fleet recovery. Third and fourth

waves of infection are probable, but they will be contained quickly and will affect only a few places.

3. Pessimistic: Effective vaccinations in 2021, but complicated distribution in a large number of emerging and developing economies, as well as restricted vaccine availability. Passengers continue to express fear of travel, exacerbated by a prolonged economic crisis and a delayed recovery of the airline fleet. Third and fourth waves of infection are probable, with the potential for widespread dissemination over numerous regions.

ACI World forecasted the following for the recovery of airport passenger traffic based on the assumptions:

- Global passenger traffic is now predicted to recover to 2019 levels by 2024, primarily due to domestic passenger traffic recovery, but slightly hampered by a slower international travel recovery (globally, domestic traffic accounts for 58 percent of total passenger traffic as of 2019).
- If new virus types are adequately suppressed, the WATF 2020–2040 scenario remains the most likely, with a rebound to 2019 levels by the end of 2023.
- In the second half of 2023, domestic passenger traffic is predicted to reach 2019 levels. International passenger traffic will take an additional year to recover, with volumes reaching 2019 levels only in 2024.
- At the country-market level, markets with a high proportion of domestic traffic are predicted to recover to pre-COVID-19 levels in 2023, whereas markets with a high proportion of foreign traffic are unlikely to reach 2019 levels until 2024 or even 2025 in some circumstances.
- The pessimistic scenario envisions a delayed recovery due to the new virus varieties, which results in governments enacting more restrictive measures, including new lockdowns and travel bans, significantly impeding efforts to securely restart. Under this scenario, passenger volume in 2021 will remain low, reaching just 46.5 percent of the level in 2019.
- In the long term, it is estimated that it will take up to two decades for global traffic to return to previously forecasted levels (pre-COVID-19 forecast). A

structural change is still a possible (traffic will never revert to its pre-COVID-19 predicted level).

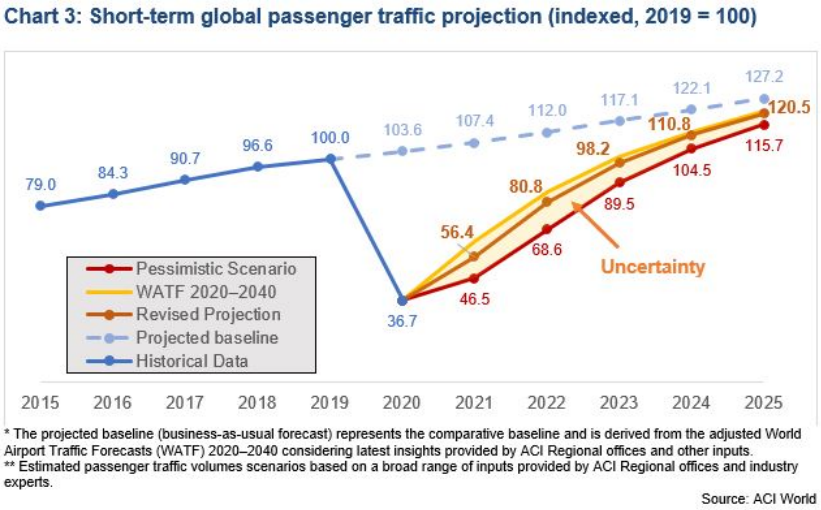

FIGURE 2.7: Short-term global passenger traffic projection (indexed, 2019 = 100)

As traffic might not return to pre-pandemic levels until 2024, aircraft's retirement is accelerating. Older, less fuel-efficient, and higher maintenance aircrafts including the Boeing 777, Airbus A380 and A3300, are replaced with newer Airbus A350 and Boeing 787s, as a surplus of used aircraft is expected until 2030 (Cirium, 2021).

While passenger flights were cancelled, the cost of sending cargo by air changed rapidly, especially across the Pacific Ocean where it is tripled by late March 2020 (Morrison, 2021). On the other hand, business aviation is less affected during the pandemic. Once lockdown restrictions are eased, it has a great opportunity to capture premium passengers who previously have chosen airlines, but prefer the social distancing offered by a private jet (Schonland, 2021).

2.3 Private Jet

A private jet, business jet, or for short, bizjet, is a jet aircraft that is designed to transport small numbers of passengers. Business jets can be used for other

roles as they can serve multipurpose, such as express cargo deliveries, medical evacuation missions equipped with mission-essential equipment such as stretchers, and some are also used by government officials, armed forces, and public bodies, which commonly equipped with meeting rooms.

2.3.1 Private Jet Industry during Pandemic

Although the Covid-19 pandemic has had a great impact on the commercial airline industry, the trends in the business jet industry actually present comparatively positive effects. The Covid-19 has shifted the trend in aviation. A business flight is no longer exclusive only for those who are in the upper class, it has now become an option for middle-class people. Private aviation, while always seems luxurious, now also truly means travelling safely, especially for those who are vulnerable to Covid-10 (Christian, 2021).

A study by McKinsey and Company presents that passengers of business jets are getting their money's worth. On commercial flights, with check-in or security procedures and boarding, passengers come into contact with other travellers and objects an average of 700 times, while on private flights the number of touchpoints is only about 20. Not to mention the roomy seating, flexible departure times, direct flight, total waiting time, privacy and access to 10 times more airports than commercial flights, and the appeal of flying privately is very obvious (GlobeAir, 2021).

Data provided by FlightAware presents the total number of flights of all types dropped sharply in March 2020. By April 2020, all global flights fell to a fifth of their 2019 volume, and business flights to 36%. They have since recovered on a small scale but still stand at around half the numbers in 2019. Business flights, nonetheless, since July 2020 have been operating at between 85% and 90% of their 2019 volume. FlightAware counts "business flights" as any which are not classified as commercial or cargo services.

According to WingX's weekly private jet tracking report, the United States private jet market has been dominated by large aircraft in March 2021. According to Richard Koe, managing director of WingX, branded charter operations in the United States are up 16%, indicating that they are currently experiencing record levels of activity. The largest rebound in March 2020 is in super-midsize and

midsize private airplanes. Flying in has increased by 20% in March 2021. The very light jet industry is rising 31% year on year.

Florida remains busy, with flight activity in March 2021, 19 percent greater than the March 2020 record, which was already greater than any March 2019 day. The primary driver has been charter demand, with March 2021's trend reaching 360 daily sectors. This compares to a March 2020 top of 304 segments and a March 2019 top of 246 daily sectors. Miami-Opa Locka Airport's growth has been robust by March 2021. Departures are up 50% year over year.

It is said that in the United States, there are indications that business jet activity in 2021 will exceed that of 2019, particularly in the charter market. In general, North America continues to be the motor of worldwide private aviation activity revival. On March 17th, 2021, there were 6,437 sectors, up from 6,326 on the same day in March 2020 and 6,815 in March 2019. Private flights have increased by 17% year to date. The most significant recoveries have occurred in Part 91k fractional operations, which are up 21% from last year's lows. Traffic on Part 91 individual owners and corporate flight departments is 15% higher than it was in March 2020 (Gollan, 2021).

According to research from AMSTAT, from 252 large, long-range jets that are currently for sale, the aircraft that is less than five years old is only 20. This is less than half of what is typically accessible, compared to approximately 17% during the financial crisis.

According to research from AMSTAT, a company that provides data on business aircraft in the US, "of 252 large, long-range jets currently for sale, just 20 of these are less than five years old". With so few jets available in the US, potential buyers have to look to Asia for possible jets.

The U.S. accounts for more than 70% of the global pre-owned jet market, with sales in the second-largest market, Europe, also climbing year-over-year in 2020. Globally, 2,227 preowned business jets were purchased in 2020, which means there is a 7.7% increase compared to 2019, which represents a total value of more than $14.5 billion (Denton, 2021).

In Europe, there was a drop in flights as the covid-19 hit in the beginning of 2020, with the average daily of European flights in the business aviation industry, including owned and rented business jets going down to 521 in April 2020. However,

in August 2020, there was a comeback to an average of 2,133 flights every day across Europe and business jet usage was at near-pre-COVID levels into April 2021, Flight routes between France, United Kingdom, Switzerland, and Italy account for most of the carbon pollution, as business jets departing from France and the United Kingdom accounting for more than a third of all business flight emissions in Europe (Euronews, 2021).

In Russia, demand for private aircraft has rocketed, with the number of trips up 32 percent from pre-pandemic levels by June 2021. While Russian commercial flights are mostly absent from European holiday destinations, with only a few flights going to the U.K. and Greece, private jet traffic does not fall under Russian and EU aviation legislation, allowing those Russians with EU residence permits or second passports to fly to otherwise closed countries. Yevgeny Bikov, from private travel business Your Charter, said there is a 50 percent rise in requests to fly privately compared with pre-pandemic 2019, largely to Western Europe (T. M. Times, 2021).

In Asia, Air Charter Services, a business jet broker with 28 global offices, reported a 150% spike in bookings when the pandemic began. Indojet Sarana Aviasi, a business jet broker based in Jakarta, Indonesia, mentioned that the business doubled in the second half of 2020 compared to the same period in 2019, although the cost of business jets is higher in Indonesia than in the U.S. and Europe (Neubauer, 2021).

Some of the private jet trends that are expected in 2021 (33, 2021):

1. **Better Sanitation Efforts**: Due to the growing concern among flyers about sanitation and the desire of private aviation firms to keep their customers safe, companies in the private jet charter business have increased their focus on cleanliness. By their very nature, private planes are significantly easier to keep clean, as there are fewer people to account for and ample room to maintain social distance while on board. Apart from social distancing, private jet charter companies are anticipated to emphasize higher cleanliness standards on private aircraft, private terminals, and FBO (fixed-base operator) facilities in order to attract consumers seeking sterile settings. Another significant private jet trend that many anticipate is an increase in COVID-19 testing for crews and workers, particularly those who have not been vaccinated. Additionally, several temperature checks each day will likely remain

a popular preventative practice, as these checks can identify crew members or staff members with fevers, allowing them to return home before spreading an illness.

2. **Increased Number of First-Time Flyers**: COVID-19 creates an opportunity for private aircraft, as consumers seek safer modes of transportation. Due to the need for a safer flying experience, the market is predicted to grow in size, with an increase in first-time private jet passengers. While some passengers may have previously shunned private travel due to the cost, the greater cleanliness and ease of social isolation may convince these potential clients that jet charters are well worth the money. Given the possibility of attracting fliers who are not accustomed to flying private, the private jet charter business will almost certainly see increased marketing efforts directed at these potential consumers. This new consumer base is likely to come from those who travel first- or business class on a regular basis. While past marketing efforts concentrated exclusively on the opulent experience and speedier flight, operators now have the option to appeal to potential fliers by emphasizing private aircraft' greater safety and hygiene. Along with safety, the private jet sector can improve the security of its facilities and boarding procedures. Rather than standing in lines, many travelers can drive directly up to a private plane and board without coming into contact with other passengers. Additionally, fliers can wait at private facilities where personnel and other fliers are kept to a minimum.

3. **Utilization of Digital Technology**: Corporate aviation has been integrating modern digital technology into their facilities and private aircraft for some time now in order to enhance the flyer experience. For instance, digital technology such as in-flight Wi-Fi is highly popular because it enables passengers to work or unwind while flying. With the adoption of COVID-19, additional digitalization is projected to minimize the number of touchpoints and improve passenger convenience at critical phases such as booking a charter flight, checking in, paying, boarding, and disembarking.

4. **A**dditional Routes to Avoid Connecting Flights Connecting flights increase the chance of getting COVID-19, as passengers are more likely to come into

touch with other people while moving to another aircraft. These risks associated with connecting flights are particularly concerning for commercial travelers, as their exposure to other people would grow considerably as they travel through airports. Private operators have considerable freedom in terms of connecting flight reductions. While commercial flights frequently require connecting flights to accommodate thousands of people, private aircraft can fly into smaller, more rural airports that commercial airlines are unable to access. This enables private aircraft to fly direct routes to the passenger's preferred destination.

5. **Eco-Friendly Aviation Fuels**: Many passengers are getting increasingly interested in airplanes that run on sustainable aviation fuels as a result of COVID-19 (SAFs). Due to the rising demand for socially responsible activities such as wearing a mask and remaining socially distant, many people's priorities have moved to include a stronger sense of social responsibility in other areas of their lives as well. According to a recent GobalData survey, 43% of respondents say that the ethical, environmental, and social responsibilities of a service or product impact their purchasing decisions. Private aircraft operators who employ SAFs can leverage these increased consumer demands for ethical and environmentally responsible products and services.

6. **Increasing the number of private jet owners**: The private aviation market may see an influx of new private jet owners seeking to travel on their own terms for business or pleasure. Small aircraft and private jet sellers may see an increase in sales as buyers seek increased safety and convenience in their flying experience. Additionally, many FBOs anticipate increased demand for their facilities and services from private jet owners. Increased demand for aircraft maintenance, hangaring, refuelling, tie-downs, and other related services may occur in 2021.

7. **Younger Passengers and Pets**: While business aviation has slowed in recent years as a result of the increased emphasis on remote meetings, leisure travel has rebounded more quickly. In 2021, families with children and pets are projected to fly charter more frequently. As a result of these expectations, private jet operators are likely to expand their pet and child accommodations.

To attract families traveling with little children, operators may equip their aircraft with booster seats and sleeping rooms large enough for a youngster to snooze peacefully. Additionally, private aircraft might invest in on-board entertainment systems specifically developed for children to keep them entertained throughout a lengthy journey.

8. **Minimizing Costs**: Due to decreased demand for trips, private jet operators have reduced their pricing and given special incentives to entice new passengers. Given the addition of a new client base comprised of those accustomed to flying first class on commercial airplanes, these passengers are likely looking for the most cost-effective but safe and secure flight conceivable. Of course, private jet owners must still contend with a variety of fees associated with the operating of their aircraft, insurance, fuel, and a limited supply of skilled pilots. Jet owners will need to acquire parts and maintenance services at a lower cost in order to remain viable and offer more inexpensive fares to clients. As a result, the market is likely to see aircraft owners looking for cost-effective suppliers that provide high-quality products and services. FBOs may potentially play a greater role in securing cheaper flights for their clients, collaborating with brokers to present more tempting proposals to potential flyers.

2.3.2 Configuration

Straight wings are commonplace although swept wings are also often used to increase cruise speed.

2.3.3 Fleet

The business jet industry was dominated by Textron Aviation that owns Beechcraft, Cessna, and Hawker aircrafts with 43.9%, Bombardier by 22.4%, Gulfstream with 13Mostly the fleet was in North America with 64.6%, Europe by 13%, then South America by 12.1%, and followed by Asia-Pacific with 5.9%. By March 31, 2019, there are 22,125 business jets around the world and the top 20 country markets account for 89% of this total fleet.

2.3.4 Class

Business jets or private jets can be categorized as:

1. Very Light Jets: Business Jets with Maximum Takeoff Weight is lighter than 12,500 pounds limit, and are approved for single pilot operation. Generally transport 6-7 passengers over a 1174 nmi average range. Cirrus SF50 G2, Phenom 100EV, Citation M2, and Honda Jet Elite.

2. Light Jets: Normally it transports 6-8 passengers over a 1953 nmi average range. (Beechcraft Premier, Cessna Citation Jet).

3. Mid-size Jets: These jets are usually used for longer-range flights such as transcontinental flights with larger passenger capacity. Generally, it accommodates 9 passengers over a 2450 nmi average range.

4. Super Mid-size Jets: TThese jets feature transatlantic capability and long-range. It accommodates 10-11 passengers over a 3420 nmi average range.

5. Large Jets: It accommodates 13-14 passengers over a 4001 nmi average range.

6. Long-range Jets: It can accommodate 12-19 passengers over a 6498 nmi average range.

7. VIP airliners: VIP airliners. Converted airliners into business jets are commonly used. Such aircraft can face operational restrictions based on runway length or local noise restrictions. It can be the most expensive type of business jet as it provides greater space and capabilities. Boeing, Embraer, and Airbus have these VIP airliners.

2.4 Aircraft Performance

Performance is a term that refers to an aircraft's ability to complete specific tasks that make it valuable for specific purposes. For instance, an aircraft's landing capability and the ability to take off in a very short distance is critical to the pilot who operates in and out of unimproved, short runways airports. The ability to

transport large loads and fly at high altitudes at high speeds and/or over long distances is necessary for an airliner and executive aircraft performance.

The primary factors that have the greatest impact on performance are the distance between takeoff and landing distance, rate of climb, ceiling, and payload, range, speed, maneuverability, stability, and fuel efficiency are all factors to consider. Several of these factors are frequently diametrically opposed: for instance, high speed at the expense of a short landing distance, and extended range at the expense of excellent payload and a strong rate of climb in relation to fuel economy.

The predominance of one or more of these criteria is what determines aircraft distinctions and discusses the high degree of specialization found in modern aircraft. The varied performance characteristics of an aircraft are the outcome of the interaction of the aircraft's and powerplant's characteristics. Aerodynamic characteristics of the aircraft generally describe the required power and thrust for various flight situations, whereas powerplant characteristics generally define the available power and thrust for various flight circumstances. The manufacturer matches the aerodynamic arrangement to the powertrain in order to achieve maximum performance under the specified design conditions (e.g., range, endurance, and climb).

There are mainly four types of forces that impacts an aircraft's performance, namely:

1. Lift L, which is perpendicular to the flight path direction.
2. Drag D, which is parallel to the flight path direction.
3. Thrust T, which in general is inclined at the angle α_T with respect to the flight path direction.
4. Weight W, which acts vertically toward the center of the earth (and hence is inclined at angle θ with respect to the lift direction)

2.4.1 Steady Straight Nonsideslipping Flight

Referring to this specific case, all the lateral variables are zero in value: $\beta = 0, C = 0, S = 0$. The aerodynamic angle of roll is also zero ($\mu = 0$). The force equation is

simplified into=

$$-D + T\cos\alpha_T - W\sin\gamma = 0 \tag{2.1}$$

$$-L - T\sin\alpha_T + W\cos\gamma = 0 \tag{2.2}$$

Additionally, there is a requirement when aerodynamic forces generate moments, it must be entirely balanced by proper settings of the control surfaces (in trimmed flight condition where $M_x = M_y = M_z = 0$). The aerodynamic elements of the aircraft will be affected by the utilization of the controls. Nevertheless, in consideration of particular flight types, it is assumed that the impact from control surface deflections to drag, lift, and side forces are adequately minimum in value in magnitude, that it can be ignored (Ruijgrok, 2012).

Furthermore, since the main concern is the translational motion of the aircraft, limitation to only the application of the force equations is needed. Based on the previously spoken conclusive statement which states that $\mu = 0$ determines that Y_a-axis lies in the horizontal plane thus the plane of symmetry of the aircraft occupy the same place in space or time with one and the same vertical plane. The motion identified in this case concerns the basic type of flight in performance analyses which is the steady symmetric flight.

2.4.2 Lift, Drag, and Moment Coefficients

The precise magnitudes of L, D and M is not only dependent on α, but also influenced by velocity and altitude factors. These are the following factors that are expected to generate variations of L, D and M.

1. Free-stream velocity V_∞
2. Free-stream density ρ_∞ (that is, altitude)
3. Size of the aerodynamic surface. For aircrafts, we will use the wing area S to indicate size.
4. Angle of attack α
5. Shape of the airfoil

6. Viscosity coefficient μ_∞ (because the aerodynamic forces are generated in part from skin friction distributions).

7. Compressibility of the airflow. Its effects are governed by the value of the free-stream Mach number $M = V_\infty/a_\infty$. Because V_∞ is already listed, we can designate a_∞ as our index for compressibility.

Therefore, for a given shape of airfoil at a given angle of attack:

$$L = f(V_\infty, \rho_\infty, S, \mu_\infty, a_\infty) \tag{2.3}$$

and D and M are similar functions.

2.4.3 Parabolic Lift-Drag Polar

There are two main forces that acts on the body surface, which are the aerodynamics forces and moments. These forces are exerted on a body moving through a fluid stem, namely:

1. The pressure distribution.

2. The shear stress distribution.

A plane's total drag can be categorized into the drag of the wing w and the amount of the components D_W:

$$D = D_W + D_n \tag{2.4}$$

As observed in figure 2.8 , the wing drag composes in accordance with the amount of the induced drag D as well as the profile drag D_p. Thus the equation is as follows:

$$D = D_i + D_p + D_n \tag{2.5}$$

The profile drag consists of:

1. Skin friction drag

2. Pressure drag

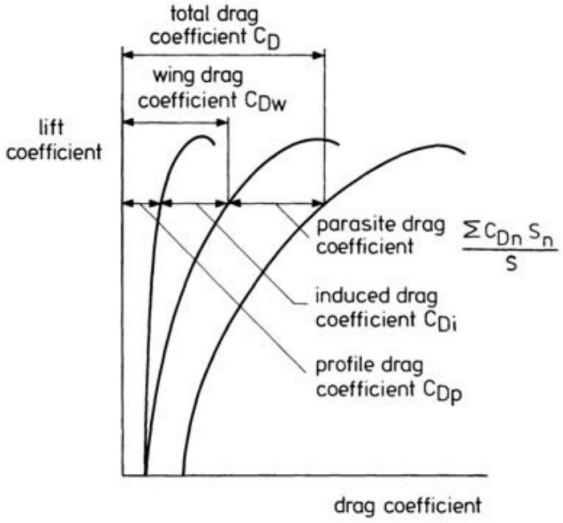

H

FIGURE 2.8: Elements of drag components.

3. Wave drag

The wave drag is zero for subsonic velocities below the critical Mach number. The drag force of the aircraft components is formed by skin contact drag, wave drag, and pressure drag. As drag coefficient for every component part C_{Dn}, is based on a certain area S_n as the reference area, the total aircraft drag equation is:

$$C_{D_i}\frac{1}{2}V^2\rho S = C_{D_p}\frac{1}{2}V^2\rho S + (\Sigma C_{D_n}S_n)\frac{1}{2}\rho V^2 \tag{2.6}$$

The total drag equation of the aircraft can be reduced by dismissing the common variables on both sides to form:

$$C_D = C_{D_i} + C_{D_p} + \frac{\Sigma C_{D_n}S_n}{S} \tag{2.7}$$

Due to the fact that the drag coefficient of each component part, C_{Dn} is referenced on a certain area Sn as the reference area, thus giving the total aircraft drag value. Streamlined features based on a hypothesis estimates that the induced drag coefficient is directly relative to the square of the lift coefficient C_L, and inversely relative to the angle proportion An and a wing effectiveness factor 0.

The factor 0 depends on the wing platform due to the fact that it demonstrates how close the elliptic spanwise lift conveyance is gathered. For an elliptic lift circulation 0=1 (least initiated drag coefficient). In any remaining cases, 0 will be short of what one. Hence, the drag coefficient of the plane would be:

$$C_D = \frac{C_L^2}{\pi AR\phi} + C_{D_p} + \frac{\Sigma C_{D_n} S_n}{S} \tag{2.8}$$

Additionally speaking, both the profile drag and parasite drag coefficients are dependent on the angle of attack, thus the equation can be formulated as follows:

$$C_D = \frac{C_L^2}{\pi AR\phi} + XC_L^2 + C_{D_p} + \left(\frac{\Sigma C_{D_n}}{S_n}\right)_{C_L=0} \tag{2.9}$$

The variables within the parenthesis can be calculated to find zero lift drag coefficient, also known as C_{D_0}. The variables XC_L^2 is the assumed parabolic change of the profile drag and the parasite drag due to its lift coefficient. Hence, the equation can be modified as:

$$C_D = C_{D_o} + \frac{C_L^2}{\pi ARe} \tag{2.10}$$

Where Oswald's proficiency factor stated as factor e, represents profile varieties and parasite drag coefficients with lift coefficient, and the impact of the actual spanwise lift distribution on the induced drag coefficient. For most aircraft types, the estimation of e differs somewhere in the range of 0.6 and 0.9 (Anderson, 2005).

$$\frac{1}{e} = X\pi AR + \frac{1}{\phi} \tag{2.11}$$

In some cases, the induced drag factor or the k factor which can be calculated as $\frac{1}{\pi ARe}$, can be used to simplify the equation in the previous segment as:

$$C_D = C_{D_0} + kC_L^2 \tag{2.12}$$

From 2.9, the deviation from the parabolic form is identified based on the difference from the straight (specked) line. We are able to observe an extensive piece of the lift-drag polar is undoubtedly a parabola, nevertheless, there are several additional drags at lift coefficients that past about 1.0.

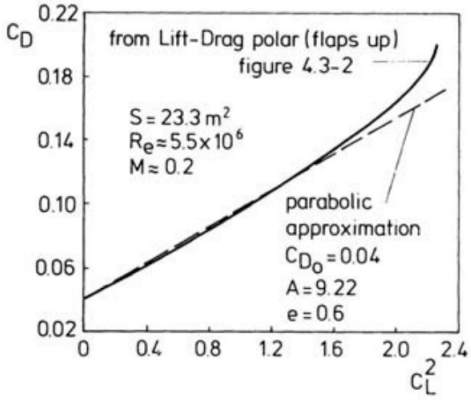

H

FIGURE 2.9: Parabolic lift-drag estimation of low-subsonic aircrafts.

The graphically portrayed lift-drag polar can be used at subsonic velocities. Moreover, in both transonic and supersonic velocities, the estimated C_{Do} and k are changed accordingly. It can be observed that in multiple cases, the aircraft is calculated based on the accompanying aerodynamic ratios: C_L/C_D, C_L^3/C_D^2 and C_L/C_D^2. These maximum values for the ratios are highly crucial. In regards to maximum C_L/C_D, the ratios can be divided based on C_L and set the main derivative equivalent to zero. To find the C_L/C_D maximum value, the final formula can be derived from:

$$\begin{aligned} \frac{d(C_L/C_D)}{dC_L} &= 0 \\ \frac{\frac{dC_D}{dC_L}C_D - C_L\frac{dC_D}{dC_L}}{C_D^2} &= 0 \\ C_D - C_L\frac{dC_D}{dC_L} &= 0 \\ C_D &= C_L\frac{dC_D}{dC_L} \\ \frac{dC_D}{dC_L} &= \frac{C_D}{C_L} \end{aligned} \tag{2.13}$$

Where

$$\begin{aligned} C_D &= C_{Do} + kC_L^2 \\ C_D &= C_{Do} + \frac{C_L^2}{\pi ARe} \\ \frac{dC_D}{dC_L} &= 0 + \frac{2C_L}{\pi ARe} \end{aligned} \tag{2.14}$$

By using the substitution method for 2.13 and 2.14, C_L value can be determined as follows:

$$\begin{aligned} \frac{C_D}{C_L} &= \frac{2C_L}{\pi ARe} \\ 2C_L^2 &= \pi ARe C_D \\ 2C_L^2 &= \pi ARe(C_Do + \frac{C_L^2}{\pi ARe}) \\ 2C_L^2 &= \pi ARe C_Do + C_L^2 \\ C_L^2 &= \pi ARe C_Do \\ C_L &= \sqrt{\pi ARe C_Do} \end{aligned} \tag{2.15}$$

By utilizing the insertion method in equation 2.15 into equation 2.11, C_D can be calculated as follows:

$$\begin{aligned} C_D &= C_{Do} + \frac{(\sqrt{\pi ARe C_Do})^2}{\pi ARe} \\ C_D &= C_{Do} + C_Do \\ C_D &= 2C_{Do} \end{aligned} \tag{2.16}$$

Using the substitution method based on equation 2.15 and 2.16, (C_L/C_Dmax) can be calculated as follows:

$$\begin{aligned} \left(\frac{C_L}{C_D}\right)_{\max} &= \frac{C_L}{C_D} \\ &= \frac{\sqrt{\pi ARe C_Do}}{2C_Do} \\ &= \frac{1}{2}\frac{piARe}{C_Do} \end{aligned} \tag{2.17}$$

Figure 2.10 and 2.11 illustrates the point where maximum C_L/C_D and the maximum lift drag polar ratio can be achieved. In order to find the maximum value of C_L^3, the value can be obtained by separating it in accordance with C_L and equating it to zero. The final formula can be derived from:

$$\frac{dC_D}{dC_L} = \frac{3C_D}{2C_L} \tag{2.18}$$

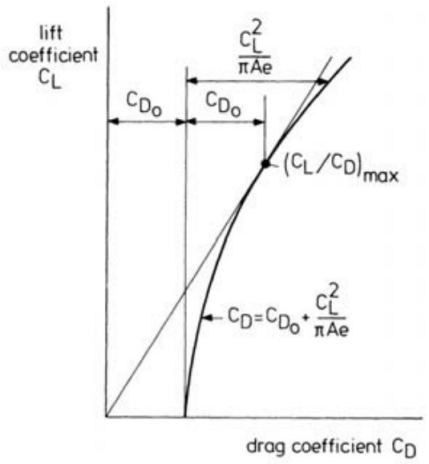

H

FIGURE 2.10: Maximum C_L/C_D value

Furthermore, differentiate the value of C_D in accordance to C_L to get

$$\frac{dC_D}{dC_L} = \frac{2C_L}{\pi ARe} \tag{2.19}$$

By utilizing the substitution method in equation 2.18 and2.19, C_L can be calculated as follows:

$$C_L = \sqrt{3C_{Do}\pi ARe} \tag{2.20}$$

By utilizing the substitution method in equation 2.20 and 2.11, C_D can be calculated as follows:

$$C_D = 4C_{Do} \tag{2.21}$$

By utilizing the substitution method in equation 2.20 and 2.21, C_L^3/C_D^2 can be calculated as follows:

$$\left(\frac{C_L^3}{C_D^2}\right)_{\max} = \frac{3\sqrt{3}}{16}\pi ARe\sqrt{\frac{\pi ARe}{C_{Do}}} \tag{2.22}$$

In order to find (C_L/C_D^2) max, it can be calculated by separating it in accordance to C_L and equating it to zero. Thus the final formula can be derived from:

$$\frac{dC_D}{dC_L} = \frac{C_D}{2C_L} \tag{2.23}$$

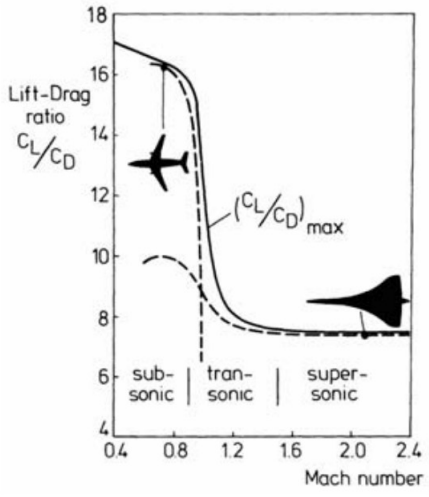

H

FIGURE 2.11: Maximum lift-drag ratio

Separate C_D in accordance to C_L to calculate:

$$\frac{dC_D}{dC_L} = \frac{2C_L}{\pi ARe} \tag{2.24}$$

By utilizing the substitution method in equation 2.23 and 2.24, C_L can be calculated as follows:

$$C_L = \sqrt{\frac{C_{D}o\pi ARe}{3}} \tag{2.25}$$

By utilizing the substitution method in equation 2.25 and 2.11, C_D can be calculated as follows:

$$C_D = \frac{4C_{D}o}{3} \tag{2.26}$$

Lastly, by utilizing the substitution method in equation 2.25 and 2.26, (C_L/C_D^2) max can be calculated as follows:

$$(C_L/C_D^2)max = \frac{3\sqrt{3}}{16}\sqrt{frac\pi ARe C_{D}o^3} \tag{2.27}$$

Note that the maximum lift-to-drag ratio $(C_L/C_D)max$ is an important aerodynamic quantity of an aircraft.

2.5 Cruising Performance

2.5.1 Range and Endurance

In a cruising flight, range measures the horizontal straight-line distance, while total range, stage length, or block distance measures the distance travelled during the climb, cruise as well as descent. Furthermore, the distance an aircraft can fly between takeoff and landing limited by its fuel capacity is defined as the maximum total range.

In order to achieve an aircraft's maximum total range, the fuel consumption per unit time has to be calculated initially. This is due to the fact that the distance an aircraft can fly between takeoff and landing is determined and limited to its fuel capacity. For a jet aircraft, the specific fuel consumption is defined as the weight of fuel consumed per unit thrust per unit time.

$$F = \frac{dW_f}{dt} \tag{2.28}$$

W_f is noted as the total fuel load. The weight of the aircraft plays a factor towards its fuel weight flow rate. Because $dW_f = -dW$, the equation 2.28 can be rewritten as

$$F = \frac{dW}{dt} \tag{2.29}$$

Based on the following definite integral, range can be defined as

$$R = \int_{t1}^{t2} V dt = \int_{W1}^{W2} -\frac{V}{F} dW = \int_{W2}^{W1} dW \tag{2.30}$$

Where V/F is used as the range per unit fuel weight (specific range)

The length of time spent during a cruising flight is defined as endurance. Based on the following definite integral, endurance can be calculated by

$$E = \int_{t1}^{t2} dt = \int_{W1}^{W2} -\frac{dW}{F} = \int_{W2}^{W1} \frac{dW}{F} \tag{2.31}$$

In symmetric flight, it is crucial to keep in mind that the time history of the flight condition relies on the specification of two control laws, as a matter of fact, the description of the variation of two control variables with time. Typically, both

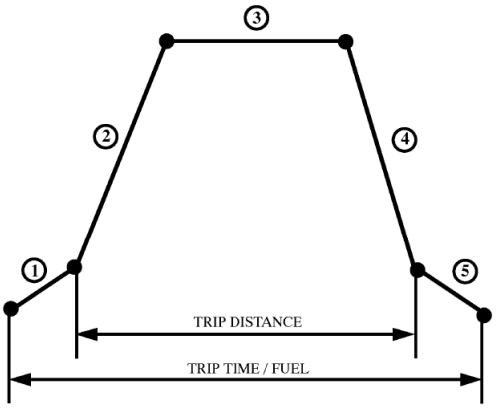

FIGURE 2.12: Bombardier CRJ1000 Flight Mission.

control variables hold a constant value throughout the journey so that the flight condition only varies under the influence of fuel consumption on the weight of the aircraft.(M. H. Sadraey, 2017).

As observed from the figure 2.13, for jet engine aircraft, fuel flow rates can be calculated by using the following formula:

$$F = C_T T \tag{2.32}$$

C_T is a specific value of fuel consumption and T is the value for thrust

Based on the figure 2.14, it is conclusive that once the range and endurance of an aircraft is determined, the average airspeed V_{avg} can be calculated by using the following formula:

$$V_{avg} = \frac{Range}{Endurance} \tag{2.33}$$

2.5.2 Approxiate Analytic Expression for Range and Endurance (Jet Propulsion)

By using the relationship of drag

$$D = \frac{C_D}{C_L} W \tag{2.34}$$

The thrust can be identified as

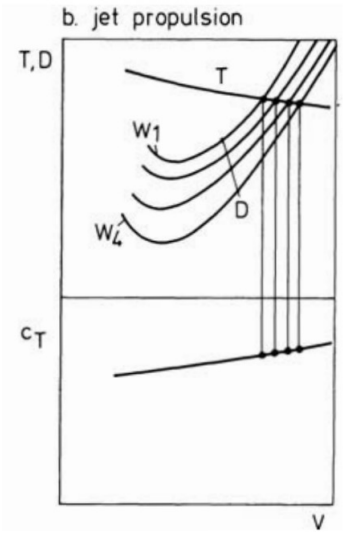

FIGURE 2.13: Determination of V/F and F for jet engine aircraft during constant altitude and engine control flight.

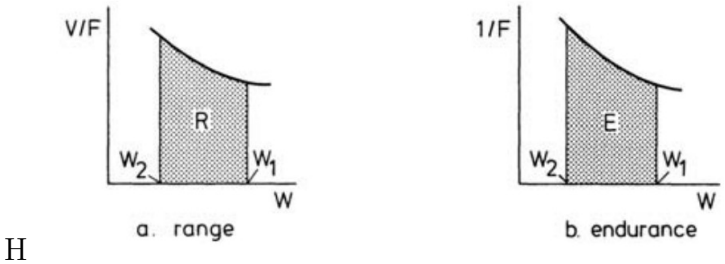

FIGURE 2.14: Calculation of Range and Endurance.

$$T = D = \frac{C_D}{C_L} W \tag{2.35}$$

By utilizing the relationship of airspeed

$$V = \sqrt{\frac{W}{S} \frac{2}{\rho} \frac{1}{C_L}} \tag{2.36}$$

The substitution method for equation 2.36 and 2.30 can be used to determine range as follows:

$$R = \int_{W2}^{W1} \frac{1}{C_T W} \sqrt{\frac{W}{S} \frac{2}{\rho} \frac{1}{C_L} dW} \tag{2.37}$$

Endurance can be calculated by using the insertion method referring to equation 2.35 and 2.32 as follows:

$$E = \int_{W2}^{W1} \frac{1}{C_T} \frac{C_L}{C_D} \frac{dW}{W} \tag{2.38}$$

To derive analytic expression in regards to range and endurance, factors to be considered is cruising at a fixed height and at a constant angle of attack. Furthermore, the process will continue to assume that specific fuel consumption remains at a constant level during the flight duration. A simplification towards the analysis will be implemented by neglecting the variation of compressibility effects on the aerodynamic characteristics of the aircraft as the flight speed reduces during the course of the flight. Combining equation 2.37, range can be calculated as follows:

$$\begin{aligned} R &= \frac{1}{C_T} \sqrt{\frac{2}{S\rho} \frac{C_L}{C_D^2} \int_{W2}^{W1} \frac{dW}{\sqrt{W}}} \\ &= \frac{2}{C_T} \sqrt{\frac{2}{S\rho} \frac{C_L}{C_D^2}} |\sqrt{W}|_W 2^W 1 \\ &= \frac{2}{C_T} \sqrt{\frac{2}{S\rho} \frac{C_L}{C_D^2} [\sqrt{W_2} - \sqrt{W_1}]} \end{aligned} \tag{2.39}$$

Taking $\sqrt{\rho}$ presence into account, it is important for jet-powered aircraft to be in high cruising altitudes. Therefore, equation 2.39 can be rewritten as follows:

$$\begin{aligned} R &= \frac{2}{C_T}\sqrt{\frac{W_1}{S}\frac{2}{\rho}\frac{C_L}{C_D^2}}[1-\sqrt{\frac{W2}{W1}}] \\ &= 2\frac{V_1}{C_T}\frac{C_L}{C_D}[1-\sqrt{\frac{W_2}{W_1}}] \end{aligned} \tag{2.40}$$

By stating that initial airspeed is V_1, an integration with equation 2.38, endurance can be calculated as follows:

$$\begin{aligned} E &= \int_{W2}^{W1}\frac{1}{C_T}\frac{C_L}{C_D}\frac{dW}{W} \\ &= \frac{1}{C_T}\frac{C_L}{C_D}|lnW|_{W_2}^{W_1} \quad = \frac{1}{C_T}\frac{C_L}{C_D}ln\frac{W1}{W2} \end{aligned} \tag{2.41}$$

Flight at a constant airspeed and angle of attack is a cruise technique for turbojet and turbofan aircraft. The flight-path angle occurring during a cruise-climb schedule's value is sufficiently small thus the level-flight conditions are approved of use, whereas lift is equal to weight and thrust is equal to drag. Assuming that C_T and $\frac{C_L}{C_D}$ have constant values throughout the flight, both range and endurance can instantly be distinguished as

$$R = \frac{V}{C_T}\frac{C_L}{C_D}ln\frac{W1}{W2} \tag{2.42}$$

$$E = \frac{R}{V} = \frac{1}{C_T}\frac{C_L}{C_D}ln\frac{W1}{W2} \tag{2.43}$$

The value of $\frac{V}{C_T}\frac{C_L}{C_D}$ is identified as the range factor. The maximum value of endurance can be calculated and identified when C_L/C_D is maximum.

Next, by placing an assumption that C_T and C_L/C_d hold constant values throughout the flight, the range does not have an absolute maximum value. With compressibility drag's absence, a constrained optimum can be obtained during a specific airspeed level. During this state, the maximum range takes place at maximum C_L/C_D.

This scenario can be conducted with conditions that the height at which the minimum drag speed is equal to the desired airspeed. With the condition of constant speed of sound at lower stratosphere for cruise-climb flight, a fixed airspeed

is directly proportional to a fixed flight Mach number (Syauqi, 2021). This results in the constant aerodynamics ratio as shown in equation 2.42.

Taking the thrust equation as a reference

$$T = C_D \frac{1}{2} \rho V^2 S \tag{2.44}$$

Which then V is defined as

$$V = \sqrt{\frac{W}{S} \frac{2}{\rho} \frac{1}{C_L}} \tag{2.45}$$

Thrust can also be defined that it is directly proportional to air density ρ, whereas, at different altitudes, air density varies. In this particular scenario, where T/ρ and specific fuel consumption is constant and the engine control settings are fixed, the expression to find range can be modified by using substitution method based on equation 2.44 and 2.42 in order to obtain

$$R = \frac{1}{C_T} \sqrt{\frac{T}{S} \frac{2}{\rho} \frac{C_L^2}{C_D^3}} ln \frac{W1}{W2} \tag{2.46}$$

In which case the maximum range requires maximum (C_L^2/C_D^3) during flights at different altitudes at a specific airspeed and engine setting.

2.6 Airfield Performance

A maneuver movement can be identified during the takeoff phase where the aircraft accelerates from rest on the runway, whereas v=0 condition towards velocity increase. The two main phases of takeoff distance are:

- The ground run distance
- Airborne distance

There are several phases within the takeoff distance, which begins with the pre-rotation phase from rest v=0 until rotation speed v_R, followed with rotation phases from rotation speed v_R until liftoff speed v_{LOF}. v_R is a very important factor during the takeoff path, with the reason that in this particular phase, a pilot will make a

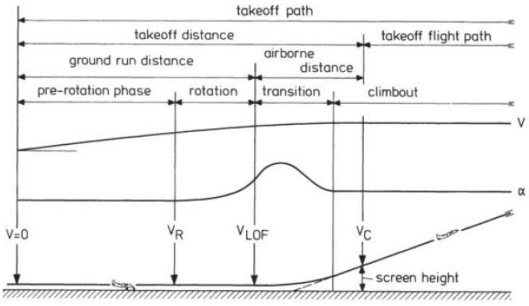

FIGURE 2.15: Take-off maneuver.

decision to set up the upward aircraft rotation. And in this case, the overall takeoff maneuver safety can be affected and identified from this reference speed based on the numerous shifting of rotation speed v_R.

During the ground run phase, the aircraft rate remains unchanged. The angle of attack will then start expanding from the ground stage towards the liftoff condition, as soon as it passes the rotation speed. The next phase is the airborne phase which begins as soon as the lift force is equal to the aircraft weight.

The airborne distance is normally isolated within the transition phase as it reaches climbing flight and the rectilinear climb to the screen height. Within the transition stage, the flight path angle increases from zero liftoff speed to the steady climb phase at screen velocity v_c, is flown with a steady lift coefficient in order to provide sufficient lift force in aiming to achieve the adequate shape of the flight path. The flap deflection and engine control setting remain consistent during the takeoff maneuver. In order to improve climb performance, the landing gear is withdrawn not long after the aircraft has entered the airborne phase. After passing through the screen, the aircraft follows through the takeoff flight path until it achieves protected flight condition at an altitude of around 450m (1500ft) in which the flight proceeds to climb to cruising elevation starts (Anderson, 2005).

In the airworthiness requirements, during takeoff ground run, a multi engine aircraft must have to wait until there is no machine failure in certain range and speed. This is done so that safety in flight is maintained and no passenger felt threatened (Yong, 2021). To fulfill it, a pilot must watch the speed indicator in every takeoff phase, figure 2.16 explains about the order.

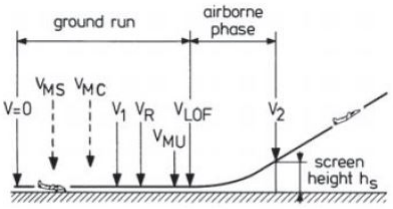

H

FIGURE 2.16: Take-off reference speeds for conventional transports.

2.6.1 Takeoff Ground Run

Figure 2.17 shows all forces acting on an aircrafts ground run. The aircraft's weight is balanced by the lift force and wheel's normal force from the ground. And the thrust is countered by drag and wheel's friction. The frictional force from the wheels is:

$$\begin{aligned} D_g &= D_{gm} + D_{gn} \\ &= \mu(N_m + N_n) \\ &= \mu(W - L) \\ &= \mu(W - \frac{1}{2}\rho v^2 S C_{L_g}) \end{aligned} \tag{2.47}$$

C_L=Lift coefficient in the ground run attitude. μ= Rolling friction coefficient where for concrete ground and the asphalted runway, $\mu = 0.02$ and for a short cut grass, μ=0.05. By neglecting the wind and runway does not have any slope, the motion's equation could be determined, such as: (Torenbeek, 2010)

$$\begin{aligned} F &= T - D - D_g \\ &= T - [\frac{1}{2}\rho v^2 S(C_{Do} + \frac{\Phi C_L^2}{\pi ARe})] - D_g \end{aligned} \tag{2.48}$$

ϕ=ground effect for some explanation. This phenomenon is the cause of an airplane's tendency to float above the ground near the moment of landing. In the presence of a ground effect, the decreased drag is accounted for by ϕ. Where,

$$\phi = \frac{(16h/b)^2}{1 + (16h/b)^2} \tag{2.49}$$

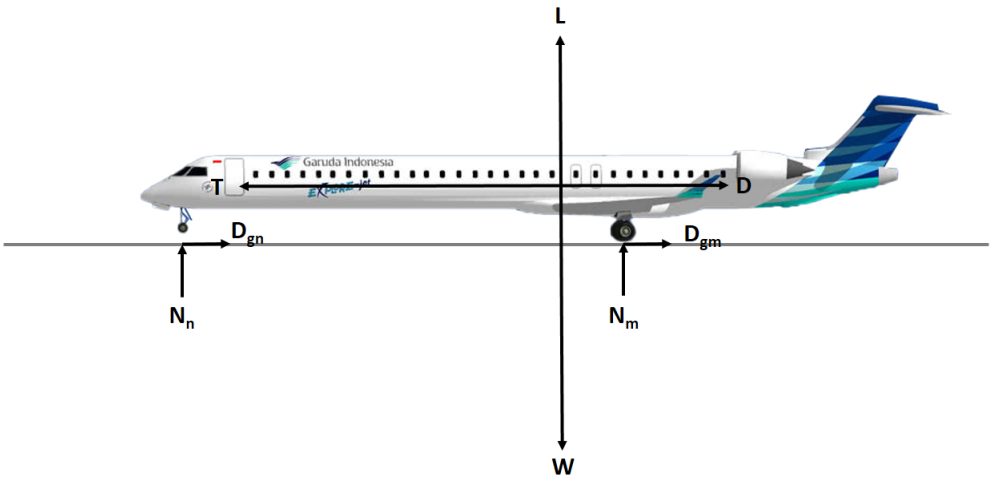

H

FIGURE 2.17: Force acting on Bombardier CRJ 1000.

During the ground run rotation phase, the C_{L_g} and C_{D_g} will vary. To get the aircraft acceleration during the ground run, indicate that a-dv/dt and v=ds/dt, the distance accelerating from rest (s=0, t=0) to liftoff speed (s=Sg, t=t) can be written as:

$$\begin{aligned} a &= \frac{dv}{dt} \\ adt &= dv \\ \int_0^t adt &= \int_0^v dv \\ at &= v \\ t &= \frac{v}{a} \\ t &= \frac{v}{(\frac{F}{m})} \\ t &= \frac{vm}{F} \end{aligned} \tag{2.50}$$

Or

$$v = \frac{F}{m}t \tag{2.51}$$

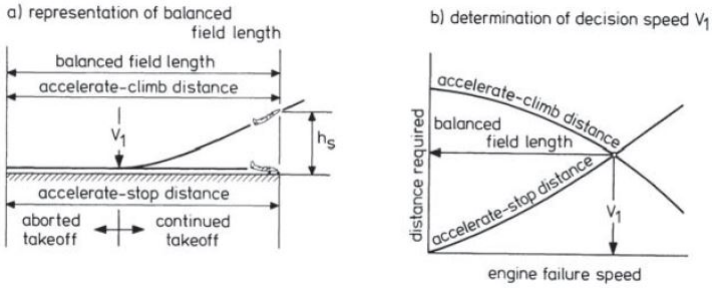

H

FIGURE 2.18: Balanced field length concept (Ruijgrok, 2012)

And for,

$$\begin{aligned} v &= \frac{ds}{dt} \\ ds &= vdt \\ \int_0^{S_g} ds &= \int_0^t vdt \\ S_g &= \int_0^t vdt \end{aligned} \tag{2.52}$$

Substitute equation 2.51 and 2.52

$$\begin{aligned} S_g &= \int_0^t \frac{F}{m} t dt \\ S_g &= \frac{F}{m}\frac{t^2}{2} \end{aligned} \tag{2.53}$$

Then, by substituting 2.50 to 2.53

$$\begin{aligned} S_g &= \frac{F}{m}\frac{t^2}{2} \\ S_g &= \frac{F}{m}\frac{(\frac{vm}{D})^2}{2} \\ S_g &= \frac{F}{n}\frac{v^2m^2}{2F^2} \\ S_g &= \frac{v^2m}{2F} \end{aligned} \tag{2.54}$$

Then the next step and also inserting that mass=W/g (Anderson, 2005),

$$S_g = \frac{v_{LOF}^2 W/g}{2[T - D - \mu(W - \frac{1}{2}\rho v^2 S C_{L_g})]} \tag{2.55}$$

For takeoff safety, the takeoff speed (v_{LOF}) must be 20 percent higher than the stalling speed ($V_S stall$). So,

$$\begin{aligned} v_{LOF} &= 1.2 v_{stall} \\ &= 1.2\sqrt{\frac{2W}{\rho S C_{L_{max}}}} \end{aligned} \tag{2.56}$$

Yield for the ground run distance (Ruijgrok, 2012),

$$\begin{aligned} Sg &= 1.2\sqrt{\frac{2W}{\rho_\infty S C_{L_{max}}}} \\ Sg &= \frac{1.44\frac{2W^2}{\rho S C_{L_{max}}}}{2g[T - D - \mu(W - \frac{1}{2}\rho v^2 S C_{L_g})]} \\ Sg &= \frac{1.44 W^2}{g\rho S C_{L_{max}}[T - D - \mu(W - \frac{1}{2}\rho v^2 S C_{L_g})]} \end{aligned} \tag{2.57}$$

2.6.2 Airborne Takeoff

The airborne distance is heavily dependent on how the aircraft is operated by the pilot and can thus be measure only when two control laws are determined. The continuous engine control setting conditions during takeoff maneuvers decide one of them. The second control rule concern the lift coefficient time history, natural acceleration, or pitch rate from the moment the aircraft leaves the ground until at the end of the transfer, it enters a comfortable climbing attitude.

The exact specification of the flight path between the takeoff point and the screen's height is usually carried out by step-by-step calculations, following those control rules. (Francis J. Hale,1984)

In a transition flare, the equation can be written as

$$\frac{W}{g} v \frac{dv}{ds} = T\cos\alpha_T - D - W\sin\gamma \tag{2.58}$$

$$\frac{W}{g}\frac{v^2}{R} = L + T\sin\alpha_T - W\cos\gamma \tag{2.59}$$

If the thrust and velocity vector overlap (α_T=0) and the angle of the flight path is small ($\sin\gamma$ and $\cos\gamma = 1$), the equation is reduced to

$$\frac{W}{g}v\frac{dv}{ds} = T - D - W\gamma \tag{2.60}$$

$$\frac{W}{g}\frac{v^2}{R} = L - W \tag{2.61}$$

A basic analytical solution to the issue is rendered here, considering a circular path of radius R. Thus, if the pilot automatically raises the angle at the take-off stage, we must consider shifting. Angle of attack and increase lift, move along the curve path Figure 2.19 section a. The lift shifting coefficient, C_{Lt}, can be presented immediately after lift off as:

$$(C_{Lt})_{LOF} = (C_{L_{LOF}}) + \Delta(C_L)_{LOF} \tag{2.62}$$

At any stage on the next transition flight path, the lift coefficient could be written as Figure 2.19 section b.

$$C_{Lt} = (C_L)_{LOF} + \Delta C_L \tag{2.63}$$

By substituting equation 2.50 into 2.48 the equation become:

$$\frac{1}{gR} = \frac{1}{v_{LOF}^2} - \frac{1}{v^2} + \frac{\Delta C_L}{\frac{2}{\rho}\frac{W}{S}} \tag{2.64}$$

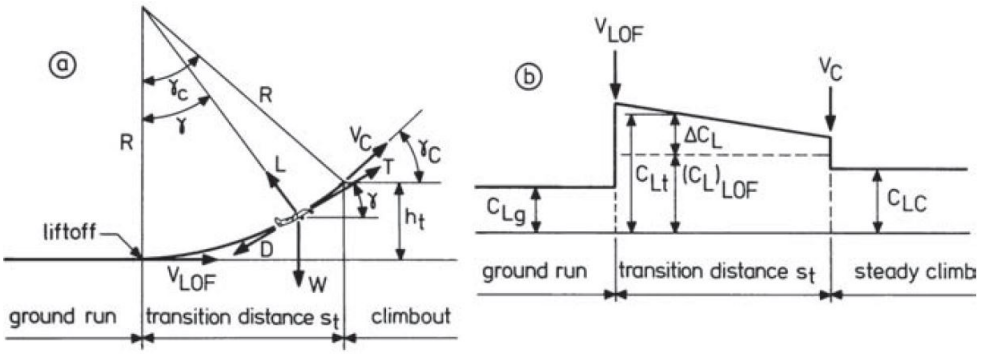

H

FIGURE 2.19: Schematic for transition to steady climb (Ruijgrok, 2012)

This term illustrates that ΔC_L and $C_L t$ quantities during displacement would decline over time Figure 2.8 section b. We can express the radius R by the combination of equations 2.48 and 2.49.

$$\begin{aligned} R &= \frac{2\frac{W}{S}}{\rho g \Delta(C_L)_{LOF}} \\ &= \frac{v_{LOF}^2 (C_L)_L OF}{g \Delta(C_L)_{LOF}} \\ &= \frac{v_{LOF}^2}{g(n_{LOF} - 1)} \end{aligned} \tag{2.65}$$

Where $n_L OF$ is the load factor of lift off (Raymer, 1989)

$$\begin{aligned} n &= \frac{L}{W} \\ &= \frac{\frac{1}{2}\rho S 0.9 C_{L_{max}} (1.15 v_{stall}^2)}{W} \end{aligned} \tag{2.66}$$

Flight-path angle reaches the value

$$\sin \gamma_c = (\frac{T - D}{W}) \tag{2.67}$$

The transition is done and the steady climb starts at vc airspeed. The sporadic value of the shifting coefficient at that stage in the flight path is unexpectedly

reduced to the C_LC value concerning the vc velocity's stability.

$$C_{LC} = \frac{W}{S}\frac{2}{\rho}\frac{1}{v_c^2} \tag{2.68}$$

This is conveniently obtained from geometric patterns if R and C are known. The following relationship occurs in Figure 2.8 section a:

$$S_t = R\sin\gamma_c \tag{2.69}$$

$$h_t = R(1-\cos\gamma_c) \tag{2.70}$$

2.6.3 Landing Ground run

Figure 2.20 shows all forces acting on an aircraft's ground run. Due to the landing performance, the motion's equation doesn't change too much. As we know that the jet engines create a thrust reversal, the thrust goes in the same direction with drag force and the wheels' friction force. The equation is shown as:

$$\begin{aligned} F &= -T - D - D_g \\ &= -T - [\frac{1}{2}\rho v^2 S(C_D o + \phi\frac{C_L^2}{\pi ARe})] - D_g \end{aligned} \tag{2.71}$$

The distance itself will also have different parameters, the distance accelerating condition is from landing speed ($s = S_L, t = 0$ to rest (s=0,t=t). So,

$$\begin{aligned} v &= \frac{ds}{dt} \\ ds &= vdt \\ \int_{S_L}^{0} ds &= \int_0^t vdt \\ -S_L &= \int_0^t vdt \\ -S_L &= \frac{v^2 m}{2F} \\ -S_L &= \frac{V_T^2 W}{2g[T + D + \mu(W - \frac{1}{2}\rho v^2 S C_{L_g})]} \end{aligned} \tag{2.72}$$

Where for safety factor V_T need extra 30 percent speed from $V_S tall$,

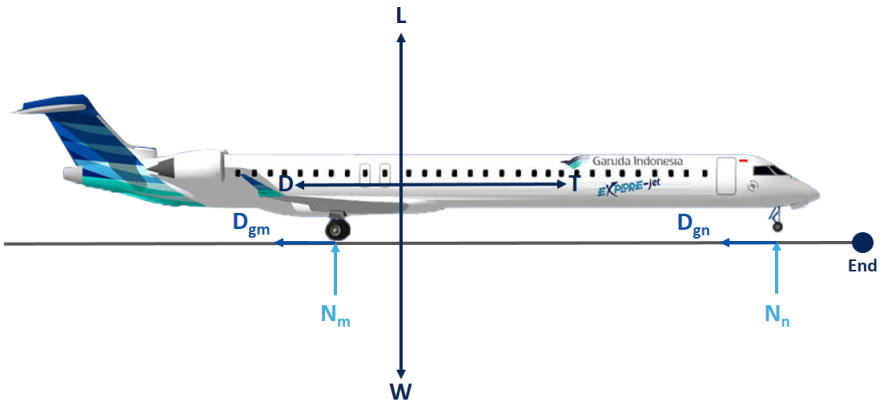

H

FIGURE 2.20: Forces acting on Bombardier CRJ 1000 during landing

$$\begin{aligned} v_T &= 1.3 v_S stall \\ &= 1.3\sqrt{\frac{2W}{\rho S C_{L_{max}}}} \end{aligned} \tag{2.73}$$

By having the same substitution steps, the landing distance became:

$$S_L = \frac{1.69W^2}{g\rho S C_{L_{max}}[T + D + \mu(W - \frac{1}{2}\rho v^2 S C_{L_g})]} \tag{2.74}$$

Where μ=0.4 because the pilot is applying a brake system (Anderson, 2005).

2.7 Aircraft Limitations

2.7.1 Limiting Speeds

Stall Speed

The term "stall" refers to a loss of lift caused by the breakdown of airflow over the wing when the angle of attack passes a critical point, or when the speed drops below a critical value at a fixed angle of attack. As air velocity increases over

the wing with angle of attack, air pressure decreases, increasing the lift coefficient. Stall speed is equal to the reference stall speed (V_{SR}). V_{SR} is equal to 1.02 V_{S1G} for a FLAPS 0/ Gear Up configuration. V_{SR} is also equal to 1.0 V_{S1G} for all other configurations. This can be seen across the blue section of the figure below:

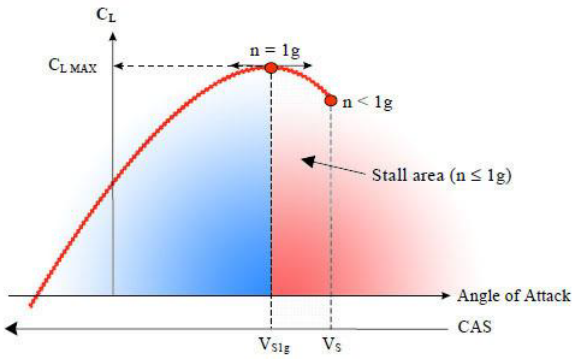

FIGURE 2.21: C_L versus angle of attack.

The lift coefficient increases until it reaches its maximum lift point (C_{LMAX}). From this point on, the lift coefficient rapidly decreases. This is referred to as a stall, and it occurs at two different speeds:

- V_{S1g}, which is the maximum lift coefficient at a load factor of one.
- V_S, which corresponds to the conventional stall in the presence of a load factor less than one.

Minimum Control Speed on the Ground (V_{MCG})

The Minimum Control Speed on the Ground (V_{MCG}) specifies the minimum speed required to keep the aircraft's control during the takeoff roll in the event of a ground engine failure. The lateral excursion should be lower than 30 feet following an engine failure on the ground, according to regulations.

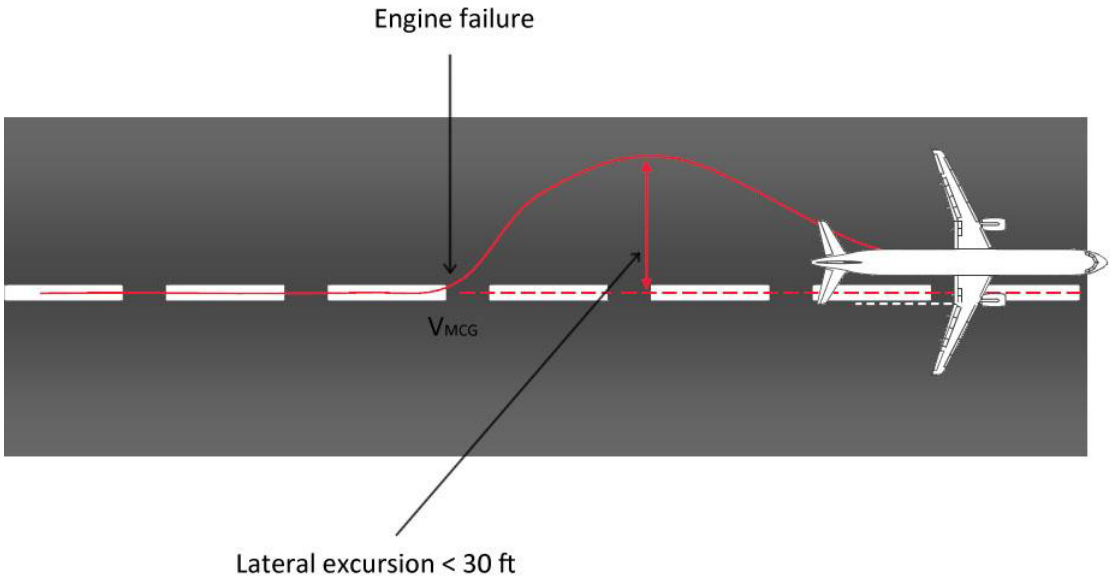

FIGURE 2.22: V_{MCG}

The conditions below are the assumptions to obtain V_{MCG}:

- Most critical takeoff configuration
- Most unfavorable takeoff weight
- Most unfavorable center of gravity
- Aircraft trimmed for takeoff
- Operating engines on takeoff power

V_{MCG} depends mostly on:

- Engine(s) thrust and position
- Pressure altitude

For CRJ1000, the (V_{MCG}) at flaps 8 is 96 KIAS (96KCAS) and at flaps 20 is 97 KIAS (97 KCAS).

Minimum Control Speed in the Air (V_{MCA})

The Minimum Control Speed in the Air (V_{MCA}) is the speed at where aircraft is still under control with a maximum bank angle of 5 degrees if an engine failure occurs.

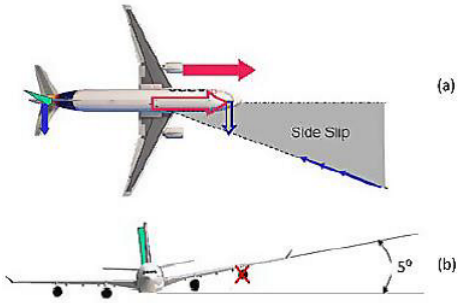

FIGURE 2.23: Sideslip angle (a) and bank angle (b) in a one-engine-inoperative condition.

These conditions necessary for determining V_{MCG} are assumed, including:

- The aircraft is in the airborne phase and out of ground effect
- Retracted Landing Gear
- Inoperative engine windmilling

For CRJ1000, the (V_{MCA}) at flaps 8 is 101 KIAS (102 KCAS) and at flaps 20 is 99 KIAS (99 KCAS).

Minimum Unstick Speed (V_{MU})

The regulation states that "V_{MU} is the calibrated airspeed at which the airplane can safely lift off the ground and continue the takeoff". V_{MU} is determined during a demonstration of low speed flight test (Figure 2.24). The control stick is pulled to the limit of the control surfaces' aerodynamic efficiency, slowly rotating the aircraft to an angle of attack when either the maximum lift coefficient is reached or the tail strikes the runway (for geometrically limited aircraft).

FIGURE 2.24: V_{MU} determination.

During flight tests, two minimum unstick speeds must be identified and validated:

- all engines operatives (AEO) : $V_{MU(AEO)}$
- with one engine inoperative (OEI) : $V_{MU(OEI)}$

In the case of a single inoperative engine, $V_{MU(OEI)}$, sufficient lateral control must be maintained to avoid an engine or wing colliding with the ground.

Minimum Speed During Approach and Landing (V_{MCL})

V_{MCL} "is the calibrated airspeed at which it is practicable to to keep aircraft under control while the crucial engine remains off and sustain straight flight with a bank angle of no more than 5°" Three or more engines aircraft, a minimum speed during approach and landing with a critical engine inoperative $V_{MCL(OEI)}$ is also determined.

Maximum Brake Energy Speed (V_{MBE})

Assume that the aircraft's brakes absorb the entire amount of kinetic energy. VMBE is dependent on the following:

- Aircraft weight
- Meteorological conditions
- Runway slope

Maximum Tire Speed (V_{TIRE})

V_{TIRE} is the specified maximum ground speed so it can avoid damaging the tire structure due to heat and centrifugal forces. The speed is specified by the tire manufacturer $V_{TIRE} = 195$ knots for the majority of Airbus aircraft variants.

2.8 Weight and Balance Control

2.8.1 Weight Control

Weight is a significant component for both design and operation of the aircraft. It requires special attention from both pilots and maintenance professionals Excessive

weight affects an aircraft's efficiency and available safety margin in the event of an emergency (FAA, 2016).

In the aircraft design process, the structure should be kept the lightest it can be while maintaining the required strength. The maximum permissible weight should be able to be sustained by the wings. As a consequence of increased weight, the wings should generate greater lift force. The structure should withstand both the increased static and dynamic stress.

A wing's lift is determined by the shape of its airfoil, its AoA, its airspeed, and the density of air. The aircraft must accelerate faster than it would at sea level to generate adequate lift for takeoff when it takes off from the airport with a high-density altitude, thus a longer takeoff run is required.

The required distance may exceed the length of the available runway. When the aircraft is operating at the airport with a high-density of altitude, the Airplane Flight Manual or Pilot's Operating Handbook has to be reviewed to ascertain the aircraft's maximum weight allowance for the altitude, temperature, wind, and runway conditions.

2.8.2 Effects of Weight

When all seats are occupied, the baggage compartment is full, and all fuel tanks are full, the majority of modern aircraft are substantially overloaded. If maximum range is desired, either passengers or baggage should be lesser, or the maximum load will be used, reducing the range indicated by the onboard fuel. Overloaded aircraft will result in a number of complications:

1. The aircraft will need takeoff speed higher than usual, therefore resulting in extended takeoff run.
2. The reduction of both angle of climb and rate.
3. Lowered service ceiling.
4. Reduction of the cruising speed.
5. Shortened cruising range.
6. Reduced maneuverability.

7. Landing roll is extended as higher landing speed.

8. Mainly the landing gear will be imposed because of the excessive load.

2.8.3 Weight Changes

The maximum weight that is permitted to carry is regulated by design factors. The maximum operational weight, on the other hand, may less than the maximum permitted weight because of factors such as high-density altitude or high drag field conditions produced by wet grass or water on the airport runway. The maximum operational weight may also be limited by the runway length at the departure or arrival airport.

A critical preflight consideration is the weight distribution throughout the aircraft. Loading the airplane to the maximum permitted gross weight is insufficient. This weight must be allocated in such a way that the CG remains within the prescribed limits in the POH or AFM.

If the center of gravity is positioned too forward, the heavier passenger is relocated to the back or baggage can be transferred to a rear baggage compartment. If CG is positioned too far aft, passengers or luggage can be moved forward. Laterally, the balance of the fuel load should be maintained.

The pilot has to give close attention to the POH or AFM about the operating of fuel system in order to maintain the aircraft's balance in flight. When an aircraft gets older, the weight is often increased due to the accumulation of dirt or debris in difficult spots and the absorption of moisture by the cabin insulation. Although the gain of the weight is typically insignificant, it is able to be confirmed only by measuring the aircraft weight.

The replaced fixed instrument might impact the aircraft's weight significantly. By replacing older and heavier electrical instruments with lighter and brand new models can save a lot in weight. While the weight adjustment is beneficial, it may result in a shift in the CG, which has to be estimated then noted at the weight and balance record.

Weight changes are primarily caused by repairs and adjustments. The FAA-certified mechanic or repairman doing the repair or alteration is responsible for determining the weight and position of the modification, computing the CG, taking

note of the updated empty weight and EWCG in the aircraft's weight and balance record, and updating the equipment lists. If the updated of calculated EWCG value falls beyond the EWCG range, an adverse-loading check must be performed. This requires an adverse-loading check in both directions and a check of the maximum weight.

The adverse-loading check is such an attempt to load an aircraft in such way that the aircraft achieves the most critical balance condition while remaining within the aircraft's design CG limitations. If any of the checks result in an out-of-range loaded CG, the aircraft has to be modified to prevent the aircraft being loaded incorrectly by the pilot. Occasionally, a fixed ballast can be installed to bring the aircraft back into the typical CG range.

The FAA-certified technician or repairman performing the annual or condition check must ensure that the aircraft records include current and accurate weight and balance data. The PIC is responsible for operating the aircraft with the most recent weight and balance data (FAA, 2016).

2.8.4 The Importance of Weight and Balance

Pilots tend to underestimate the serious importance of optimum aircraft weight and balance. Load sheets are taken for granted, and hasty calculations of the aircraft's center of gravity are produced. Sadly, each year, a number of accidents happen as the effect of weight and balance concerns. Numerous incidents could have been prevented if greater attention had been paid to weight and balance.

In the maximum gross weight formula, there is a safety factor. Aircraft can fly when it takes off at a weight greater than maximum gross weight if there is a long enough runway and also the density altitude is low enough. Landing, on the other hand, is a different story. While all aircraft are designed to endure an occasional hard landing, when the aicraft was significantly overweight, some structure would certainly be broken at the moment, or the structure will be damaged sufficiently to break later when everything would appear as usual to a pilot that is unaware of this scenario.

Even worse than an overloaded, hard landing is surpassing the structural integrity of the metal or composite design values while maneuvering or encountering

turbulence. Hidden damage may result, resulting in an unanticipated catastrophic breakdown at a later point in time.

2.9 Weight and Balance Theory

Weight and balance in aircraft are determined by the law of the lever. Two factors are critical in determining an aircraft's weight and balance:

1. The total weight of the aircraft has to be lower compared to the FAA's maximum weight allowance for the aircraft's model.

2. The aircraft's center of gravity, or the point at which all the weight is concentrated, has to be kept within the permitted range for the aircraft's operational weight.

2.10 Weight and Balance Control-Commuter Category and Large Aircraft

2.10.1 Establishing the Initial Weight of an Aircraft

Before entering service, every aircraft is weighed along with the empty weight and also the center of gravity (CG) position are determined. Normally, new aircraft are weighed at the manufacturer and are suitable for service without having to reweight if the weight and balance records have been changed to account for aircraft alterations and modifications, such as interior reconfigurations.

Prior to use by the receiving operator, an aircraft sent from an operator with an approved weight and balance program to another operator with an approved program does not need to be weighed, if 36 calendar months have not passed since the last individual or fleet weighing, or unless some other modification to the aircraft requires weighing.

Aircraft that have been transferred, leased, or bought from an operator without an approved weight and balance program and that have not been modified or have been modified minimally may be placed into operation without being reweighed if the last weighing was performed in accordance with an acceptable method not

more than the past 12 calendar months, and the operator maintained a record of weight and balance changes. Failure to reweight an aircraft after modification might be dangerous. Compliance with applicable manuals, operations standards, and management specifications is necessary when weighing large aircraft to guarantee that the weight and balance criteria established in the Aircraft Flight Manual (AFM) are satisfied within permitted limitations. This supplies the flight crew with information that enables the maximum payload to be safely carried.

After cleaning the aircraft, it should be weighed in still air or an enclosed facility. Ascertain that the aircraft is configured for weighing in terms of flight controls, oil, ballast, unusable fuel, and other operational fluids, and equipment in accordance with the governing weight and balance procedure. Generally, large aircraft are not weighed by raising them off the floor on jacks; instead, they are weighed on ramp-type scales.

Scales has to be calibrated, zeroed, and used according to the manufacturer's specifications. Each scale has to be calibrated on a regular basis in accordance with the manufacturer's schedule for calibration, either by the manufacturer or a recognized facility, such as a civil department of weights and measures. Without access to the schedule of the manufacturer, the interval between calibrations should not pass 12 months.

2.10.2 Operating Empty Weight (OEW)

Operational empty weight (OEW) is the sum of the basic empty weight and the fleet empty weight. The operator has two options for OEW maintenance. The loading schedule can be used to determine an aircraft's operational weight and balance, or the operator can establish fleet empty weights for a fleet or group of aircraft.

Reestablishing the OEW

Each aircraft's OEW and CG positions should be reestablished during the reweighing. Additionally, it has to be calculated if the total change in the weight and balance log reaches plus or minus one-half of one percent (0.5 percent) of the maximum landing weight, or whenever the total change in the CG position pass one-half of one percent (0.5 percent) of the MAC. Weight changes can be calculated while reestablishing the aircraft's OEW between reweighing periods if the

weight and CG location of the adjustments are known; if not, the aircraft has to be reweighed.

2.11 Aircraft Payload-Range Diagram

The payload-range diagram is beneficial for airliners in the following ways:

- it enables them to compare the payload range capabilities of various aircraft types.
- calculating the maximum cargo that can be flown over which distances given the restrictions.

The payload-range diagram's specific shape is determined by the aircraft's aerodynamic design, structural efficiency, engine technology, fuel capacity, and passenger/cargo capacity.

Payload-Range Trade-off

A typical payload-range diagram is depicted in the Figure 2.25.

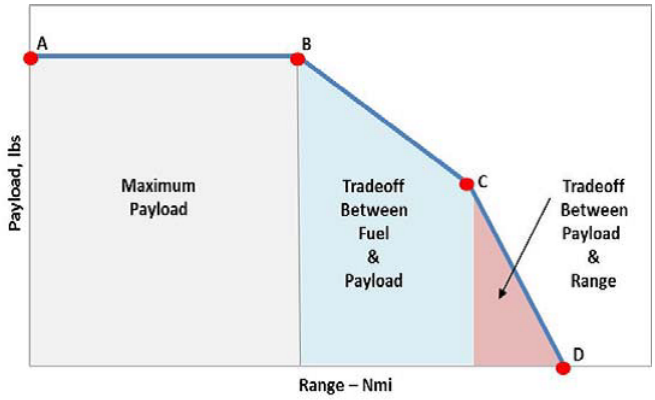

FIGURE 2.25: Payload-Range trade-offs.

The shape of the curve is such that the aircraft can carry a maximum payload with specific range — as indicated by the grey area between points "A" and "B."

Payload-Range Diagram Boundaries & Limitations

The figure shows an usual version of payload-range diagram, emphasizing the various weight categories of an aircraft. While the shape of the diagram is determined by the aerodynamic design, engine technology, fuel capacity, and usual

passenger/cargo configuration of the aircraft, the diagram's boundary is determined by the aircraft's structural design parameters.

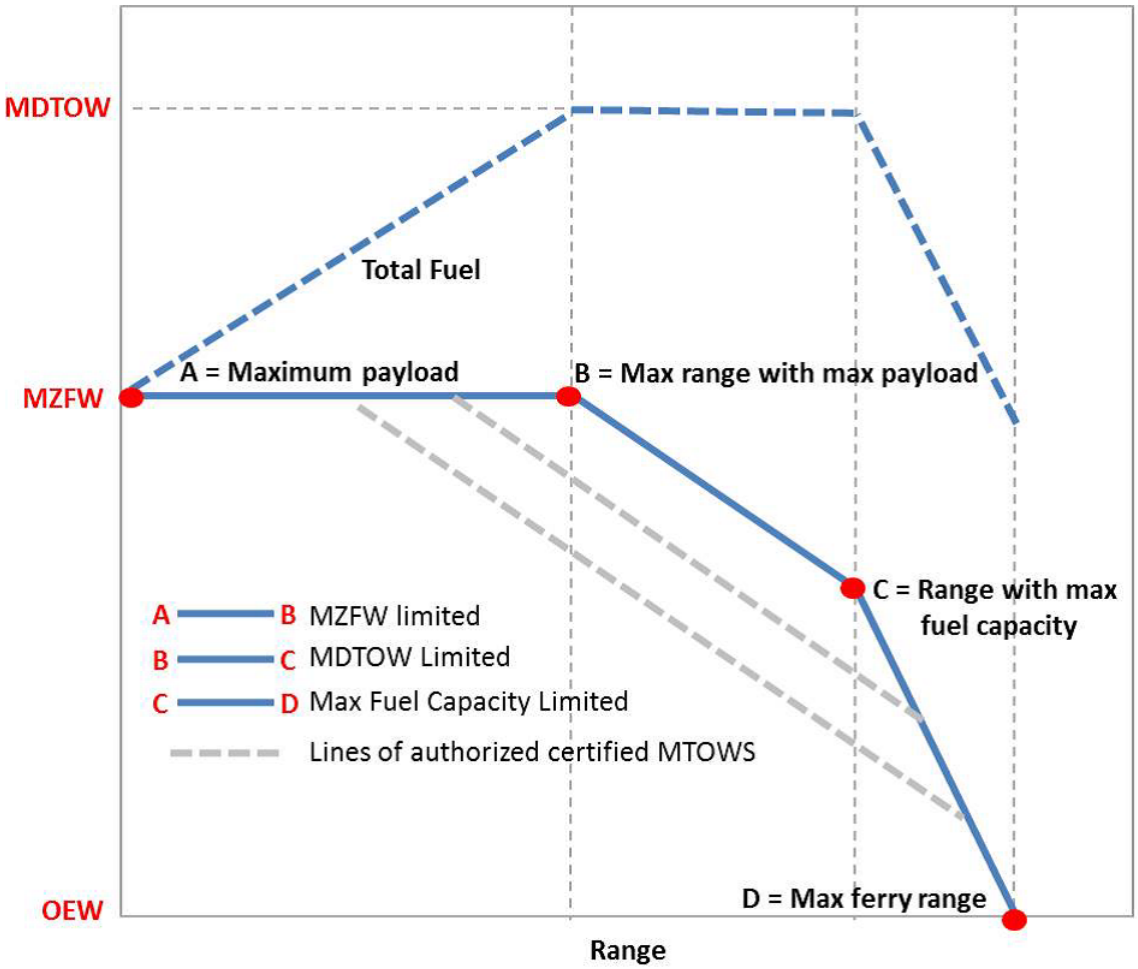

FIGURE 2.26: Payload-Range Boundaries and Limitations.

The following are critical design criteria inherent in payload-range diagrams:

- **At Point A** , the aircraft is carrying its maximum payload and is empty of fuel. When carrying the maximum payload, the aircraft's capacity is limited by its MZFW. Because the MZFW is a constant value, and the OEW varies due to the airline's operational expenses, lowering the OEW enables the aircraft to carry greater payload.

- **Along Points A to B**- maximum payload range; fuel is provided to allow for flight within a certain range. The envelope's topside is constrained by the Maximum Zero Fuel Weight (MZFW).
- **Point B** indicates the aircraft's maximum range when carrying the maximum payload.
- **Along Points B to C** - payload is restricted by the MTOW; payload is exchanged for fuel to extend range. The greater the MTOW, the greater the amount of fuel or payload that can be carried. The bigger the amount of fuel transported, the longer the range. This is often the region of most performance interest. The envelope's first angled section is limited by the Maximum Design Takeoff Weight (MDTOW).
- **At Point C**, the aircraft's maximum fuel volume capacity has been reached; this is the most structurally efficient point for fuel carriage and reflects the maximum range possible with full fuel tanks and a fair payload. This, however, can be misleading, as the reduced payload at this stage, may not be economically viable
- **Along Points C to D** - payload is limited by fuel; only payload can be offloaded to reduce the aircraft's weight and therefore increase its range capabilities. Generally speaking, operating in this zone is not financially viable because of the huge payload reductions required to accomplish minor increase of range. The envelope's second angled section is constrained by the aircraft's Maximum Fuel Capacity (MFC).
- Finally, the aircraft is at Operator's Empty Weight (OEW) at Point D, and the range flown at this point is assumed as maximum ferry- range.
- The region inside the boundary shows possible payload and range mission combinations. A contour line drawn inside the MDTOW boundary and parallel to it represents alternate, approved MTOWs. The authorized weight limitations are determined by airline and are frequently referred to as purchased weights.

Figure 2.27 shows the graph between payload and range of CRJ1000 aircraft.

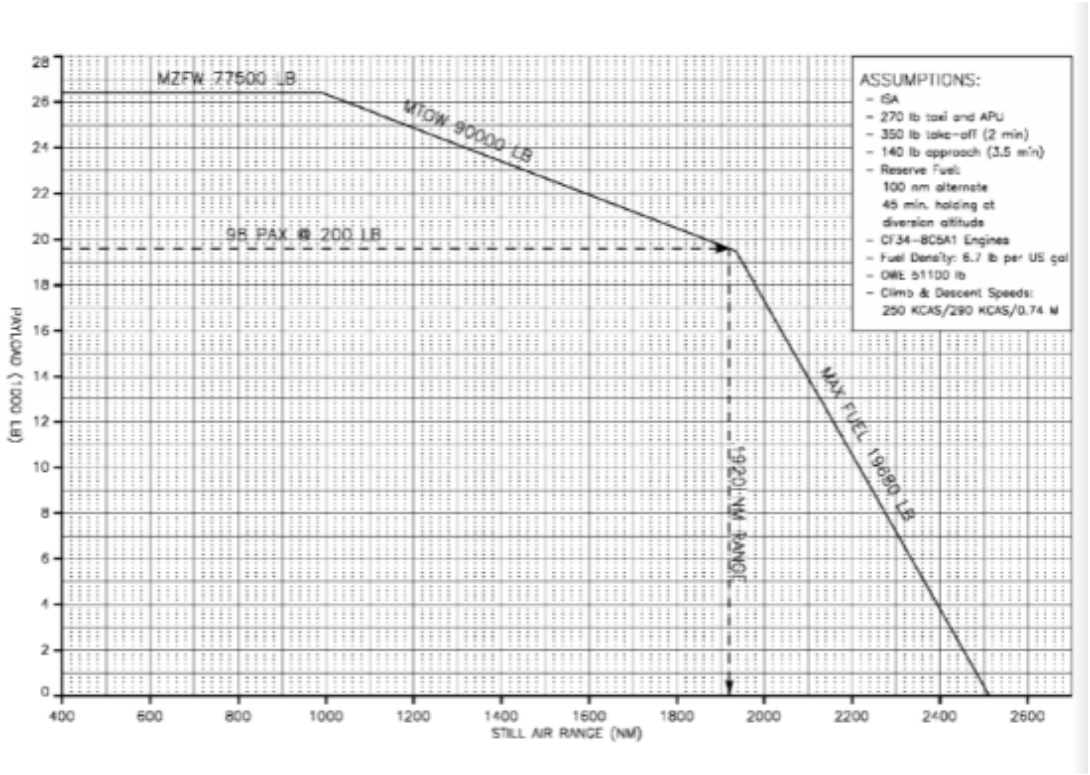

FIGURE 2.27: Payload-Range of CRJ1000 Aircraft.

2.12 How Design Change Affect The Payload-Range Diagram

Changing the MZFW limit It can be seen in Figure ?? that the increased of Maximum Zero-Fuel Weight (MZFW) effects. The maximum payload is obtained by subtracting the MZFW from the OEW (operational empty weight)

Figure 2.28 illustrates the effects of increasing the Maximum Zero-Fuel Weight (MZFW). The maximum payload can be calculated as the MZFW minus the OEW (operational empty weight). $MaxPayload = MZFW - OEW$ If the manufacturer can increase this certificated value by showing the airframe's structural integrity, further payload can be added.

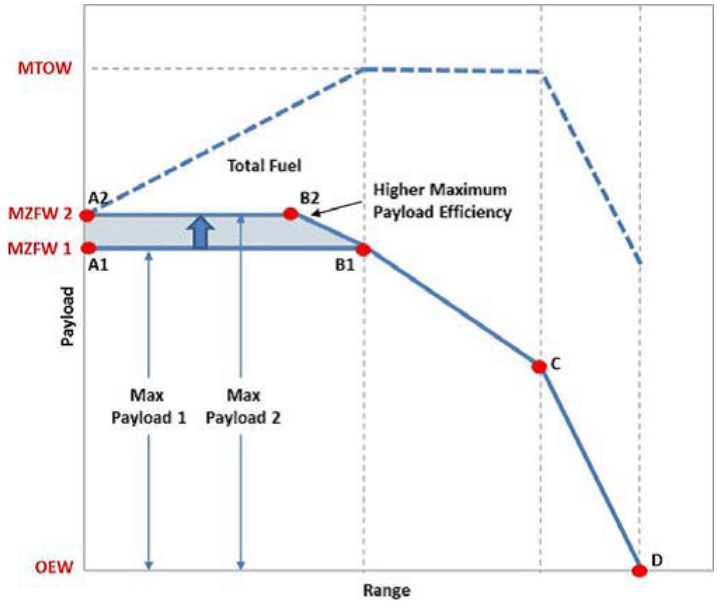

FIGURE 2.28: The Effects of Increasing the MZFW.

The OEM allows operators to increase weight in 1,000-pound amounts up to the limitation. Additionally, increasing MZFW typically does not result in an increase in MTOW, as this is a fixed, approved weight. As a result, at maximum payload efficiency, the MZFW drops linearly with increasing MTOW - as represented by the section along with points B2 to B1.

Changing the OEW limit

If the MZFW is constant, the OWE varies according to the operator item weight. Although reducing an aircraft's OEW allows more payload to be carried, the primary reason why an airline would focus on reducing weight is to improve aircraft performance and save on fuel expense. Excess weight reduces the flight performance of an airplane in almost every respect, including higher takeoff speeds, longer takeoff run, and reduced rate and angle of climb. Adding weight to an airplane requires a greater lifting force as it moves through the air - which also increases the drag.

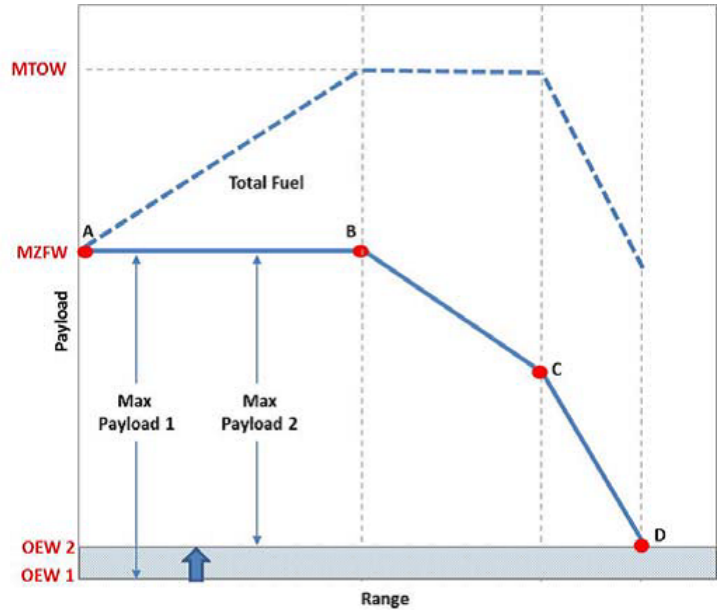

FIGURE 2.29: Changing the OEW limit.

Changing the MTOW limit

Figure 2.30 demonstrates the impacts of raising the Maximum Capacity of the Fuel Tank. Typically, the aircraft manufacturer will make accessible the option to install additional fuel tanks, allowing the aircraft to fly greater ranges.

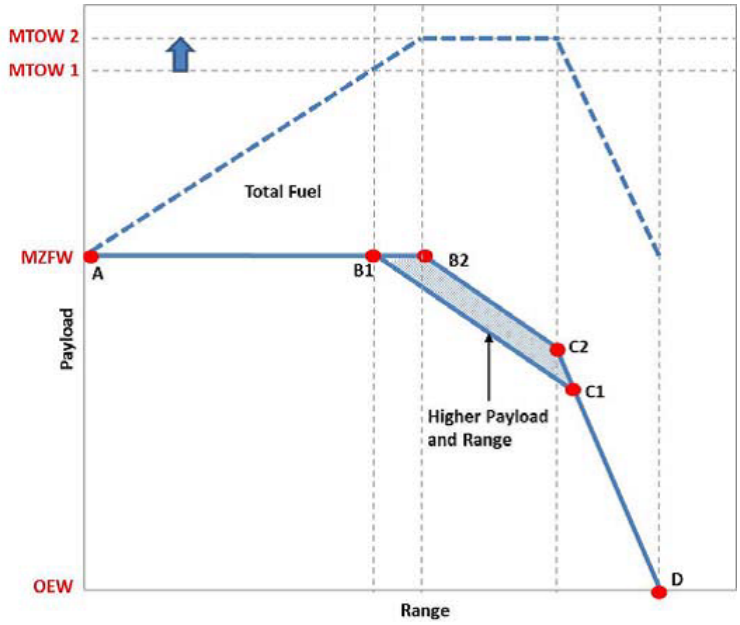

FIGURE 2.30: Changing the MTOW limit.

All things being equal, if the manufacturer can improve this certificated value by demonstrating the structural integrity of the airframe, then more payload-range can be made available. As previously discussed, while higher MTOWs enhance an aircraft's utility, airframe manufacturers routinely charge premiums for these higher design weights.

Changing the MFC limit Figure 2.31 illustrates the effects of increasing the Maximum Fuel Capacity. What typically happens under this circumstance is the aircraft manufacturer will make available the option to add fuel tank(s) allowing the aircraft to fly longer ranges.

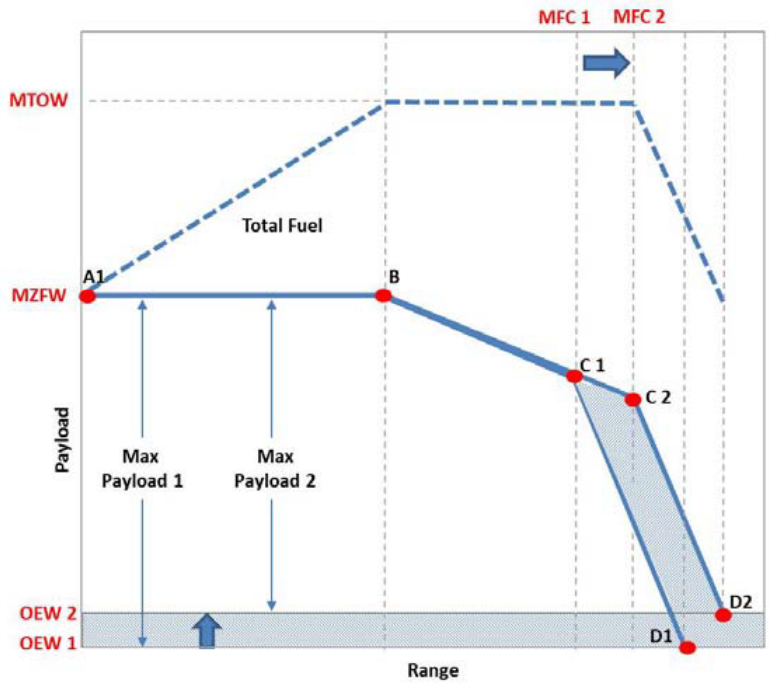

FIGURE 2.31: Changing the MFC limit.

While the addition of extra fuel tanks extends the range of the aircraft, there are certain drawbacks to this choice, as indicated in Figure 2.31 below, which shows the 737-900ER's optional fuel tank capabilities. To begin, because the tanks themselves contribute weight to the aircraft, they raise the Manufacturer's Empty Weight (MEW), which results in an increase in OEW. As a result, the maximum payload available is reduced. Second, the installation of cargo tanks frequently results in the loss of space that could be utilized for goods. Thirdly, the range enhancements are accessible only when the payload reaches the point on the envelope where range would have been otherwise limited by MFC – as indicated in Figure above by the shaded envelope.

CHAPTER 3
RESEARCH METHODOLOGY

3.1 Research Methodology Flow Chart

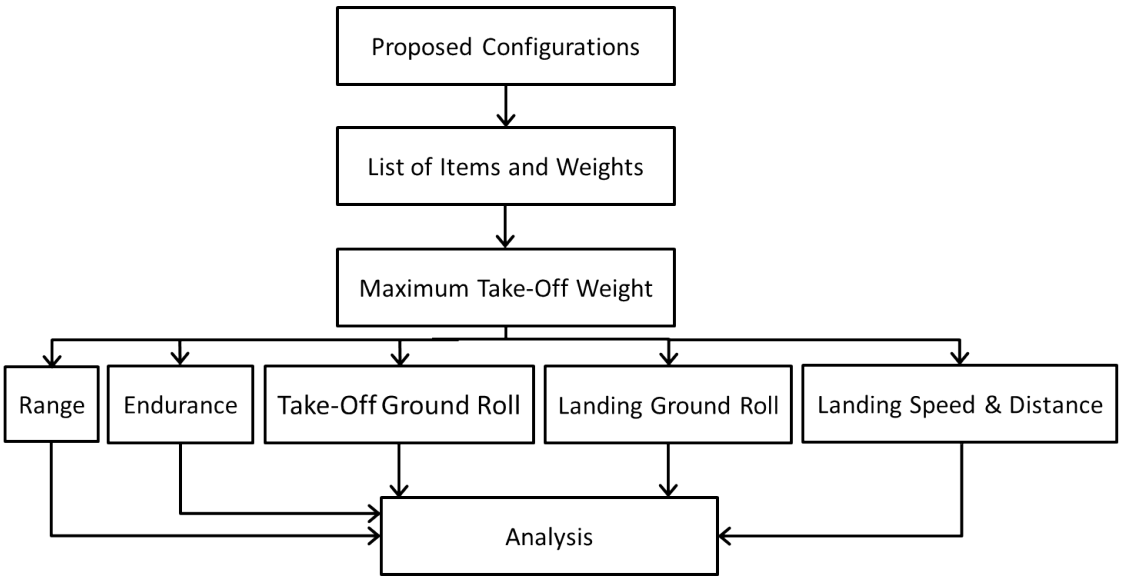

FIGURE 3.1: Research Methodology for this study.

This is the the flow chart of the research methodology used for this thesis. First, two configurations of CRJ1000 as business jets are proposed. Then, the items and weight for the configurations are listed, to calculate the Maximum Take-Off Weight. From the MTOW, then the range, endurance, take-off and landing ground roll, actual and required landing distance, and landing speed can be calculated. Finally, the analysis is made from the calculations.

3.2 CRJ1000 Operational Condition

According to the Route Profitability data from Airline X since CRJ1000 first operated until 2019, the total expenditure is higher than the income received by the company (Jacky, 2020). Figure shows the graph of the income and expenditure of CRJ1000 operational from 2012 to 2019. Based on Figure 3.2, the expenditure is always higher than the income received.

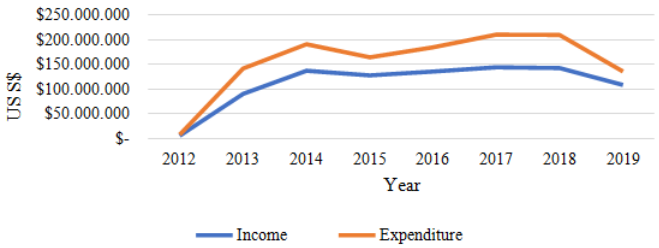

FIGURE 3.2: Income and Expenditure of CRJ1000 Operational.

Figure 3.3 shows the average annual utilization of CRJ1000 aircraft. As can be observed, CRJ1000 aircraft are underutilized. Both in 2017 and 2018, utilization is nearly identical to that of Air Nostrum. However, when compared to the utilization standard of 8 hours, the CRJ1000's utilization is quite low. In 2019, the CRJ1000 aircraft are operated for just 3,36 hours per day, significantly less than the standard.

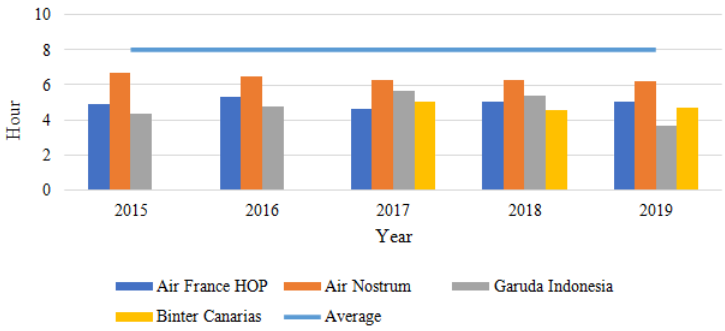

FIGURE 3.3: Average Annual Utilization of CRJ1000

As illustrated in Figure 3.4 by the seat load factor aspect, the load factor obtained is less than the break-even load factor (BELF). This situation is worse when BELF is greater than 100%, implying that the CRJ1000 operates inefficiently. This

indicates that either the operational costs are excessive or the revenue is insufficient, as the BELF is greater than 100% (Jacky, 2020). Given the CRJ1000's operational condition and the ongoing trend toward business jets, converting CRJ1000 aircraft to business jets is one of the most likely solutions for the current situation.

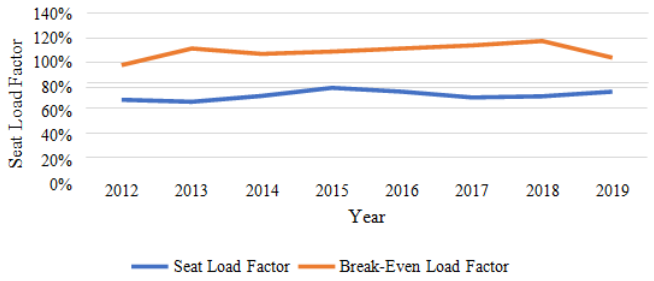

FIGURE 3.4: Seat Load Factor of CRJ1000

3.3 Configuration Layout of Current CRJ1000

Figure 3.5 shows the current configuration layout of CRJ1000 aircraft with the capacity of 96 seats.

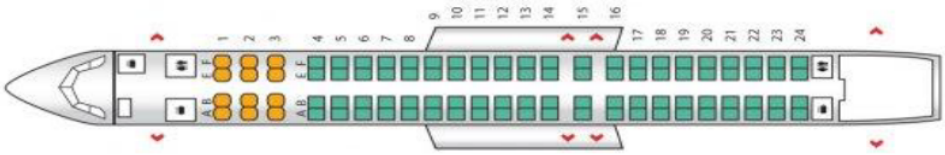

FIGURE 3.5: Configuration of Current CRJ1000 Aircraft.

Table 3.1 shows the list of items and weights of current CRJ1000 configuration.

Items	Quantity	Weight (kg)	Total Weight (kg)
Economy Class Seat	84	30	2520
Business Class Seat	12	40	480
Lavatory	1	100	100

TABLE 3.1: List of Items and Weights of Current Configuration

3.3.1 Aircraft Operating Weights

Weights of aircraft can be classified according to how they are certified. The two authorities that certify weight limits are those certified by the manufacturer during the aircraft's design and certification process, and those by the operator. Operator-certified weights are often reliant on the aircraft's specification/configuration and are considered into the determination of certain manufacturer-certified weights.

Manufacturer Certified Weights

Certified manufactured operating weights are obtained throughout the aircraft design and certification phases and are documented in the aircraft type certificate and manufacturer's specification documents such as the Aircraft Flight Manual and Aircraft Weight Balance Manual. Manufacturer-certified operating weights are classified as follows:

- **Maximum Taxi Weight (MTW)** implies the maximum weight an aircraft can carry on the ground, as limited and/or approved by the aircraft's strength and airworthiness regulations (this includes the weight of fuel for taxiing to the takeoff position).
- **Maximum Takeoff Weight (MTOW)** (Brake Release Gross Weight) refers to the maximum takeoff weight permitted and/or limited by the aircraft's strength and airworthiness criteria.
- **Maximum Landing Weights (MLW)** is the maximum landing weight permitted by the aircraft's structural strength and regulations.
- **Maximum Zero-fuel Weight (MZFW)** refers to the maximum weight that can be loaded prior to the addition of useable fuel and other fluids that is usable.

Manufacturer certified weights are frequently differentiated by the following limitations:

- The aircraft's structural design
- The permitted weight limitations that an operator may lawfully use.

Maximum structural design weights are the absolute maximum weights permitted by aircraft strength and airworthiness regulations. They are developed to avoid overloading the structure or to ensure that the structure maintains appropriate performance or handling characteristics during operation. Maximum Design Taxi Weight (MDTW), Maximum Design Takeoff Weight (MDTOW), Maximum Design Landing Weights (MDLW), and Maximum Design Zero-fuel Weight (MDZFW) are included in these weights.

Maximum authorized weights are weight limits that an operator or airline may legally use. Authorized weights may be equal to or less than the weight restrictions specified in the structural design.

When certified weights are less than the design thresholds, the lower values are termed as Maximum Taxi Weight (MTW), Maximum Takeoff Weight (MTOW), Maximum Landing Weights (MLW), and Maximum Zero-fuel Weight (MZFW). The airline determines the permissible weight restrictions, which are frequently referred to as "purchased weights." An operator may purchase a certified weight that is less than the maximum design weights in order to avoid paying expenses (such as airport landing and navigation fees) that are indexed to certain maximum weights (e.g. MTOW, MLW, etc.).

Operator Certified Weights

While many weight parameters are regulated on a manufacturer-by-manufacturer basis, others are defined by the operator and vary according to the aircraft's specification/configuration. Operator weights are made up of:

- Operating Empty Weight (OEW)
- Maximum Structural Payload (MSP)

Operator's Empty Weight (OEW) refers to the weight of an aircraft that has been prepared for service. It is calculated by adding the Manufacturer's Empty Weight (MEW), Standard Items (SI), and Operator Items (OI).

Maximum Structural Payload (MSP) means the maximum design payload (passengers, baggage, and cargo) as a structural limit weight.

Operator Weight Build-Up

The figure illustrates the weight categories that are represented in the majority of transport aircraft. Begin with the Manufacturer's Empty Weight (MEW) and add elements necessary to operate the aircraft. This figure provides a mathematical overview of the process of calculating a variety of weight categories, which can be seen below:

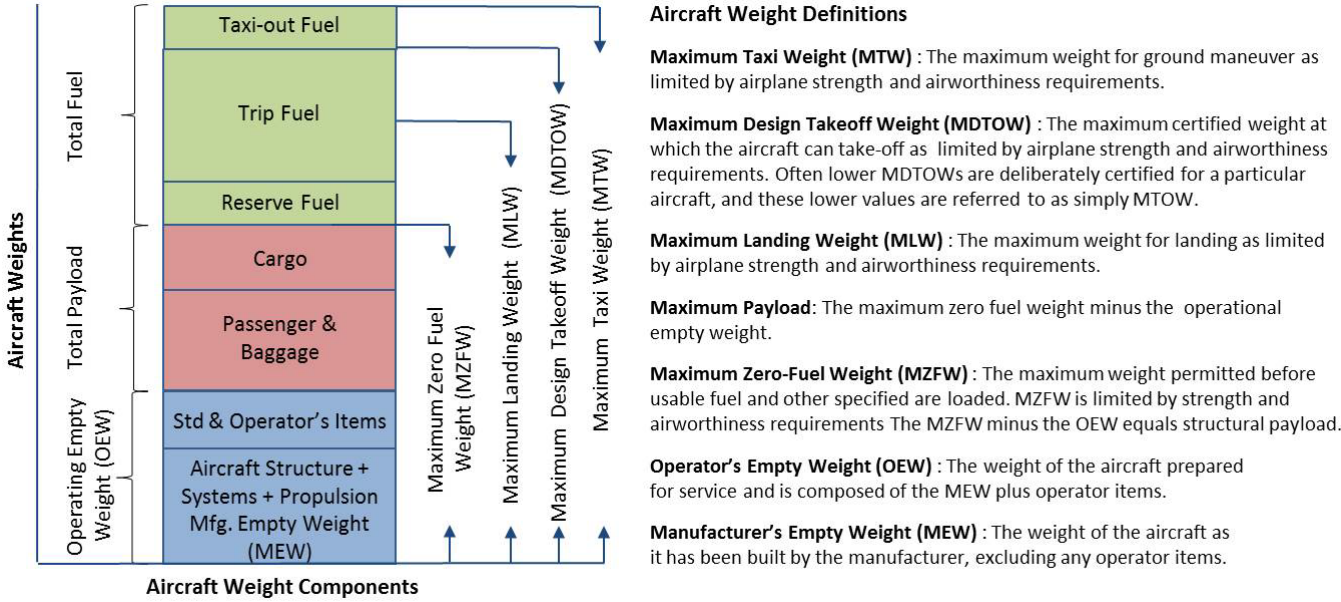

FIGURE 3.6: Aircraft Weight Component

- For any aircraft with a specified maximum take-off weight, the MTOW can be computed as the MZFW plus the Reserve & Trip Fuel Capacity:MTOW = MZFW + Reserve Fuel + Trip Fuel
- For any aircraft with a specified MTW, the MTW can be computed as the MTOW plus the Taxi-out Fuel: MTW = MTOW + Taxi-out Fuel

The following table is the list of CRJ 1000 weight and cargo volume limitations. For the fuel, the weight is calculated determined with a fuel density of 6.7 lb/US gal (0.809 kg/L).

Maximum Ramp Weight (MRW)	92300 lb (31867 kg)
Maximum Landing Weight (MLW)	81500 lb (36968 kg)
Maximum Flight Weight (MFW)	51000 lb (23133 kg)
Maximum Zero Fuel Weight (MFZW)	77500 lb (35153 kg)
Maximum Fuel Tank Capacity	2903 US gal (10989 L) 228.2 lb (103.5 kg)
Maximum Cargo Volume - Aft Baggage Compartment	14.41 m^3
Maximum Cargo Volume - Forward Under Floor Baggage	5.26 m^3
Maximum Cargo Volume - Under-seat storage	4.16 m^3
Maximum Cargo Volume - Overhead bins	5.08 m^3

TABLE 3.2: List of Weight of CRJ1000

3.4 Aircraft Performance

Takeoff and landing performance are determined by the rate of acceleration and deceleration. For example, during takeoff, an aircraft begins at zero speed and gradually accelerates to the takeoff speed in order to gain altitude. The airplane touches down at the landing speed and decelerates to zero speed throughout the landing. The critical elements affecting takeoff or landing performance are as follows:

- The takeoff or landing speed is proportional to the stall speed or minimum flying speed.
- The pace at which the aircraft accelerates or decelerates during the takeoff or landing roll. Any object's speed (acceleration and deceleration) varies directly proportional to its force imbalance and inversely proportional to its mass.
- The distance traveled during the takeoff or landing roll is a function of both acceleration/deceleration and speed.

3.4.1 Cruising Performance

Range

For range, the Breguet equation for jet engine is used for this thesis. The range ratio is used to calculate the range of proposed configurations. The final range ratio equation as follows:

$$R_{\text{Biz}} = R_{\text{Pax}} \left(\frac{\ln \frac{W_{1_{\text{Biz}}}}{W_{2_{\text{Biz}}}}}{\ln \frac{W_{1_{\text{Pax}}}}{W_{2_{Pax}}}} \right) \tag{3.1}$$

Endurance

Breguet equation for jet engine is also used to calculate the endurance in this thesis. Since the endurance of current CRJ1000 configuration is unknown, therefore the percentage of change of the endurance ratio is used. The final endurance ratio equation as follows:

$$\Delta E = \left(\frac{\ln \frac{W_{1_{\text{Biz}}}}{W_{2_{\text{Biz}}}}}{\ln \frac{W_{1_{\text{Pax}}}}{W_{2_{Pax}}}} \right) - 1 \tag{3.2}$$

3.4.2 Airfield Performance

Take-Off Ground Roll Distance

Numerous elements must be considered while determining the Take-off ground run, including the following:

- Mass: The mass can be determined by dividing the total weight by gravitation.
- Speed during take-off: For take-off safety, the take-off speed (V_{LOF}) must be 20 percent higher than the stalling speed (V_{Stall}). To determine V_{stall}, we need to find C_{Lmax}.
- Force:Thrust force, drag force (can be determined by summing the Zero lift drag force and induced drag force, where the induced drag will have an additional multiplication by the ground effect factor), and wheel friction force (could be determined by multiplying the friction coefficient with the Normal force of the aircraft where the normal is equal to Weight = Lift)

Below is the equation used to calculate the take-off ground roll distance for this study.

$$S_{L_{O_G}} = \frac{1.44W^2}{g\rho_\infty SC_{Lmax}T - D + \mu_r(W-L)_a v} \tag{3.3}$$

For cases where $T > \mu_r(W - L)$ and $T > D$, therefore:

$$S_{L_{O_G}} = \frac{1.44W^2}{g\rho_\infty SC_{Lmax}} \tag{3.4}$$

Thus,

$$S_{L_{O_{G_{\text{Biz}}}}} = S_{L_{O_{G_{\text{Pax}}}}} \left(\frac{W_{\text{Biz}}}{W_{\text{Pax}}}\right)^2 \tag{3.5}$$

Figure 3.7 shows the take-off field length with ISA of CRJ 1000.

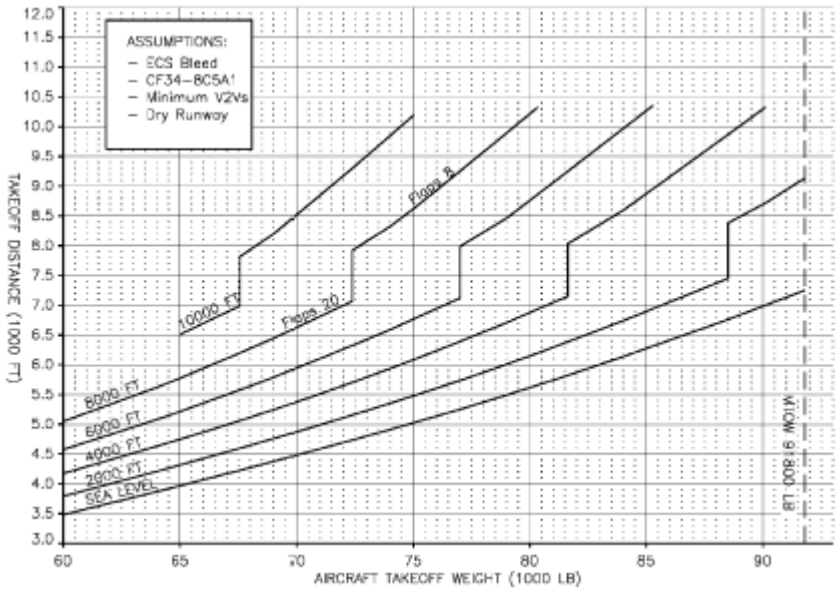

FIGURE 3.7: CRJ 1000 Take-Off Field Length - ISA.

Figure 3.8 illustrates the take-off field length with ISA + 15 degrees C of CRJ 1000.

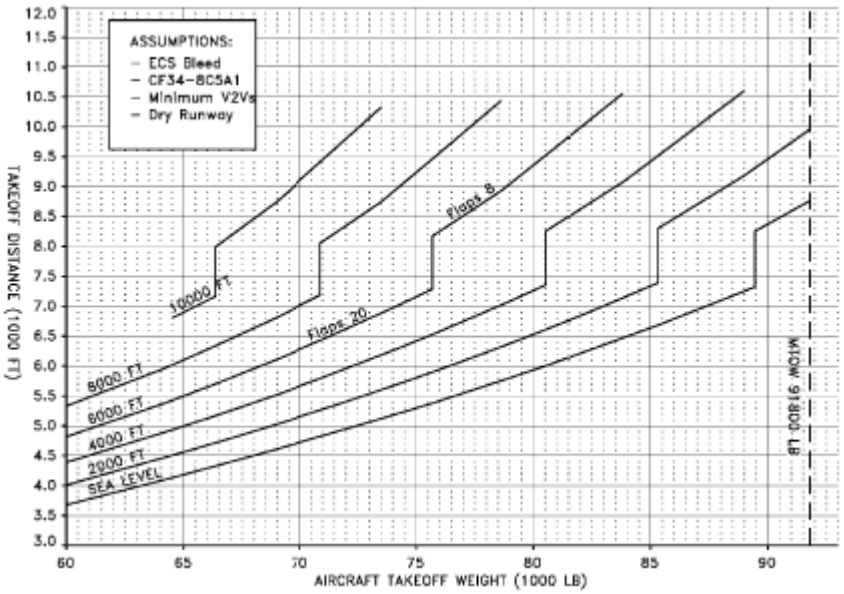

FIGURE 3.8: CRJ 1000 Take-Off Field Length - ISA + 15 Degrees C

Figure 3.9 shows the take-off field length with ISA + 20 Degrees C of CRJ 1000.

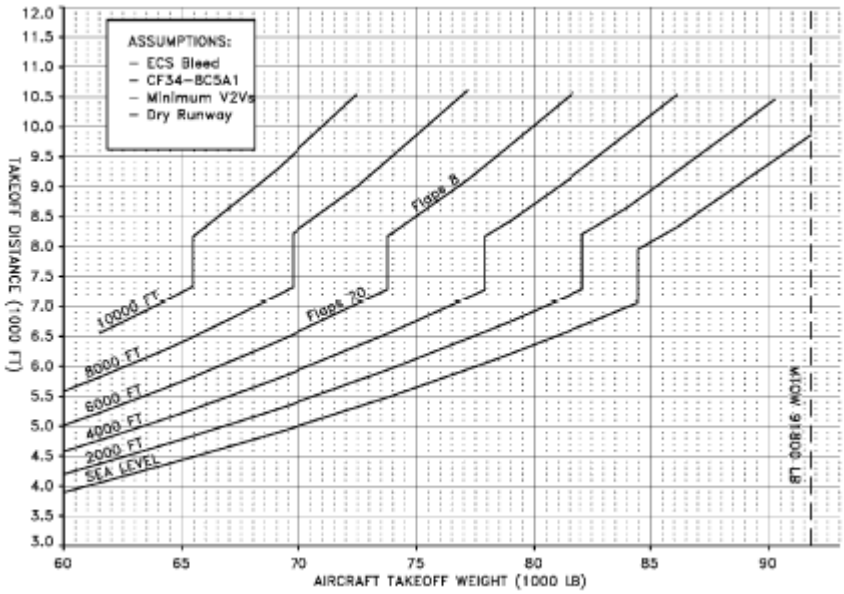

FIGURE 3.9: CRJ 1000 Take-Off Field Length - ISA + 20 Degrees C

Figure 3.10 shows the take-off field length with ISA + 25 Degrees C of CRJ 1000.

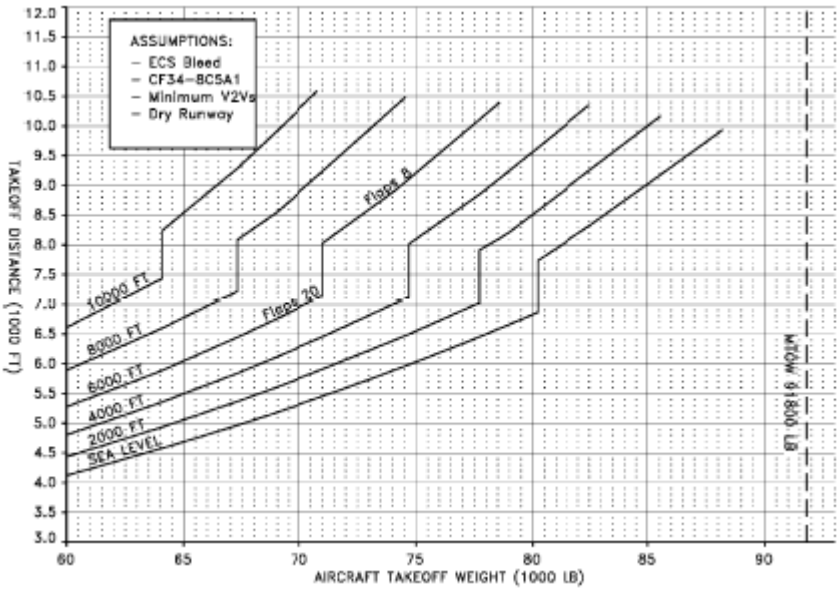

FIGURE 3.10: CRJ 1000 Take-Off Field Length - ISA + 25 Degrees C

Figure 3.11 shows the take-off field length with ISA + 30 Degrees C of CRJ 1000.

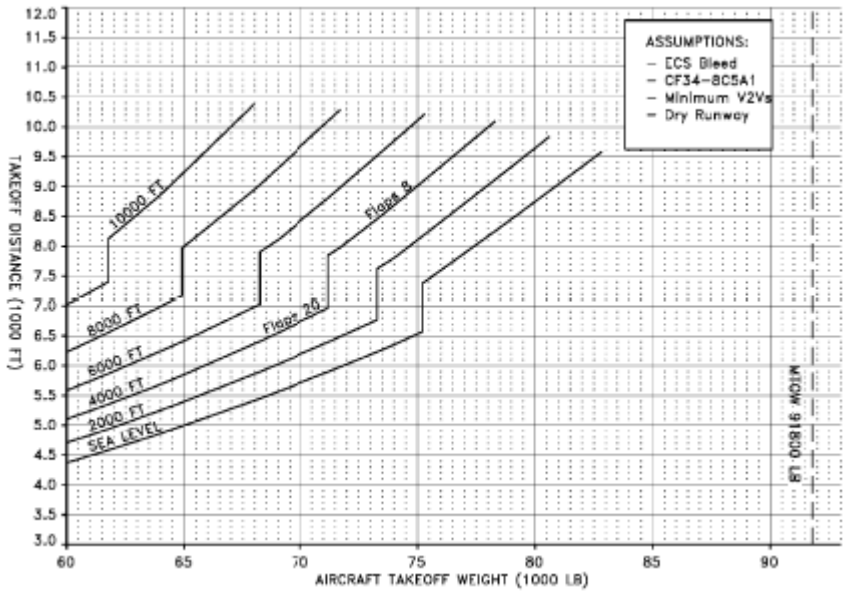

FIGURE 3.11: CRJ 1000 Take-Off Field Length - ISA + 30 Degrees C

Figure 3.12 shows the take-off field length with ISA + 35 Degrees C of CRJ 1000.

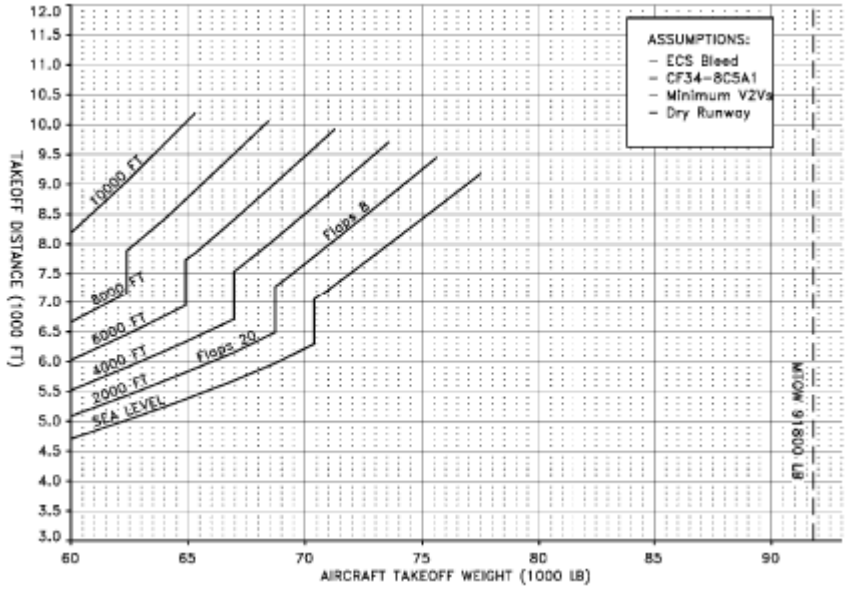

FIGURE 3.12: CRJ 1000 Take-Off Field Length - ISA + 35 Degrees C

The Airborne Phase of The Take-Off

To evaluate an aircraft's airborne performance, an aircraft needs to maintain the same radius value during the liftoff and climb phases, as well as the flight path's angle.

Landing Ground Run

Meanwhile, we continue to use total weight without regard for fuel weight decrease when determining the landing ground run. Numerous parameters must be considered while determining the landing ground run, including the following:

- Mass: The mass can be determined by dividing the total weight by gravitation.
- Landing speed:Same as when take-off, during the landing, there is also a landing safety factor, where the landing speed (V_T) must be 30 percent higher than the stalling speed (V_{Stall}).
- Force: There is a variation in the force applied as a result of the installation of reverse thrust. The reverse thrust direction becomes identical to that of the wheel friction force and drag force. Similarly, the friction coefficient has decreased to 0.4 as a result of the functioning brake system. As a result, the force value increases.

Below is the equation used to calculate the landing ground roll distance for this study.

$$S_L = \frac{1.69W^2}{g\rho_\infty SC_{Lmax}D + \mu_r(W-L)_{0.7V}} \tag{3.6}$$

For cases where spoilers are deployed then $L = 0$, and normally $D < \mu W$, therefore:

$$S_L = \frac{1.69W}{g\rho_\infty SC_{Lmax}\mu_r} \tag{3.7}$$

Thus,

$$S_{L_{G_{\text{Biz}}}} = S_{L_{G_{\text{Pax}}}} \left(\frac{W_{\text{Biz}}}{W_{\text{Pax}}}\right) \tag{3.8}$$

Figure 3.13 shows the landing field length of CRJ 1000 at flaps of 45 degrees or slats extended.

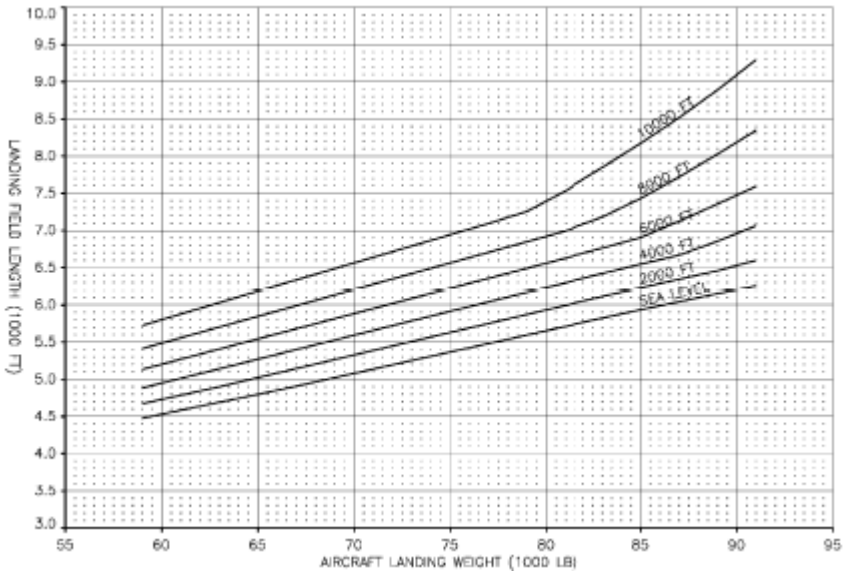

FIGURE 3.13: CRJ 1000 Landing Field Length - Flaps at 45 Degrees or Slats Extended

CHAPTER 4
RESULTS AND DISCUSSIONS

4.1 Proposed Aircraft Configuration

Figure 4.1 and 4.2 are the proposed business jets configuration of CRJ1000. The main difference of these two proposed configurations is that option 1 has 27 business class seats and 4 VIP seats while option 2 has 36 business class seats.

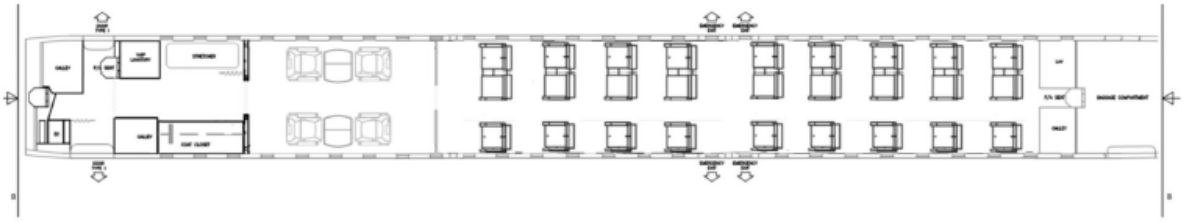

FIGURE 4.1: First option of proposed business jet configuration.

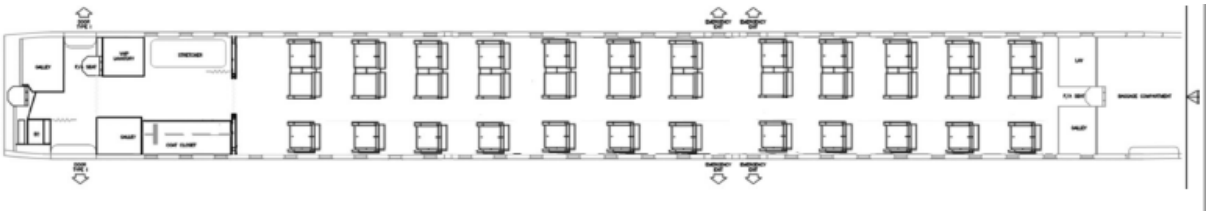

FIGURE 4.2: Second option of proposed business jet configuration.

For option one, the 4 VIP forward seats will be the rotatable with retractable tablets. Option one will also have two VIP wood finish partitions. VIP seats with the wood finish partitions behind the seats can be seen in Figure 4.3.

FIGURE 4.3: VIP Seats and Wood Finish Partitions

Figure 4.4 is the other view of rotatable VIP seats with retractable tablets.

FIGURE 4.4: Rotatable VIP Seat with Retractable Tablet.

Option one configuration will also have a table with wood finish that can be seen in Figure 4.5.

FIGURE 4.5: VIP table with wood finish

Figure 4.6 is the business seats for both new configurations.

FIGURE 4.6: Business Seats

Both configurations will have one VIP coat closet, one forward premium lavatory, one universal convertible medical stretcher, eight lining covers, six overhead

bins, two sets of renewed curtains, and renewed carpet. Figure 4.7 is the VIP coat closet.

FIGURE 4.7: VIP Coat Closet

The medical stretcher will be equipped with oxygen supply and easy access VIP wood finish sliding compartments for oxygen and medical materials. Figure 4.8, 4.9, 4.10, 4.11, 4.12, and 4.13 below are the UUDS medical stretcher from different point of views.

FIGURE 4.8: UUDS Medical Stretcher - Front View A

FIGURE 4.9: UUDS Medical Stretcher - Front View B

FIGURE 4.10: UUDS Medical Stretcher - Side View

FIGURE 4.11: UUDS Medical Stretcher - Side View and Closed A

FIGURE 4.12: UUDS Medical Stretcher - Side View and Closed B

FIGURE 4.13: Retracted UUDS Medical Stretcher.

Other than that, the medical stretcher is also equipped with a pond, portable toilet, syringe box, blanket, drawsheet, dust bag, disposable gloves, pillow, and disposable curtain. The medical stretcher kit can be seen in Figure 4.14

FIGURE 4.14: UUDS Medical Stretcher Kit

The transport container has a weight of 23.8 kg, width of 850 mm, length of 1275 mm, and height of 600 mm. Figure 4.15 and 4.16 show the transport container of UUDS Medical Stretcher.

FIGURE 4.15: UUDS Medical Stretcher Transport Container

FIGURE 4.16: UUDS Medical Stretcher - Other Point of View of the Box

Both configurations will use Flymingo wireless in-flight entertainment tablets for business class passengers. The media or movie content contract will be managed by the customer directly with Flymingo. The figure of Flymingo IFE can be seen in Figure 4.17.

FIGURE 4.17: Flymingo Wireless In-Flight Entertainment

The premium lavatory is based on the previous lavatory that will be refurbished as can be seen below. The example of the premium lavatory can be seen in Figure 4.18.

FIGURE 4.18: Premium Lavatory

The Overhead bins will be the same as the previous ones but with the new covers. Both existing curtains and carpet will be replaced in option 1 and option 2.

4.2 Weight Changes

Table below are the lists of items and its weight. On the option 1 and option 2, the curtain and carpet will replace the existing. But since the total needed of both curtain and carpet are the same on the current, option 1, and option 2 configurations, therefore they are not inserted in the table below.

Note: For the curtain, the area is calculated from the cabin aisle height (1.89 m) and width (0.41 m). For the carpet, the area is taken from the floor area, 50.3 m^2.

Figure 4.1 below is the list of items and weights of the current configuration.

Items	Quantity	Weight (kg)	Total Weight (kg)
Economy Class Seat	84	30	2520
Business Class Seat	12	40	480
Lavatory	1	100	100

Table 4.1: List of Items and Weights of Current Configuration

The table 4.2 is the list of items and weights of the option 1 configuration.

Items	Qty	W (kg)	Total W (kg)
VIP Seat	4	40	160
Table	1	10	10
Business Class Seat	27	30	810
VIP Coat Closet	1	100	100
Forward Premium Lavatory	1	120	120
Stretcher	1	30	30
Partitions	2	5	10
IFE with Tablets and Charger Rack	1+31	2	64
Lining Covers	8	0	0
Overhead Bins Covers	6	0	0
Satcom Irridium	1	10	10
LCD TV Screens	1	15	15
		Total Weight	1329

Table 4.2: List of Items and Weights of Option 1 Configuration

The following table 4.3 is the list of items and weights of the option 2 configuration.

Items	Qty	Weight (kg)	Total Weight (kg)
Business Class Seat	36	30	1080
VIP Coat Closet	1	100	100
Forward Premium Lavatory	1	120	120
Stretcher	1	30	30
IFE with Tablets and Charger Rack	1+36	2	74
Lining Covers	8	0	0
Overhead Bins Covers	6	0	0
Satcom Irridium	1	10	10
LCD TV Screens	1	15	15
		Total Weight	1429

TABLE 4.3: List of Items and Weights of Option 2 Configuration

The table 4.4 below is the total weight (basic empty weight) comparison between current, option 1, and option 2 configurations.

Items	Current (kg)	Opt_1 (kg)	Opt_2 (kg)
Economy Class Seat	2520	0	0
VIP Seat	0	160	0
Table	0	10	0
Business Class Seat	480	810	1080
VIP Coat Closet	0	100	100
Forward Premium Lavatory	100	120	120
Stretcher	0	30	30
Partitions	0	10	0
IFE with Tablets and Charger Rack	0	64	74
Satcom Irridium	0	10	10
LCD TV Screens	0	15	15
Total Weight	3100	1329	1429

TABLE 4.4: Total Weight Comparison between Current, Option 1, and Option 2 Configurations

Since the standard weight for payload is determined by the airlines, therefore the standard varies. In this thesis, since according to the CRJ 1000 fact sheet that the range is based on the weight for each passenger is 112 kg, therefore it is assumed that the passenger weight is 70 kg and the baggage weight is 32 kg. The following table 4.5 is the list of the passenger and baggage weights for the three configurations. C stands for current configuration. Opt_1 means option 1 configuration. Opt_2 means option 2 configuration.

Items	Weight	Current Quantity	Current Weight	Opt_1 Quantity	Opt_1 Weight	Opt_2 Quantity	Opt_2 Weight
Passenger	70	96	6720	31	2170	36	2520
Baggage	32	96	3072	31	992	36	1152
Total (kg)			9792		3162		3672

TABLE 4.5: List of Passenger and Baggage Total Weights

4.3 Aircraft Performance

4.3.1 Cruising Performance

Range

From equation 2.46, Range is defined as

$$R = \frac{1}{C_T}\sqrt{\frac{T}{S}\frac{2}{\rho}\frac{C_L^2}{C_D^3}}ln\frac{W1}{W2} \tag{4.1}$$

Since current range is known, the difference between the current configuration and the proposed configurations are the W_1 and W_2, therefore the equation can be written as:

$$R_{Pax} = R_{Biz} \tag{4.2a}$$

$$\frac{1}{C_T}\sqrt{\frac{T}{S}\frac{2}{\rho}\frac{C_L^2}{C_D^3}}ln\frac{W_{1pax}}{W_{2pax}} = \frac{1}{C_T}\sqrt{\frac{T}{S}\frac{2}{\rho}\frac{C_L^2}{C_D^3}}ln\frac{W_{1biz}}{W_{2biz}} \tag{4.2b}$$

$$ln\frac{W_{pax1}}{W_{2pax}} = ln\frac{W_{1biz}}{W_{2biz}} \tag{4.2c}$$

Then,

$$\frac{R_{Pax}}{R_{Biz}} = \frac{ln\frac{W_{1pax}}{W_{2pax}}}{ln\frac{W_{1biz}}{W_{2biz}}} \tag{4.3}$$

Therefore,

$$R_{\mathrm{Biz}} = R_{\mathrm{Pax}}\left(\frac{\ln\frac{W_{1_{\mathrm{Biz}}}}{W_{2_{\mathrm{Biz}}}}}{\ln\frac{W_{1_{\mathrm{Pax}}}}{W_{2_{Pax}}}}\right) \tag{4.4}$$

To find the MTOW that is assumed as W_1 for the two proposed configurations, the equation is:

$$MTOW_x = MTOW_{Current} - W_{Current} + W_x \tag{4.5}$$

Table 4.6 is the Total Weight and MTOW for the three configurations.

Items	Current (kg)	Opt_1 (kg)	Opt_2 (kg)
Basic Empty Weight	3100	1329	1429
Payload	9792	3162	3672
Total Weight Change w/o Fuel (W)	12 892	4491	5101
MTOW (W_1)	41 640	33 239	33 849
Δ MTOW		−8401	−7791

TABLE 4.6: Total Weight and MTOW for the three configurations.

These equations below are used for the calculation in the table above.

$$W = BEW - \text{Payload} \tag{4.6}$$

For W_1:

$$MTOW_x = MTOW_{\text{Current}} - W_{\text{Current}} + W_x \tag{4.7}$$

$$\Delta MTOW = MTOW_x - MTOW_{\text{Current}} \tag{4.8}$$

For W_2, the Maximum Fuel Tank Capacity is 8822 kg, with the assumption that fuel density is 0.809 kg/L.

$$W_2 = MTOW_x - W_{Fmax} \tag{4.9}$$

Table 4.7 shows the comparison between the variants of W_2.

W	Current (kg)	Opt_1 (kg)	Opt_2 (kg)
W_1	41 640	33 239	33 849
W_2	32 818	24 417	25 027

TABLE 4.7: Comparison between the variants of W_2

Table 4.8 below is the range for the three configurations and the percentage of change compared to the current configuration.

Configuration	$\ln \frac{W_1}{W_2}$	Range (km)	$\Delta(\%)$
Current	0.2381	3056	
Option 1	0.3084	3958.9	+29.5
Option 2	0.3019	3874.9	+26.8

TABLE 4.8: Range of Proposed Configurations

Endurance

Since the endurance for current CRJ1000 configuration is unknown, therefore the percentage of change of the endurance ratio is used. The endurance ratio and range ratio equations used are similar, therefore the percentage of change between endurance and range are also similar.

The equation below shows how to calculate the percentage of change of endurance ratio.

$$\Delta E = \left(\frac{\ln \frac{W_{1_{\text{Biz}}}}{W_{2_{\text{Biz}}}}}{\ln \frac{W_{1_{\text{Pax}}}}{W_{2_{Pax}}}} \right) - 1 \tag{4.10}$$

Table 4.9 shows the percentage of endurance change, compared to current configuration. The percentage of change is similar to range.

Configuration	$\ln \frac{W_1}{W_2}$	ΔE	$\Delta E(\%)$
Current	0.2381		
Option 1	0.3084	0.295	+29.5
Option 2	0.3019	0.268	+26.8

TABLE 4.9: Endurance of Proposed Configurations

4.3.2 Airfield Performance

Take-Off Ground Roll

The ground roll distance or lift off distance equation is as follows:

$$S_{L_{O_G}} = \frac{1.44W^2}{g\rho_\infty SC_{Lmax}T - D + \mu_r(W - L)_{av}} \tag{4.11}$$

For cases where $T > \mu_r(W - L)$ and $T > D$, therefore:

$$S_{L_{O_G}} = \frac{1.44W^2}{g\rho_\infty SC_{Lmax}} \tag{4.12}$$

Therefore,

$$\frac{S_{L_{O_{G_{\text{Biz}}}}}}{S_{L_{O_{G_{\text{Pax}}}}}} = \frac{\frac{1.44W_{\text{Biz}}^2}{g\rho_\infty SC_{Lmax}}}{\frac{1.44W_{\text{Pax}}^2}{g\rho_\infty SC_{Lmax}}} \tag{4.13a}$$

$$\frac{S_{L_{O_{G_{\text{Biz}}}}}}{S_{L_{O_{G_{\text{Pax}}}}}} = \left(\frac{W_{\text{Biz}}}{W_{\text{Pax}}}\right)^2 \tag{4.13b}$$

$$S_{L_{O_{G_{\text{Biz}}}}} = S_{L_{O_{G_{\text{Pax}}}}} \left(\frac{W_{\text{Biz}}}{W_{\text{Pax}}}\right)^2 \tag{4.13c}$$

$$\tag{4.13d}$$

The takeoff field length for the current configuration is 2,120 m at ISA, SL, and MTOW configurations. It is assumed from the standard practice that take-off ground roll is $\frac{3}{4}$ from the take-off field length, therefore the take-off ground roll for the current configuration is 1.590 m.

The table 4.10 shows the take-off ground roll for both configurations. Weight used is the MTOW of each configuration.

Configuration	W (MTOW) (kg)	$S_{L_{O_G}}$ (m)	$\Delta(\%)$
Current	41 640	1590	
Option 1	33 239	1013.14	-36.28
Option 2	33 849	1050.67	-33.29

TABLE 4.10: Take-off Ground Roll for Both Configurations

Landing Ground Roll

The landing ground roll distance equation is as follows:

$$S_{L_G} = \frac{1.69W^2}{g\rho_\infty SC_{Lmax}D + \mu_r(W - L)_{0.7V}} \tag{4.14}$$

For cases where spoilers are deployed then $L = 0$, and normally $D < \mu W$, therefore:

$$S_{L_G} = \frac{1.69W^2}{g\rho_\infty SC_{Lmax}\mu_r W} \tag{4.15a}$$

$$= \frac{1.69W}{g\rho_\infty SC_{Lmax}\mu_r} \tag{4.15b}$$

$$\tag{4.15c}$$

Therefore,

$$\frac{S_{L_{G_{\text{Biz}}}}}{S_{L_{G_{\text{Pax}}}}} = \frac{\frac{1.69W_{\text{Biz}}}{\mu_r g\rho_\infty SC_{Lmax}}}{\frac{1.69W_{\text{Biz}}}{\mu_r g\rho_\infty SC_{Lmax}}} \tag{4.16a}$$

$$\frac{S_{L_{G_{\text{Biz}}}}}{S_{L_{G_{\text{Pax}}}}} = \left(\frac{W_{\text{Biz}}}{W_{\text{Pax}}}\right) \tag{4.16b}$$

$$S_{L_{G_{\text{Biz}}}} = S_{L_{G_{\text{Pax}}}} \left(\frac{W_{\text{Biz}}}{W_{\text{Pax}}}\right) \tag{4.16c}$$

$$\tag{4.16d}$$

The landing field length for the current configuration is 1749 m at ISA, SL, and MLW configurations. It is assumed that take-off ground roll is $\frac{3}{4}$ from the landing field length, therefore the landing ground roll for the current configuration is 1311.75 m. The table 4.11 shows the take-off ground roll for both configurations.

Configuration	W_2	S_{L_G} (km)	$\Delta(\%)$
Current	36 968	1311.75	
Option 1	24 417	866.4	-33.95
Option 2	25 027	888.04	-32.3

TABLE 4.11: Landing Ground Roll for Both Configurations

Landing Distance and Speed

For the current configuration, the landing distance is 1749 m. The landing distance will be taken from the chart, taken from the Flight Planning and Performance

Manual of CRJ 1000 by Garuda Indonesia.

W: Weight

Alt: Altitude

Req: required

V_{ref}: Landing Speed

For configuration: APU OFF; Anti Ice OFF; Packs ON (ECS Bleed);Dry Runway; 0 wind

Below charts are the linear regressions of landing distance variation due to weight at several altitudes. The blue dots indicate the actual landing distance while the red dots indicate the required landing distance.

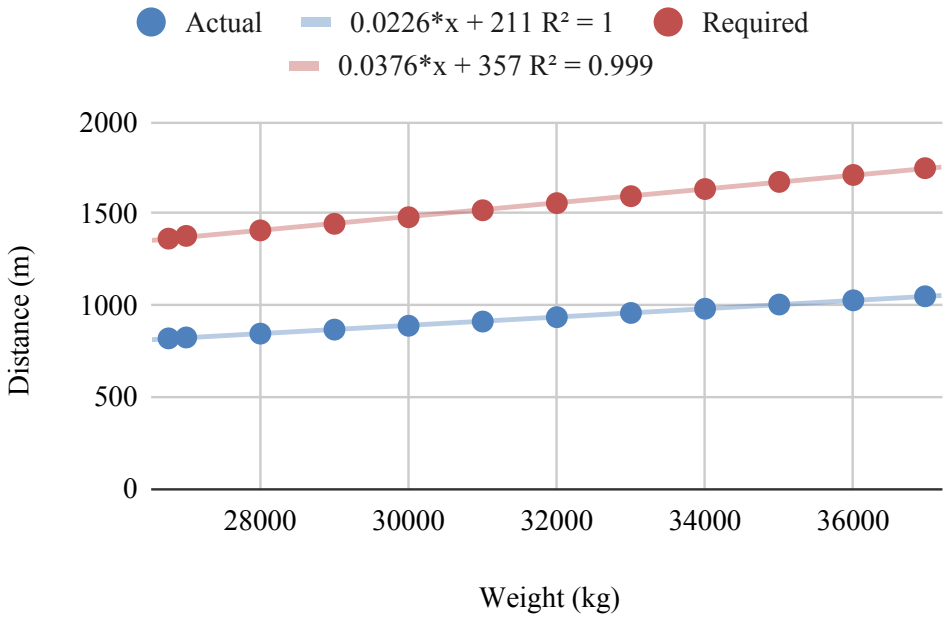

FIGURE 4.19: Landing Distance Variation Due to Weight at $h = 0\,\mathrm{m}$ ($X \triangleq W$)

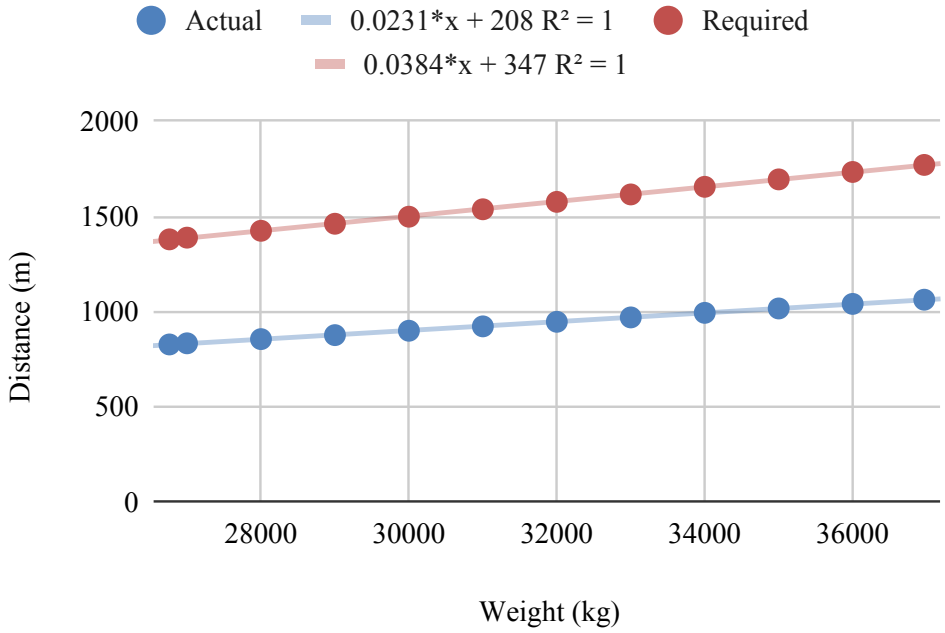

FIGURE 4.20: Landing Distance Variation Due to Weight at $h = 500\,\mathrm{m}$ ($X \triangleq W$)

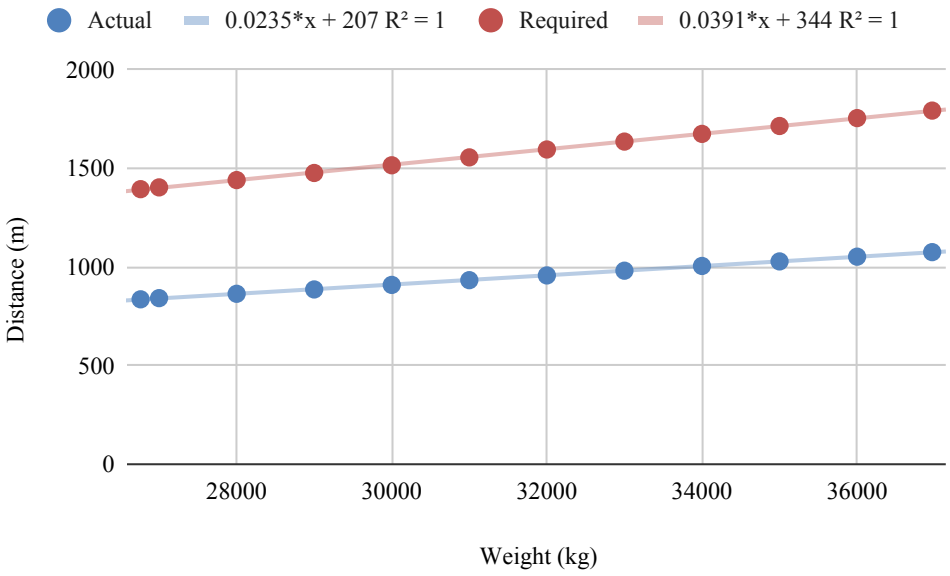

FIGURE 4.21: Landing Distance Variation Due to Weight at $h = 1000\,\mathrm{m}$ ($X \triangleq W$)

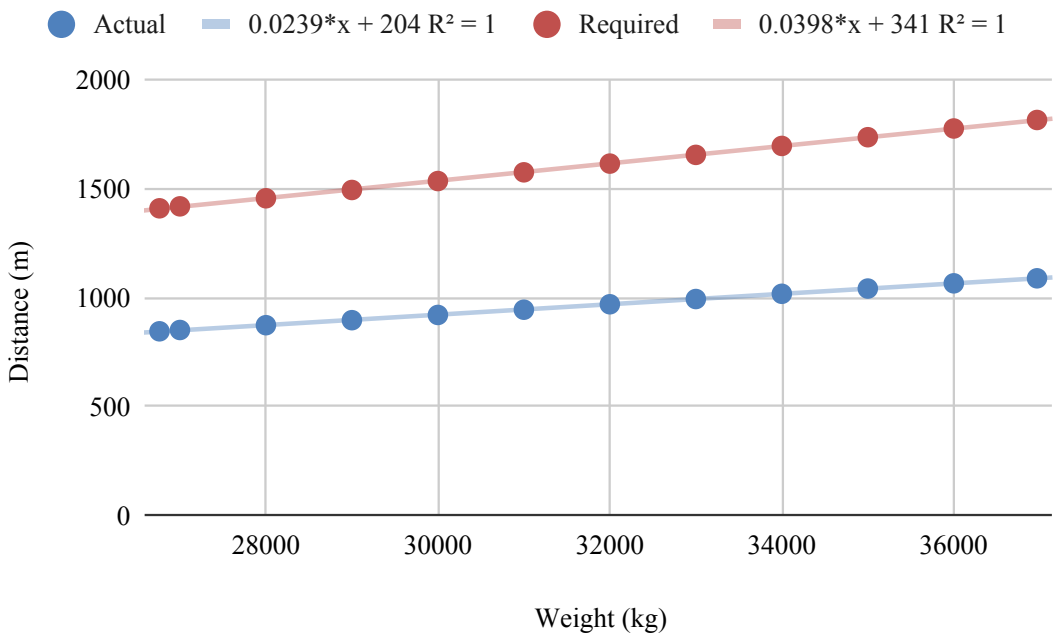

FIGURE 4.22: Landing Distance Variation Due to Weight at $h = 1500\,\mathrm{m}$ ($X \triangleq W$)

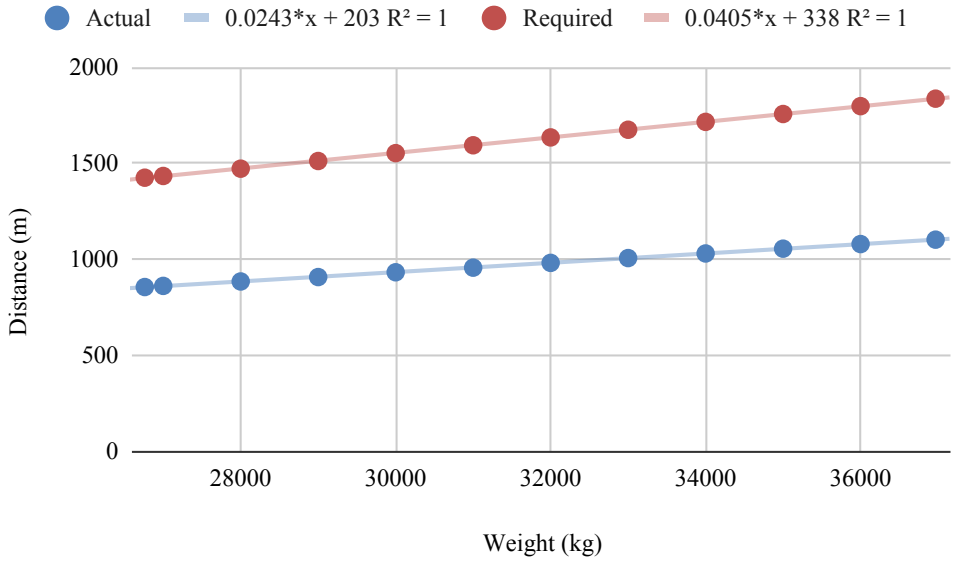

FIGURE 4.23: Landing Distance Variation Due to Weight at $h = 2000\,\mathrm{m}$ ($X \triangleq W$)

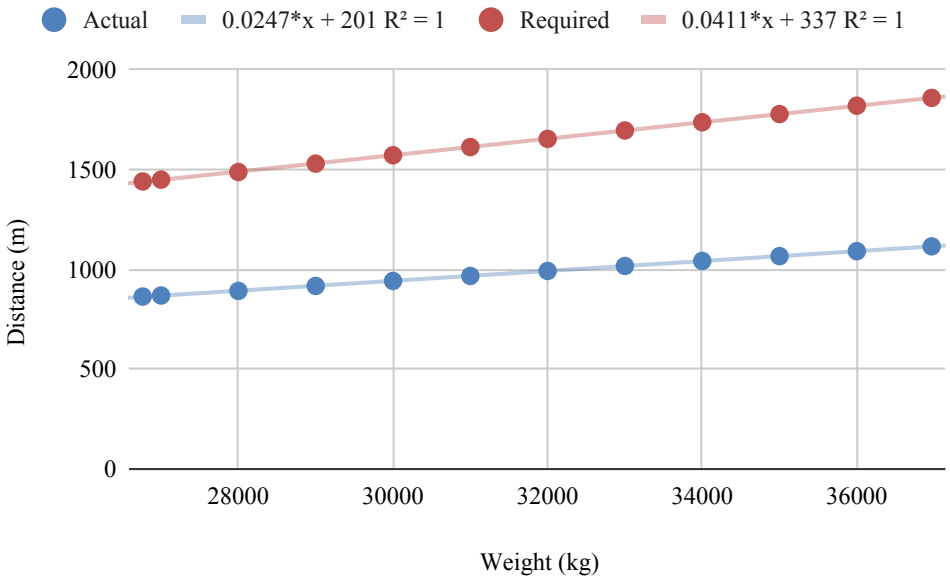

FIGURE 4.24: Landing Distance Variation Due to Weight at $h = 2500\,\mathrm{m}$ ($X \triangleq W$)

Below charts are the linear regressions of landing speed variation due to weight at several altitudes. Landing speed is more sensitive to the change of weight than to the change of altitude.

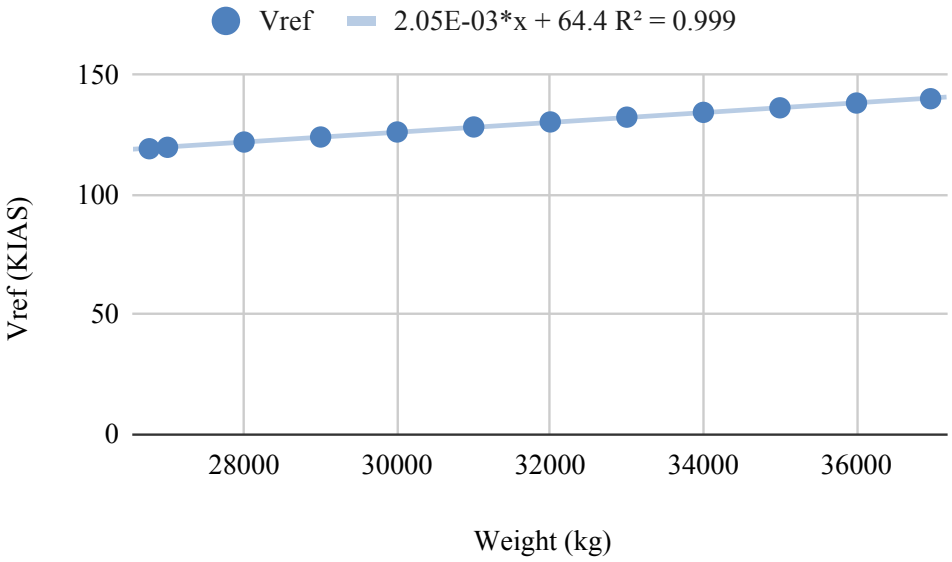

FIGURE 4.25: Landing Speed Variation Due to Weight at $h = 0\,\mathrm{m}$ ($X \triangleq W$)

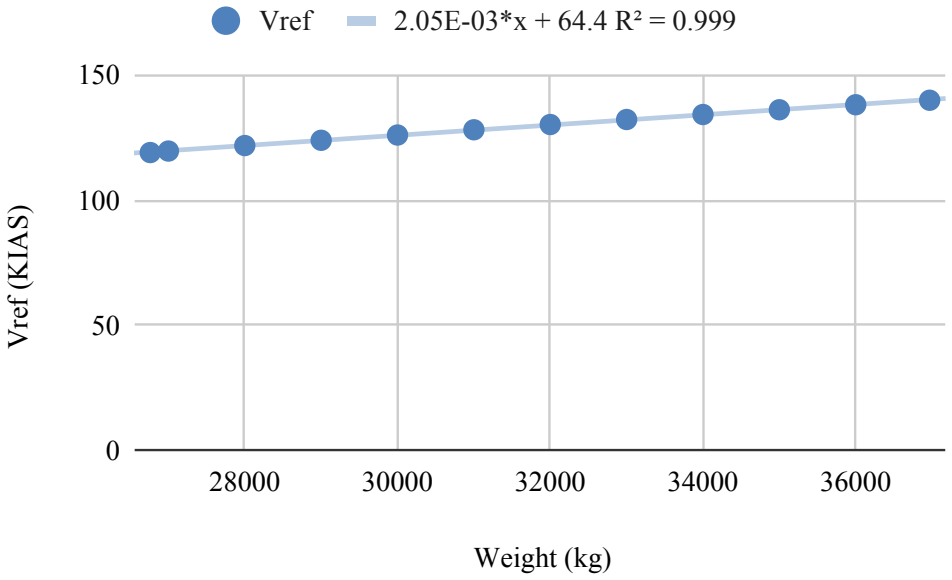

FIGURE 4.26: Landing Speed Variation Due to Weight at $h = 500\,\mathrm{m}$ ($X \triangleq W$)

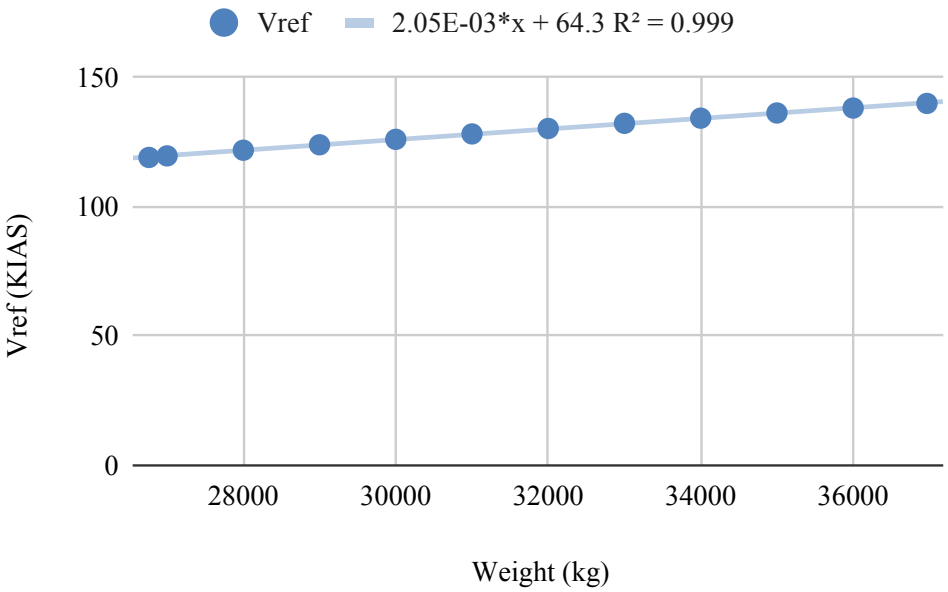

FIGURE 4.27: Landing Speed Variation Due to Weight at $h = 1000\,\mathrm{m}$ ($X \triangleq W$)

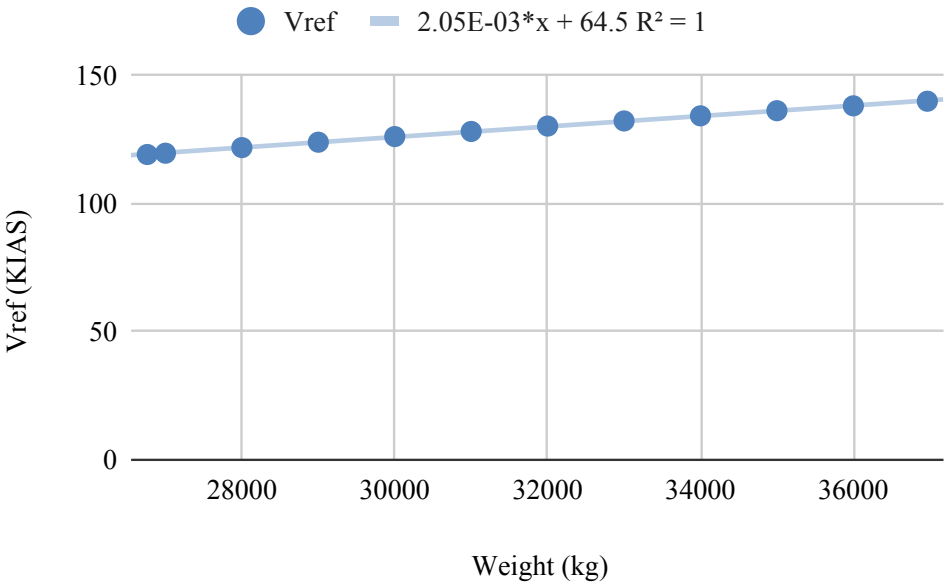

FIGURE 4.28: Landing Speed Variation Due to Weight at $h = 1500\,\mathrm{m}$ ($X \triangleq W$)

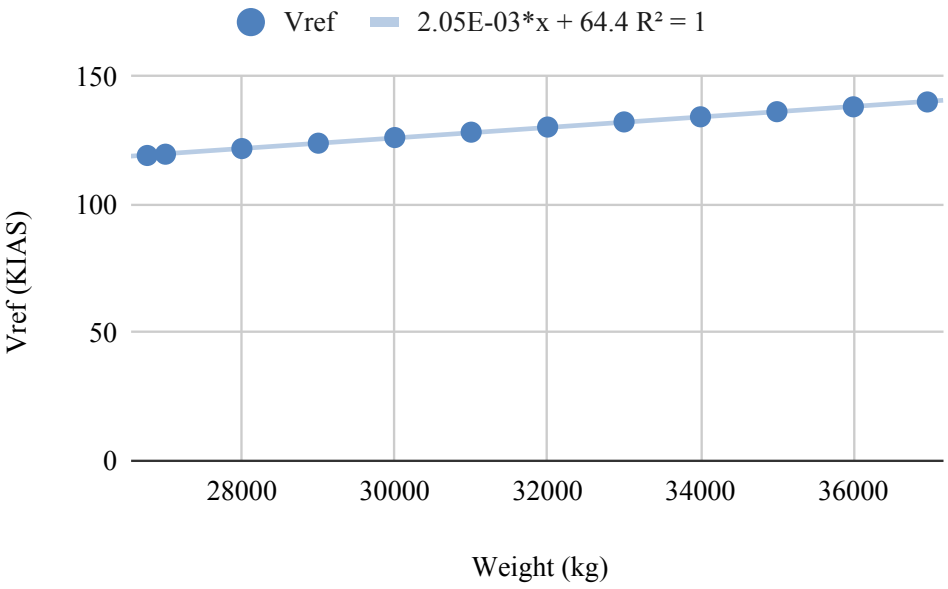

FIGURE 4.29: Landing Speed Variation Due to Weight at $h = 2000\,\mathrm{m}$ ($X \triangleq W$)

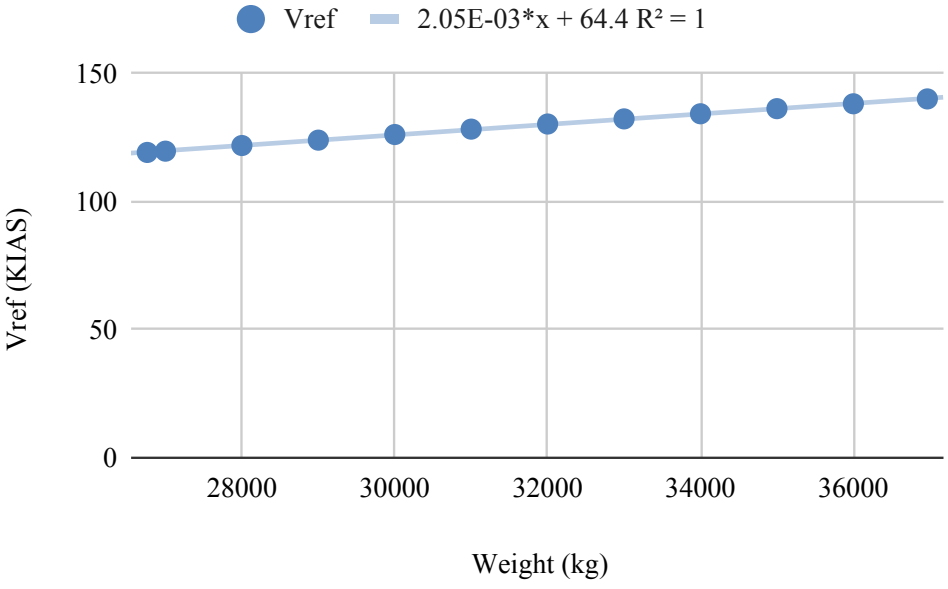

FIGURE 4.30: Landing Speed Variation Due to Weight at $h = 2500\,\mathrm{m}$ ($X \triangleq W$)

Table 4.12 is the summary of the linear regressions of landing distance and speed at several altitudes.

Alt (ft)	Actual S_L (m)	Required S_L (m)	V_{ref} (KIAS)
0	0.0226 W + 211	0.0376 W + 357	2.05E-03 W + 64.4
	R^2= 1	R^2= 0.999	R^2= 0.999
500	0.0231 W + 208	0.0384 W + 347	2.05E-03 W + 64.4
	R^2= 1	R^2= 1	R^2=: 0.999
1000	0.0235 W + 207	0.0391 W + 344	2.05E-03 W + 64.3
	R^2= 1	R^2= 1	R^2= 0.999
1500	0.0239 W + 204	0.0398 W + 341	2.05E-03 W + 64.5
	R^2= 1	R^2= 1	R^2= 1
2000	0.0243 W + 203	0.0405 W + 338	2.05E-03 W + 64.4
	R^2= 1	R^2= 1	R^2= 1
2500	0.0247 W + 201	0.0411 W + 337	2.05E-03 W + 64.4
	R^2= 1	R^2= 1	R^2= 1

TABLE 4.12: Linear Regressions of Landing Distance and Speed

W_2 for option 1 is 24 417 kg. Table 4.13 shows the result from the linear regressions for W: 24 417 kg and 0 Wind.

Alt (ft)	Actual D (m)	Required D (m)	V_{ref} (KIAS)
0	762.8	1275	114.5
500	772	1284.6	114.5
1000	780.8	1298.7	114.4
1500	787.6	1312.8	114.6
2000	796.3	1326.9	114.5
2500	804.1	1340.5	114.5

TABLE 4.13: Landing Distance for W: 24 417 kg and 0 Wind

W_2 for option 2 is 25 027 kg. Table 4.14 shows the result from the linear regressions for W: 25 027 kg and 0 Wind.

Alt (ft)	Actual D (m)	Required D (m)	V_{ref} (KIAS)
0	776.6	1298	115.7
500	786.1	1308	115.7
1000	795.1	1322.6	115.6
1500	802.1	1337.1	115.8
2000	811.2	1351.6	115.7
2500	819.2	1365.6	115.7

TABLE 4.14: Landing Distance and Speed for W:25 027 kg and 0 Wind

Landing Ground Roll Comparison

Since landing ground roll can be obtained by using approximation and linear regressions, therefore table will compare the results. To obtain $S_{L_{G_{\text{Biz}}}}$ from Required S_L from the regressions, equation below can be used:

$$S_{L_{G_{\text{Biz}}}} = \text{Required}S_L \times \frac{3}{4} \tag{4.17}$$

Table 4.15 shows the comparison of the landing ground roll results by using approximation and linear regressions.

Configuration	Req S_L Regress (m)	Regress (m)	Δ(%)	Approx (m)	Δ(%)
Current	1749	1311.75		1311.75	
Option 1	1275	956.25	-27.1	866.4	-33.9
Option 2	1298	973.5	-26	888.04	-32.3

TABLE 4.15: Landing Ground Roll Comparison between Regressions and Approximation at $h = 0$

The difference between the results is not significant. The linear regressions can be used for quick and better estimation of ground roll for both take-off and landing.

4.3.3 List of Airports

Since the take-off and landing distance needed for both proposed configurations are lower, therefore the aircraft can take-off from or landing to airports with shorter runway. The take-off distance for current configuration is 2120 m. The take-off ground roll from approximations for option 1 is 1013.14 m and for option 2 is 1050.67 m, which are $\frac{3}{4}$ from the total take-off distance. Therefore by multiplying the take-off ground roll with $\frac{4}{3}$, the total take-off distance can be obtained. For option 1, the take-off distance is 1350.83 m and for option 2 is 1400.89 m.

Table 4.16 and 4.17 below is the list of 80 new accessible airports with runway between 1350 m and 2120 m for both proposed configurations.

IATA Code	Airport	Runway	Location
ABU	A. A. Bere Tallo	1600 m x 30 m	Atambua, East Nusa Tenggara
-	Alas Lauser	1500 m x 30 m	Kutacane, Aceh
AEG	Aek Godang	1400 m x 30 m	South Tapanuli, North Sumatra
BTW	Bersujud Batu Licin	1800 m x 30 m	Batu Licin, South Kalimantan
LLO	Bua Lagaligo	1880 m x 30 m	Luwu, South Sulawesi
BTO	Budiarto	1600 m x 45 m	Curug, Banten
BUW	Beto Ambari	1800 m x 30 m	Baubau, Southeast Sulawesi
BLI	Buli	1500 m x 23 m	Pekaulang, East Halmahera, North Maluku
MEQ	Cut Nyak Dien	1800 m x 30 m	Nagan Raya, Aceh
SIQ	Dabo	1300 m x 30 m	Singkep Island, Lingga, Riau Islands
RTI	David Constantijn Saudale	1650 m x 30 m	Rote Ndao, East Nusa Tenggara
KRC	Depati Parbo	1800 m x 30 m	Kerinci, Jambi
DOB	Dobo	1500 m x 30 m	Dobo, Aru Islands
NBX	Douw Aturure Nabire	1400 m x 30 m	Nabire, Papua
-	Enggano	1600 m x 30 m	Banjar Sari, North Bengkulu, Bengkulu
RTG	Frans Sales Lega	1500 m x 30 m	Ruteng, Manggarai, East Nusa Tenggara
-	Gading Wonosari	1400 m x 45 m	Gunung Kidul, Yogyakarta
GLX	Gamar Malamo	1400 m x 30 m	Galela, North Maluku
LKA	Gewayantana	1600 m x 30 m	Tiwatobi, East Flores, East Nusa Tenggara
KBU	Gusti Sjamsir Alam	1650 m x 30 m	Laut Island, Kotabaru, South Kalimantan
KSR	H. Aroeppala Selayar	1950 m x 30 m	Selayar, South Sulawesi
SMQ	H. Asan Sampit	2060 m x 30 m	Sampit, Central Kalimantan
ENE	H.Hasan Aroeboesman	1650 m x 30 m	Ende, Flores island, East Nusa Tenggara
HMS	Haji Muhammad Sidik	1400 m x 30 m	Trinsing, North Barito, Central Kalimantan
JBB	Noto Hadinegoro	1705 m x 30 m	Jember, East Java
KBX	Kambuaya	1420 m x 30 m	East Ayamaru, West Papua
PSJ	Kasiguncu	1850 m x 30 m	Kasiguncu, Poso, Central Sulawesi
LNU	Kol RA. Bessing Malinau	1450 m x 30 m	Malinau, East Kalimantan
TJG	Kota Bangun	1400 m x 30 m	Kutai Kartanegara, East Kalimantan
KAZ	Kuabang Kao	2000 m x 30 m	Kao, Halmahera Utara, North Maluku
SMG	Lasikin	1710 m x 30 m	Sinabang, Simeulue island, Aceh
LSO	Lasondre	1400 m x 30 m	Batu Islands, South Nias, North Sumatra
LPU	Long Apung	1450 m x 30 m	Long Apung, Malinau, North Kalimantan
SBG	Maimun Saleh	1850 m x 30 m	Sabang, Aceh
ARD	Mali	1600 m x 30 m	Alor, East Nusa Tenggara
LSW	Malikus Saleh	1850 m x 23 m	Pinto Makmur, North Aceh, Aceh
RTU	Maratua	1600 m x 30 m	Maratua Island, East Kalimantan
RJM	Marinda	1400 m x 30 m	Waisai, Raja Ampat, West Papua
WNI	Matahora	2000 m x 45 m	Wangi-wangi Island, Wakatobi, Southeast Sulawesi
SXK	Mathilda Batlayeri	2000 m x 45 m	Amfutu, Tanimbar Islands, Maluku
MNA	Melongguane	1600 m x 30 m	Melangguane, Talaud Islands, North Sulawesi
IAX	Miangas	1400 m x 30 m	Miangas, North Sulawesi

TABLE 4.16: New Accessible Airports for Both Proposed Configurations Part 1

IATA Code	Airport	Runway	Location
MRB	Muara Bungo	1800 m x 30 m	Bungo Regency, Jambi
MPC	Mukomuko	1400 m x 30 m	Muko Muko, Bengkulu
NAH	Naha	1600 m x 30 m	Tahuna, Sangihe Islands, North Sulawesi
NAM	Namniwel	1600 m x 30 m	Namlea, Buru island, Maluku Islands
FOO	Biak Numfoor	1755 m x 20 m	Noemfoor, Schouten Islands
NNX	Nunukan	1450 m x 30 m	Nunukan, North Kalimantan
CJN	Nusawiru	1400 m x 30 m	Pangandaran, West Java
LAH	Oesman Sadik	1650 m x 30 m	Labuha, South Halmahera, North Maluku
OKL	Oksibil	1350 m x 30 m	Oksibil, Papua
PXA	Pagar Alam	1340 m x 30 m	Pagar Alam, South Sumatra
PPR	Pasir Pangaraian	1300 m x 30 m	Rokan Hulu, Riau
DUM	Pinang Kampai	1800 m x 30 m	Dumai, Riau
UOL	Pogogul Buol	1600 m x 30 m	Buol, Central Sulawesi
KTG	Rahadi Oesman	1400 m x 30 m	Ketapang, West Kalimantan
TJB	Raja Haji Abdullah	1400 m x 30 m	Tanjung Balai Karimun, Riau Islands
TNJ	Raja Haji Fisabilillah	2006 m x 45 m	Tanjungpinang, Riau Islands
MKW	Rendani	2000 m x 45 m	Manokwari, West Papua
KXB	Sangia Nibandera	1850 m x 30 m	Kolaka, Southeast Sulawesi
BJW	Soa	1600 m x 30 m	Soa, Ngada, East Nusa Tenggara
ZRI	Stevanus Rumbewas Serui	1600 m x 30 m	Yapen Islands, Papua
RAQ	Sugimanuru Muna	1600 m x 30 m	Muna, Southeast Sulawesi
TLI	Sultan Bantilan	1400 m x 30 m	Toli-Toli, Central Sulawesi
SWQ	Sultan Muhammad Kaharuddin	1650 m x 30 m	Sumbawa Besar, West Nusa Tenggara
BMU	Sultan Muhammad Salahuddin	1650 m x 30 m	Bima, Sumbawa, West Nusa Tenggara
TMH	Tanah Merah	1400 m x 30 m	Boven Digoel Regency, Papua
OJU	Tanjung Api Ampana	2110 m x 30 m	Ampana, Tojo Una-Una, Central Sulawesi
TJS	Tanjung Harapan	1600 m x 30 m	Tanjung Selor, North Kalimantan
TJG	Tanjung Waruking	1400 m x 30 m	Tabalong, Kalimantan Selatan
SQG	Tebelian	1820 m x 30 m	Sintang, West Kalimantan
-	Tempuling	1350 m x 30 m	Tembilahan, Indragiri Hilir, Riau
TRT	Toraja	1700 m x 30 m	Tana Toraja, South Sulawesi
SUP	Trunojoyo	1600 m x 30 m	Madura Island, East Java
CXP	Tunggu Wulung	1400 m x 30 m	Cilacap, Central Java
WGP	Umbu Mehang Kunda	1950 m x 30 m	Waingapu, Sumba, East Nusa Tenggara
KNG	Utarom Kaimana	2000 m x 30 m	Kaimana, West Papua
WET	Waghete	1400 m x 30 m	Tigi, Deiyai, Papua
WRR	Werur	1400 m x 30 m	Tambrauw, West Papua
LBW	Yuvai Semaring	1600 m x 30 m	Long Bawan, North Kalimantan

Table 4.17: New Accessible Airports for Both Proposed Configurations Part 2

CHAPTER 5
SUMMARY, CONCLUSION, RECOMMENDATION

5.1 Conclusion

The main purpose of this thesis is to propose business jet configurations and analyze the aircraft performance of the converted aircraft, especially the ones that are really related to the weight alteration because of the modification. Based on the proposed configurations and calculation results, the conclusions are:

	Current	Opt_1	$\Delta\text{Opt}_1(\%)$	Opt_2	$\Delta\text{Opt}_2(\%)$
MTOW (kg)	41 640	33 239	-20.18	33 849	-18.71
Range (km)	3056	3958.9	+29.5	3874.9	+26.8
ΔE		0.295	+29.5	0.268	+26.8
$S_{L_{O_G}}$ ($h = 0$ m) (m)	1590	1013.14	-36.28	1050.67	-33.92
S_{L_G} ($h = 0$ m) (Approx) (m)	1311.75	866.4	-33.95	888.04	-32.3
S_{L_G} ($h = 0$ m) (Regres) (m)	1311.75	956.25	-27.1	973.5	-26
Actual S_L ($h = 0$ m) (m)	1049	762.8	-27.28	776.6	-25.97
Required S_L ($h = 0$ m) (m)	1749	1275	-27.1	1298	-25.79
V_{ref} ($h = 0$ m) (KIAS)	139.9	114.5	-18.16	115.7	-17.3

Table 5.1: Summary for Three Configurations

- Both options have lesser MTOW, with a difference up to 8401 kg.
- The two options have extended range, up to 902.9 km.
- The percentage of endurance change is similar to range.

- The actual landing distance for both options are lesser, with a change up to 286.2 m.
- The required landing distance for both configurations are lower, up to 474 m.
- The take-off ground roll for both configurations are lesser, with a difference up to 576.86 m.
- Both options have lower landing ground roll, as far as 445.35 m.
- The landing ground roll difference between approximation and regressions is less than 6.85 %.
- The linear regressions can be used for better estimation of ground roll for both take-off and landing while approximations can be used to obtain quicker result.
- The two options have smaller landing speeds, as far as 25.4 KIAS.
- Landing speed is more sensitive to the change of weight than to the change of altitude.
- Overall, option 1 has better cruising and airfield performance since its MTOW is the lightest.
- Both proposed configurations will be able to take-off from and landing to another 80 airports with shorter runway, especially in the remote area, and specifically in East Indonesia.

5.2 Recommendation

Based on the result from the previous chapter, the recommendations regarding the business jets conversion are:

- Lesser weight resulting in a great fuel saving for the airline and most likely to be profitting while charging block hours.
- Converting CRJ1000 may be the most probable solution for the ongoing case.

- It is better for the airline to convert the aircraft as soon as possible, since the conversion process will take up to 8 months.
- Airline X should consider that it will be the business jet with the highest capacity across Indonesia.

References

33, L. (2021, May). *Private aviation trends for 2021.* Retrieved from https://l33jets.com/trends-in-private-aviation-2021

Anderson, J. D. (2005). *Introduction to flight.* McGraw-Hill Higher Education.

Christian, A. (2021, April). *The pandemic has created a middle class private jet boom.* Retrieved from https://www.wired.co.uk/article/coronavirus-planes-bonanza

Cirium. (2021, April). *Pandemic speeds retirement of older, high-maintenance aircraft.* Retrieved from https://www.flightglobal.com/fleets/pandemic-speeds-retirement-of-older-high-maintenance-aircraft/140831.article

Curran, A. (2021, June). *Garuda indonesia reduces leased crj1000 fleet.* Retrieved from https://simpleflying.com/garuda-indonesia-leased-crj-retur/

Denton, J. (2021, March). *Private-jet sales rose as airlines filed for bankruptcy through the pandemic.* Retrieved from https://www.marketwatch.com/story/private-jet-sales-rose-as-airlines-filed-for-bankruptcy-through-the-pandemic-11616759315

Euronews. (2021, May). *Environmentalists wary as private jet demand soars post lockdown.* Retrieved from https://www.euronews.com/travel/2021/05/27/private-jets-are-popular-covid-compliant-and-terrible-for-the-environment

FAA. (2016). Aircraft weight and balance handbook.

for Diseases Control & Prevention, C. (2021, March). *Clinical questions about covid-19: Questions and answers.* Retrieved from https://www.cdc.gov/coronavirus/2019-ncov/hcp/faq.html

GlobeAir. (2021, May). *Globeair announces a 20% volume growth for entry-level private jet charters in 2021.* Retrieved from https://www.globeair.com/

fr/n/private-jet-growth-2021

Gollan, D. (2021, March). *U.s. private jet charter market hitting record levels in march.* Retrieved from https://privatejetcardcomparisons.com/2021/03/26/u-s-private-jet-charter-market-hitting-record-levels-in-march/

Gopinath, G. (2021, April). *The great lockdown: Worst economic downturn since the great depression.* Retrieved from https://blogs.imf.org/2020/04/14/the-great-lockdown-worst-economic-downturn-since-the-great-depression/

Handayani, M., & Kuniawan, D. (2021, March). *Use a crj1000 aircraft, garuda boss: We lost idr 418 billion, more expensive than aircraft rental.* Retrieved from https://voi.id/en/news/32260/use-a-crj1000-aircraft-garuda-boss-we-lost-idr-418-billion-more-expensive-than-aircraft-rental

Herman. (2021, June). *Garuda to return 12 bombardier jets to nordic aviation capital.* Retrieved from https://jakartaglobe.id/business/garuda-to-return-12-bombardier-jets-to-nordic-aviation-capital

Jacky. (2020). Analisis dan restrukturisasi operasi pesawat bombardier crj1000.

Kingsley-Jones, M. (2021a, April). *Active mainline fleet over takes idle tally as recovery picks up.* Retrieved from https://www.flightglobal.com/fleets/active-mainline-fleet-over-takes-idle-tally-as-recovery-picks-up/138875.article

Kingsley-Jones, M. (2021b, April). *By the numbers: coronavirus effect on the global fleet.* Retrieved from https://www.flightglobal.com/fleets/by-the-numbers-coronavirus-effect-on-the-global-fleet/138943.article

Linker, R. (2021, April). *Business jet market - growth, trends, covid-19 impact, and forecasts (2021 - 2026).* Retrieved from https://www.globenewswire.com/news-release/2021/04/15/2211159/0/en/Business-Jet-Market-Growth-Trends-COVID-19-Impact-and-Forecasts-2021-2026.html

Morrison, M. (2021, April). *Transatlantic traffic keeps biggin hill's head above water.* Retrieved from https://www.flightglobal.com/business-aviation/transatlantic-traffic-keeps-biggin-hills-head-above-water/138210.article

Neubauer, I. L. (2021, April). *Private jet charters ride crosswinds of covid*

in asia. Retrieved from https://asia.nikkei.com/Business/Travel-Leisure/Private-jet-charters-ride-crosswinds-of-COVID-in-Asia

Puspa, A. W. (2021, June). *Garuda (giaa) kembalikan 12 crj-1000, ini sikap serikat karyawan.* Retrieved from https://ekonomi.bisnis.com/read/20210217/98/1357229/garuda-giaa-kembalikan-12-crj-1000-ini-sikap-serikat-karyawan

Ruijgrok, G. J. (2012). *Elements of airplane performance.* VSSD.

Schonland, A. (2021, April). *Rolls-royce's pearl.* Retrieved from https://airinsight.com/rolls-royces-pearl/

Sun, X., Wandelt, S., Zheng, C., & Zhang, A. (2021). Covid-19 pandemic and air transportation: Successfully navigating the paper hurricane. *Journal of Air Transport Management*, 102062.

Swindells, K. (2021, April). *Private jet industry trends upwards due to covid-19 pandemic.* Retrieved from https://www.elitetraveler.com/cars-jets-and-yachts/aviation/private-jet-trends-upwards-covid-19-pandemic

Syauqi, R. (2021, January). Performance review and analysis of guav-190417 target drone: Cruising and turning.

Team, Q. C. O. W. A. (2021, March). *Coronavirus is spreading turbulence in the airline industry.* Retrieved from https://www.oliverwyman.com/media-center/2020/mar/coronavirus-is-spreading-turbulence-in-the-airline-industry.html

Times, F. (2021, June). *China private jet use soars as economy hits pre-pandemic levels.* Retrieved from https://www.ft.com/content/2cebf46e-417e-42bc-b281-a6813529c1c4

Times, T. J. (2021, March). *Business jets drawing keen interest in japan amid pandemic.* Retrieved from https://www.japantimes.co.jp/news/2020/12/31/business/business-jets-interest-pandemic/

Times, T. M. (2021, June). *Demand for private jets surges as rich russians skirt pandemic rules to holiday in europe.* Retrieved from https://www.themoscowtimes.com/2021/06/08/demand-for-private-jets-surges-as-rich-russians-skirt-pandemic-rules-to-holiday-in-europe-a74148

University, J. H. (2021, June). Covid-19 dashboard by the center for systems

science and engineering (csse) at johns hopkins university (jhu).

www.alternativeairlines.com. (2021, May). *Regional jet.* Retrieved from `https://www.alternativeairlines.com/regional-jets`

Yong, J. Y. H. (2021, January). Performance review and analysis of guav-190417 target drone: Airfield, symmetric climb, and gliding.